AD-A037 737 OPTICAL SOCIETY OF AMERICA WASHINGTON D C F/G 20/6
OPTICAL PHENOMENA IN INFRARED MATERIALS.(U)
1976 AF-AFOSR-3061-76
UNCLASSIFIED AFOSR-TR-77-0163 NL

1 OF 3
AD A037737

OPTICAL PHENOMENA IN INFRARED MATERIALS

Technical Digest

December 1-3, 1976

Annapolis, Maryland

UNCLASSIFIED

SECURITY CLASSIFICATION OF THIS PAGE (When Data Entered)

MASTER COPY

REPORT DOCUMENTATION PAGE		READ INSTRUCTIONS BEFORE COMPLETING FORM
1. REPORT NUMBER AFOSR - TR- 77-0163	2. GOVT ACCESSION NO.	3. RECIPIENT'S CATALOG NUMBER
4. TITLE (and Subtitle) OPTICAL PHENOMENA IN INFRARED MATERIALS		5. TYPE OF REPORT & PERIOD COVERED INTERIM 6. PERFORMING ORG. REPORT NUMBER
7. AUTHOR(s)		8. CONTRACT OR GRANT NUMBER(s) AFOSR 76-3061
9. PERFORMING ORGANIZATION NAME AND ADDRESS Optical Society of America 2000 L Street N. W. Washington DC		10. PROGRAM ELEMENT, PROJECT, TASK AREA & WORK UNIT NUMBERS 9763-02 61102F
11. CONTROLLING OFFICE NAME AND ADDRESS AFOSR/NE Bldg 410 Bolling AFB, DC 20332		12. REPORT DATE 1976 13. NUMBER OF PAGES 206
14. MONITORING AGENCY NAME & ADDRESS(if different from Controlling Office)		15. SECURITY CLASS. (of this report) UNCLASSIFIED 15a. DECLASSIFICATION/DOWNGRADING SCHEDULE

16. DISTRIBUTION STATEMENT (of this Report)

Approved for public release; distribution unlimited

17. DISTRIBUTION STATEMENT (of the abstract entered in Block 20, if different from Report)

18. SUPPLEMENTARY NOTES

Proceedings of topical meeting Dec 1-3 1976 Annapolis Maryland p1-206

19. KEY WORDS (Continue on reverse side if necessary and identify by block number)

20. ABSTRACT (Continue on reverse side if necessary and identify by block number)

A digest of technical papers presented at topical meeting on Optical Phenomena in Infrared Materials

DD FORM 1 JAN 73 1473 EDITION OF 1 NOV 65 IS OBSOLETE

UNCLASSIFIED

SECURITY CLASSIFICATION OF THIS PAGE (When Data Entered)

OPTICAL PHENOMENA IN INFRARED MATERIALS.

A digest of technical papers presented at the topical meeting on
Optical Phenomena in Infrared Materials
December 1-3, 1976, Annapolis, Maryland

(9) Technical digest.

(11) 1976 (12) 188p. (15) AF-AFOSR-3061-76

(16) 9763 (17) $2

(18) AFOSR

(19) TR-77-0163

Sponsored by:
Optical Society of America,
2000 L Street, N. W.
Washington, D. C. 20036

and supported in part by:
Air Force Office of Scientific Research
Air Force Systems Command, USAF
Grant No. AFOSR-76-3061 as a portion of
the research program in Electronic
Technology at Rome Air Development Center

1473 S/C

392813

AB

WEDNESDAY, December 1, 1976

WASHINGTON NORTH

9:00 A.M. INTRODUCTORY REMARKS
B. Bendow and S.S. Mitra

9:15 A.M. SOLAR ENERGY I
J. J. Loferski, Presider

WA1 Invited Paper: OPTICAL PROPERTIES OF SOLIDS RELEVANT TO PHOTOTHERMAL SOLAR ENERGY, A. S. Barker, Jr., Bell Laboratories.

WA2 SILICON FILMS AS SELECTIVE ABSORBERS FOR SOLAR ENERGY CONVERSION, D. E. Ackley and J. Tauc, Brown University.

WA3 NORMAL SPECTRAL REFLECTANCE AND THE NORMAL SPECTRAL EMITTANCE OF THE METAL COATED GLASS CERAMICS, S. Tanemura and T. Noguchi, Solar Research Laboratory, Nagoya, Japan; and, K. Hirose, K. Yamada, and Y. Takenaka, Ishizuka Glass Ltd.

WA4 SELECTIVE ABSORPTION OF TUNGSTEN LAYER FABRICATED BY C.V.D. METHOD, S. Tanemura and T. Noguchi, Solar Research Laboratory, Nagoya, Japan; and, S. Umezu and T. Yoshiwa, Toho Metal Ltd.

10:55 A.M. SOLAR ENERGY II
D. M. Mattox, Presider

WB1 TOTAL HEMISPHERICAL EMISSIVITIES OF COPPER, ALUMINUM, AND SILVER, K. G. Ramanathan, San Ho Yen, and Edward Estalote, University of New Orleans.

WB2 INFRARED SPECTRAL EMITTANCE PROFILES OF SPECTRALLY SELECTIVE SOLAR ABSORBING LAYERS AT ELEVATED TEMPERATURES, D. E. Soule and D. W. Smith, Western Illinois University.

WB3 INFRARED, HEMISPHERICAL REFLECTOMETER FOR CHARACTERIZING SELECTIVE SURFACES FOR SOLAR THERMAL ENERGY CONVERSION, Keith D. Masterson, University of Arizona.

WB4 STRUCTURAL COMPOSITION AND OPTICAL PROPERTIES OF GOOD SOLAR BLACKS: GOLD BLACK, P. O'Neill, C. Doland and A. Ignatiev, University of Houston.

WB5 OPTICAL COATINGS FOR SOLAR HEATING AND COOLING, H. Y. B. Mar, R. E. Peterson, and J. H. Lin, Honeywell, Inc.

LUNCH

WEDNESDAY, December 1, 1976

WASHINGTON NORTH

2:00 P.M. MEASUREMENT TECHNIQUES I
L. Skolnik, Presider

WC1 Invited Paper: RECENT ADVANCES IN MEASUREMENT TECHNIQUES FOR SMALL ABSORPTION COEFFICIENTS, A. Hordvik, Rome Air Development Center.

WC2 PHOTOACOUSTIC SPECTROSCOPY: A MEASUREMENT TECHNIQUE FOR LOW ABSORPTION COEFFICIENTS, H. S. Bennett and R. A. Forman, National Bureau of Standards.

WC3 ANALYSIS OF LASER CALORIMETRIC DATA, H. B. Rosenstock and M. Hass, Naval Research Laboratory, and D. A. Gregory and J. A. Harrington, University of Alabama.

WC4 NEW THECHNIQUE FOR MEASURING THE INFRARED ABSORPTION IN THIN FILM COATINGS, James A. Harrington, Morris Braunstein, and J. Earl Rudisill, Hughes Research Laboratories.

3:40 P.M. MEASUREMENT TECHNIQUES II
G. Birnbaum, Presider

WD1 PARALLELICITY CRITERION FOR SAMPLES TO BE STUDIED USING FABRY PEROT INTERFERENCES, Raoul Well and Dalia Neshmit, Israel Institute of Technology.

WD2 10.6 μm ELLIPSOMETER MEASUREMENTS OF REFRACTIVE INDICES OF IR MATERIALS, M. E. Pedinoff and M. Braunstein, Hughes Research Laboratories, and O. M. Staffsud, University of California, Los Angeles.

WD3 A BRDF MEASURING INSTRUMENT, F. O. Bartell, A. G. DeBell, D. S. Goodman, J. E. Harvey, and W. L. Wolfe, University of Arizona.

WD4 TOPOGRAPHICAL INVESTIGATION OF THE VARIATIONS IN STOICHIOMETRY IN $Hg_{1-x}Cd_xTe$ USING ELECTROLYTE ELECTROREFLECTANCE, P. E. Vanier, Fred H. Poll Pollak, and Paul M. Raccah, Yeshiva University.

WD5 INFRARED TECHNIQUE FOR OBSERVATION OF SUPERCOOLING, Edward M. Alexander, Naval Research Laboratory.

WASHINGTON CENTER

2:00 P.M. THIN FILMS I
E. Burstein, Presider

WE1 Invited Paper: INFRARED PROPERTIES OF THIN FILMS, F. Abèles, Laboratoire d'Optique des Solides.

WE2 RETROREFLECTANCE MEASUREMENTS OF PHOTOMETRIC STANDARDS AND COATINGS - II, W. G. Egan and T. Hilgeman, Grumman Aerospace Corporation.

WE3 STUDY OF OPTICAL TRANSITIONS IN DISORDERED THIN FILMS OF IONIC COMPOUNDS AS A FUNCTION OF CONDITIONS OF PREPARATION, A. Barrière and A. Lachter, Université de Bordeaux.

WE4 INFRARED IMPURITY AND FREE-CARRIER ABSORPTION IN SILICON-SILVER FILMS, S. O. Sari, P. Hollingsworth, and H. S. Gurev, University of Arizona.

3:40 P.M. THIN FILMS II
F. Abèles, Presider

WF1 Invited Paper: SURFACE, GUIDED, AND INTERFERENCE EM-WAVES IN ATTENUATED INTERNAL REFLECTION (AIR) PRISM SPECTROSCOPY, A. Hjortsberg, W. P. Chen, and E. Burstein, University of Pennsylvania.

WF2 EVALUATION OF THIN FILM COATINGS BY ATTENUATED TOTAL REFLECTION, R. T. Holm, E. D. Palik, and J. W. Gibson, Naval Research Laboratory, and M. Braunstein and B. Garcia, Hughes Research Laboratory.

WF3 TEMPERATURE DEPENDENCE OF THIN FILM POLARIZER, D. W. Ricks, S. Seitel, and E. A. Teppo, Naval Weapons Center.

WF4 INFRARED LIGHT SCATTERING FROM SURFACES COVERED WITH MULTIPLE DIELECTRIC OVERLAYERS, J. M. Elson, Naval Weapons Center.

THURSDAY, December 2, 1976

WASHINGTON NORTH

9:00 A.M. LASER WINDOWS I
Harry Winsor, Presider

ThA1 Invited Paper: RESIDUAL ABSORPTION IN INFRARED MATERIALS, M. Hass, Naval Research Laboratory; and, B. Bendow, Rome Air Development Center.

ThA2 MECHANISMS FOR PRODUCING LATTICE ABSORPTION: ONE OR TWO? Herbert B. Rosenstock, Naval Research Laboratory.

ThA3 TEMPERATURE DEPENDENCE OF MULTI-PHONON ABSORPTION IN ZINC SELENIDE, P. A. Miles, Raytheon.

ThA4 IMPURITY ABSORPTION IN CVD ZnSe, Herbert G. Lipson, Rome Air Development Center.

10:25 A.M. LASER WINDOWS II
D. Stierwalt, Presider

ThB1 INFRARED ABSORPTION IN GERMANIUM AND SILICON, Don A Gregory and James A. Harrington, University of Alabama; and, Marvin Hass, Naval Research Laboratory.

ThB2 FREQUENCY AND TEMPERATURE DEPENDENCE OF RESIDUAL LATTICE ABSORPTION IN SEMI-CONDUCTING CRYSTALS, Bernard Bendow and Herbert G. Lipson, Rome Air Development Center; and, Stanford P. Yukon, Parke Mathematical Laboratories.

ThB3 BULK AND SURFACE CALORIMETRIC MEASUREMENTS AT CO WAVELENGTHS, S. D. Allen and J. E. Rudisill, Hughes Research Laboratories.

ThB4 SURFACE AND BULK ABSORPTION IN HF/DF LASER WINDOW MATERIALS, A. Hordvik and L. Skolnik, Rome Air Development Center.

ThB5 MIXED FLUORIDES FOR MID-IR LASER WINDOWS, J. J. Martin, Oklahoma State University; and, Herbert G. Lipson, Bernard Bendow, and Audun Hordvik, Rome Air Development Center; and, Shashanka S. Mitra, University of Rhode Island.

WASHINGTON CENTER

9:00 A.M. INFRARED DETECTION
H. Levinstein, Presider

ThC1 Invited Paper: FAR-IR PHOTOCONDUCTIVITY IN SILICON DOPED WITH SHALLOW DONOR IMPURITIES, P. Norton, Bell Laboratories, Murray Hill.

ThC2 MERCURY CADMIUM SELENIDE INFRARED DETECTOR MATERIALS, C. J. Summers, D. A. Nelson, and C. R. Whitsett, McDonnell Douglas Corporation.

ThC3 THALLIUM SELENIDE INFRARED DETECTOR, P. S. Nayar and W. O. Hamilton, Louisiana State University.

ThC4 STRUCTURAL AND IR PROPERTIES OF $Pb_{1-x}Hg_xS$ THIN FILMS, N. C. Sharma, D. K. Pandya, H. K. Sehgal, and K. L. Chopra, Indian Institute of Technology.

10:25 A.M. REFLECTANCE AND SCATTERING
J. Howard, Presider

ThD1 Invited Paper: LIGHT SCATTERING FROM SURFACES OF INFRARED OPTICAL COMPONENTS, H. E. Bennett, J. M. Bennett, J. M. Elson, and D. L. Decker, Naval Weapons Center.

ThD2 SURFACE EVALUATION TECHNIQUES AND SURFACE STATISTICS FOR INFRARED OPTICAL MATERIALS, Jean M. Bennett, Naval Weapons Center.

ThD3 SCATTERING PROPERTIES OF OPTICAL SURFACES AND BAFFLE MATERIALS FOR INFRARED SYSTEMS, J. E. Harvey, J. A. Gunderson, R. V. Shack, and W. L. Wolfe, University of Arizona.

ThD4 RELATIONSHIP BETWEEN SURFACE SCATTERING AND MICROTOPOGRAPHIC FEATURES, E. L. Church, H. A. Jenkinson, and J. M. Zavada, Frankford Arsenal

ThD5 INFRARED OPTICAL REFLECTIVITY OF LIQUID METALS, Edward Siegel, Public Service Electric and Gas Company, Maplewood, NJ.

LUNCH

THURSDAY, December 2, 1976

WASHINGTON NORTH

2:00 P.M. LASER WINDOWS AND DAMAGE I
A. Gunther, Presider

ThE1 SURFACE CHEMISTRY AND ABSORPTION OF CaF_2 AND SrF_2 AT DF AND CO WAVELENGTHS, P. Kraatz and S. J. Holmes, Northrop Corporation.

ThE2 RESIDUAL ABSORPTION IN HF AND DF LASER WINDOW MATERIALS FROM CONTAMINATION BY CARBONACEOUS AND OTHER IMPURITIES, Philip H. Klein, Naval Research Laboratory.

ThE3 REFRACTIVE PROPERTIES OF INFRARED LASER WINDOW MATERIALS, Marilyn Dodge, National Bureau of Standards.

ThE4 PHOTOELASTIC CONSTANTS OF POTASSIUM CHLORIDE AT 10.6 μm, Albert Feldman, Deane Horowitz, and Roy M. Waxler, National Bureau of Standards.

ThE5 ABSORBING PRECIPITATES IN CADMIUM TELLURIDE: ESTIMATES FOR CATASTROPHIC LASER DAMAGE THRESHOLDS, Herbert S. Bennett, National Bureau of Standards; and, Cyrus D. Cantrell, Los Alamos Scientific Laboratory.

3:45 P.M. LASER WINDOWS AND DAMAGE II
A. Gunther, Presider

ThF1 Invited Paper: PULSE LASER DAMAGE IN INFRARED MATERIALS, Michael Bass, University of Southern California.

ThF2 IRREVERSIBLE LASER DAMAGE IN IR DETECTOR MATERIALS, F. Bartoli, L. Esterowitz, M. Kruer, and R. Allen, Naval Research Laboratory.

4:20 P.M. GLASSES
J. Tauc, Presider

ThG1 Invited Paper: INFRARED STUDY OF ANOMALOUS EXCITATIONS IN GLASSES, A. J. Sievers, Cornell University.

ThG2 MULTIPHONON ABSORPTION IN MIXED As_2S_3-GeS_4 GLASSES, D. S. Ma, P. S. Danielson, C. T. Moynihan, and P. B. Macedo, Catholic University of America.

ThG3 ASSESSMENT OF Ge-As-Se 8-12 μm INFRARED OPTICAL GLASSES FOR APPLICATIONS IN THERMAL IMAGING SYSTEMS, A. N. Pitt, Jr., J. A. Savage, and P. J. Webber, Royal Signals and Radar Establishment, Malvern, England.

WASHINGTON CENTER

2:00 P.M. FUNDAMENTAL INFRARED PROPERTIES

ThH1 TEMPERATURE DERIVATIVE OF THE REFRACTIVE INDEX OF DIAMOND, John Fontanella and Richard Johnston, US Naval Academy; and, Carl Andeen, Case Western Reserve University.

ThH2 ANALYSIS OF INFRARED REFLECTIVITY IN THE PRESENCE OF ASYMMETRICAL PHONON LINE, F. Gervais and J. L. Servoin, C. N. R. S.

ThH3 FIR EMISSION FROM n-TYPE $Hg_{.8}Cd_{.2}Te$ IN ELECTRIC FIELDS, G. Nimtz and E. Tyssen, Universität zu Köln.

ThH4 INFRARED PROPERTIES OF STOICHIOMETRIC AND NON-STOICHIOMETRIC RUTILE TiO_2, F. Gervais and J. F. Baumard, C. N. R. S.

ThH5 MAGNETOREFLECTION STUDIES OF $Hg_{1-x}Cd_xTe$ ALLOYS, M. H. Weiler, R. L. Aggarwal, and B. Lax, Massachusetts Institute of Technology.

3:45 P.M. POST-DEADLINE PAPERS

FRIDAY, December 3, 1976

WASHINGTON NORTH

9:00 A.M. NONLINEAR AND INTEGRATED OPTICS I
B. Lax, Presider

FA1 Invited Paper: HIGH ENERGY $LiNbO_3$ TUNABLE SOURCE, R. L. Byer and R. L. Herbst, Stanford University; and, H. Ito, Tohoku University.

FA2 PHONON INDUCED TRANSPARENCY OF TELLURIUM NEAR 11 μm WAVELENGTH, K. -H. Müller and G. Nimtz, Universität zu Köln.

FA3 EFFICIENT NEAR INFRARED STIMULATED RAMAN SCATTERING IN GLASS FIBER WAVEGUIDES, Chinlon Lin, R. H. Stolen, L. G. Cohen, G. W. Tasker, and W. G. French, Bell Laboratories, Holmdel and Murray Hill.

FA4 INFRARED GENERATION BY NONLINEAR 4-PHOTON MIXING IN GERMANIUM, N. Lee, R. L. Aggarwal, and B. Lax, Massachusetts Institute of Technology.

COFFEE

10:25 A.M. NONLINEAR AND INTEGRATED OPTICS II

FB1 Invited Paper: SECOND AND FOURTH ORDER NONLINEAR PROCESSES IN CHALCOPYRITES, H. Kildal, G. W. Iseler, N. Manyuk, and J. C. Mikkelsen, Massachusetts Institute of Technology.

FB2 STUDY OF THIN FILMS USING LEAKY SURFACE EM (SEM) AND INTERFERENCE EM (IEM) WAVES IN THE INFRARED, W. P. Chen, A. Hjortsberg, and E. Burstein, UNiversity of Pennsylvania.

FB3 OPTICAL CONSTANTS OF THE ACCUMULATION LAYER IN SILICON MOS STRUCTURES, H. C. Chien and G. Sadasiv, University of Rhode Island.

FB4 Invited Paper: SEMI-CONDUCTOR BASED INFRARED INTEGRATED OPTICS, I. Melngailis, Massachusetts Institute of Technology.

OPTICAL PROPERTIES OF SOLIDS RELEVANT TO PHOTOTHERMAL SOLAR ENERGY

by

A. S. Barker, Jr.
Bell Laboratories, Murray Hill, NJ 07974

A study of the process of absorbing the sun's energy and converting it to useful heat to provide space heating or to operate air conditioning machinery shows that one requires more than the simple hothouse effect or the use of ordinary black paint. In this talk we examine the notion of an ideal photothermal absorber and describe the need for a different type of absorption and emission characteristic, depending on the operating temperature of the surface. Optical processes of bulk materials, such as interband transitions and free carrier absorption in metals and in semiconductors are examined and compared with the ideal absorber. The constraints on any material due to the Kramers-Kronig relations are also presented. Recent work of several groups trying to create a near ideal absorption characteristic using multilayer films or composite media is assessed and compared with the Tabor selective surface. Studies of the motion of defects, vacancies and host-ions have shown the importance of considering stability and degradation in potential candidates for solar absorbers. Finally, some comments are made about the need for flat plate collectors whose cost is less than $5

per square foot in the context of the energy crisis and national fuel reserves.

SILICON FILMS AS SELECTIVE ABSORBERS FOR SOLAR ENERGY CONVERSION

D. E. Ackley and J. Tauc
Division of Engineering and Department of Physics
Brown University, Providence, Rhode Island 02912 USA

Introduction

In some photothermal solar energy conversion systems semiconductor films are deposited on highly reflecting metals to form absorber-reflector tandems that absorb the solar energy and reduce the thermal radiation from the system.[1] Silicon has been proposed as a suitable material for this application. We determined the optical contents below the absorption edge (to 4 μm) at high temperatures (up to 800°C) of crystalline silicon (c-Si) and amorphous silicon films (a-Si), and calculated the efficiencies of c-Si (or a-Si) - metal selective absorbers.

Experimental

Crystalline Si samples were cut from an ultrahigh purity ($\rho \approx 4 \times 10^4$ ohm cm) Si single crystal. Amorphous films were prepared by rf. sputtering onto sapphire substrates in a high purity Ar atmosphere at 5×10^{-3} Torr; deposition rate was 1.7 Å/sec and the thicknesses ranged from 7.5 to 8.5 μm. Annealing at 500°C for 5 hours shifted the absorption edge to significantly higher energies but subsequent heating up to 800°C had little effect. The samples were very stable against crystallization and remained amorphous even after extended exposure to 800°C.

For the high temperature measurements we used an equipment designed by De Fonzo[2]. For the calculation of the optical constants, we assumed a temperature and wavelength independent index of refraction; an approximate method based on fringe averaging was used.

Absorption constants

The absorption coefficients are shown in Fig. 1. We represent their temperature and wavelength dependences as follows:

c-Si:
$$\alpha = \alpha_{edge} + \alpha_{car} \qquad (1)$$

where the edge absorption

$$\alpha_{edge} = 4 \times 10^3 (\hbar\omega - E_g(T))^2 / \hbar\omega \qquad (cm^{-1}) \qquad (2)$$

$$E_g(T = 300K) = 1.12 \text{ eV} \ , \ dE_g/dT = 5 \times 10^{-4} \text{ eV/degree for } T > 300K.$$

The parameters were determined from Ref. 3.

The free carrier contribution was shown[4] to be approximately:

$$\alpha_{cm} = 5 \times 10^{-17} \, n_i(T)(T/873)(0.37/\hbar\omega)^{1.5} \quad (cm^{-1}) \tag{3}$$

T is in K, $\hbar\omega$ in eV , $n_i(T)$ is the intrinsic carrier concentration (cm^{-3}).

a-Si: It was shown[4] that in our samples at high temperatures the low energy tail of the absorption is determined by transitions involving a density of states tail with an exponential energy dependence:

$$\hbar\omega\alpha = A(T) \exp(\hbar\omega/E_t)[\exp(-\hbar\omega - E_F)/kT + 1]^{-1} \tag{4}$$

where E_t is the slope of the exponential state distribution, E_F is the Fermi level. The constants $A(T)$, E_t and E_F were determined from fits to the experimental data[4].

As seen in Fig. 1, the main difference between c-Si and a-Si is the lack of free-carrier absorption in a-Si. We are presently checking this point by measurements out to 6 μm. Our preliminary data appears to be consistent with a much smaller free carrier absorption in a-Si than in c-Si.

Photothermal efficiency

We calculated the efficiency

$$\eta = (E_{abs} - E_{emit})/E_{abs} \tag{5}$$

assuming that the reflectivity at the silicon-metal interface is one, that the reflectivity R of the silicon-air interface is constant in the whole wavelength and temperature range and that the solar energy distribution can be represented by a suitably normalized black body radiation at 6100K. The absorptance of the film is

$$A(\lambda) = \frac{(1-R)[1-\exp(-2\alpha d)]}{1-R\exp(-2\alpha d)} \tag{6}$$

where α is the absorption constant and d is the film thickness. The absorbed and emitted energies are

$$E_{abs} = C \int W(\lambda, T = 6100K) \, A(\lambda, T) d\lambda \tag{7}$$

$$E_{emit} = \int W(\lambda, T) \, A(\lambda, T) d\lambda \tag{8}$$

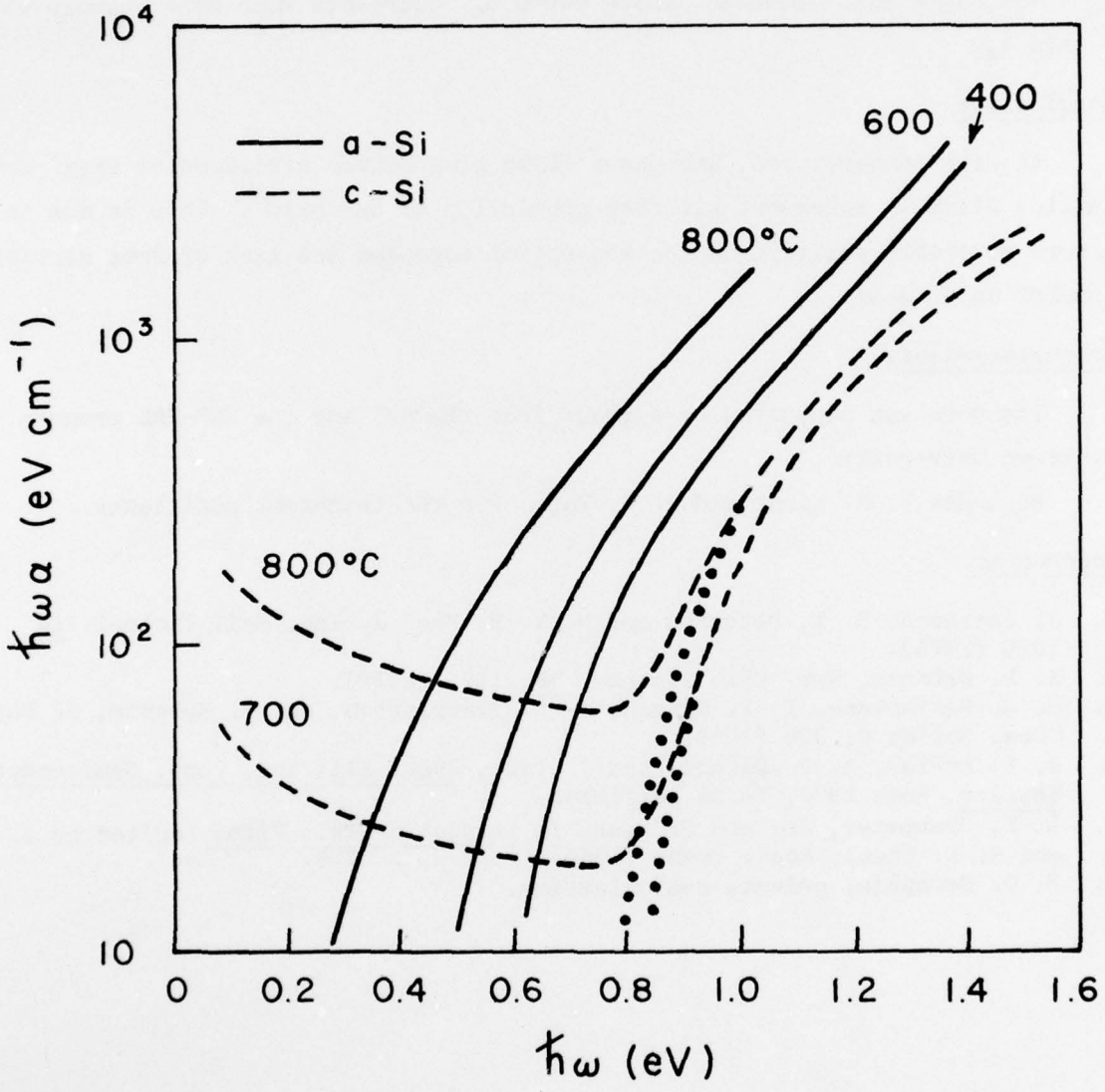

Fig. 1 Absorption in silicon. The dotted line is the absorption edge of c-Si when the free carrier absorption is neglected.

where $C \simeq 1.85 \times 10^{-5}$, $W(\lambda, T)$ is the black body radiation.

We calcuated η for $d = 8.6$ μm and found that at low temperatures there is little difference between efficiencies of a-Si (η_a) and c-Si (η_c): at 400°C $\eta_a = 99\%$, $\eta_c = 95\%$. However, above 400°C η_c decreases much more sharply with T than η_a.

Conclusions

At high temperatures, amorphous films give better efficiencies than crystalline films in agreement with the prediction of Seraphin[6]. This is due to a more favorable position of the absorption edge and the lack of free carrier absorption in a-Si.

Acknowledgements

The work was supported by a grant from the NSF and the NSF-MRL program at Brown University.

We thank T. R. Kirst and J. O. White for the technical assistance.

References

1. J. Jurisson, R. E. Peterson and H. Y. B. Mar, J. Vac. Sci. Technol. 12, 1010 (1975).
2. A. P. DeFonzo, Rev. Sci. Instrum. 46, 1329 (1975).
3. G. G. Macfarlane, T. P. McLean, J. E. Quarrington, and V. Roberts, J. Phys. Chem. Solids 8, 388 (1959).
4. D. E. Ackley, A. P. DeFonzo and J. Tauc, Proc. XIII Int. Conf. Semiconductor Physics, Rome 1976, to be published.
5. L. F. Drummeter, Jr. and G. Hass, in Physics of Thin Films (edited by G. Hass and R. E. Thun), Acad. Press (1964), vol. 2, p. 305.
6. B. O. Seraphin, private communication.

THE NORMAL SPECTRAL REFLECTANCE AND THE NORMAL SPECTRAL EMITTANCE OF THE METAL COATED GLASS CERAMICS

S. Tanemura & T. Noguchi

Solar Research Laboratory
Government Industrial Research Institute, Nagoya, Japan

and
K. Hirose, K. Yamada & Y. Talemaka

Ishizuka Glass Ltd., Nagoya, Japan

1. Sample Preparation

Glass Ceramics (sample 1) is fabricated by heating of spodumen glass and mineralizer such as ZrO_2, TiO_2 and MgO etc. The sample has an optical flat surface and is opaque.

When a glass ceramics which contains CuO is heat-treated in a reducing atmosphere, metallic copper particles are crystalized on the surface due to the diffusion process of Cu^{++}. Sample 2 and 3 are prepared by this process with the heat-treatment at 980°C for about an hour and at 980°C for about 5 minutes respectively. The SEM image of sample 3 is given in Fig. 1a. The average size of Cu particles observed in sample 2 is about twice as large as that of sample 3. A composite layer with about 10 μm in thickness of glass ceramics and Cu ions is observed under the metallic Cu layer.

After the above mentioned heating processes of sample 2, sample 2 is treated further in an oxidizing gas at over 400°C into sample 4. The X.M.A. analysis shows CuO with about several microns in thickness is coated on metalic Cu particles. The SEM image of this sample is given in Fig. 1b. Sample 4 is again treated in a reducing gas at under 400°C into sample 5, and the surface of which shows Cu_2O film by the X.M.A. analysis.

2. Experiments

The normal spectral reflectance(N.S.R.) of above samples at a room temperature and at about 141 °C in situ were obtained at wavelength range from 0.5 μm to 15.0 μm with an accuracy of about $\pm$ 1.5 %. The normal spectral emittance (N.S.E.) at about 141°C were also obtained at wavelength range from 5.0 μm to 15.0 μm with an accuracy of about $\pm$ 5 %. Both measurements were done alternately by setting the respective auxiliary optical system to the scanning monochrometer without any change

of the sample position in the optical path. The principles of the measurements are based on the double beam optical null method.

3. Results and Discussion

The N.S.R. and N.S.E. data of samples 1, 3, 4, and 5 are given in Fig. 2 to Fig. 5. Those of sample 2 are similar to the data of sample 3 but show the low peak value at 6.8 μm. No significant difference between N.S.R. data at a room temperature and at about 141°C exists, except samples 2 and 3 for which N.S.R. data at wavelength range from 0.5 μm to 1.0 μm at about 141°C give the lower values due to the slight oxidation of the samples.

The N.S.R. data and [1 - N.S.E.] data of sample 1 coincides with each other within experimental errors. For other samples, the coincidence is entirely depend on wavelength.

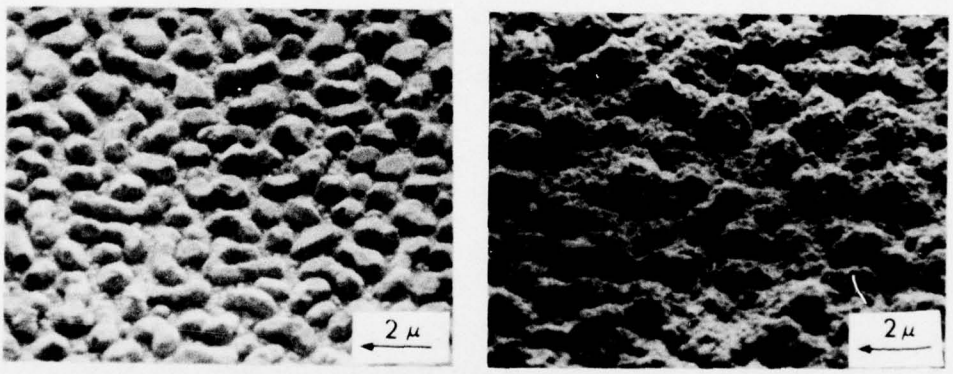

(a) (b)

Fig. 1 a; SEM image of glass ceramics with Cu particles precipitated.

b; SEM image of sample 4. The small cupric oxide crystals formed on individual copper particles coalesced.

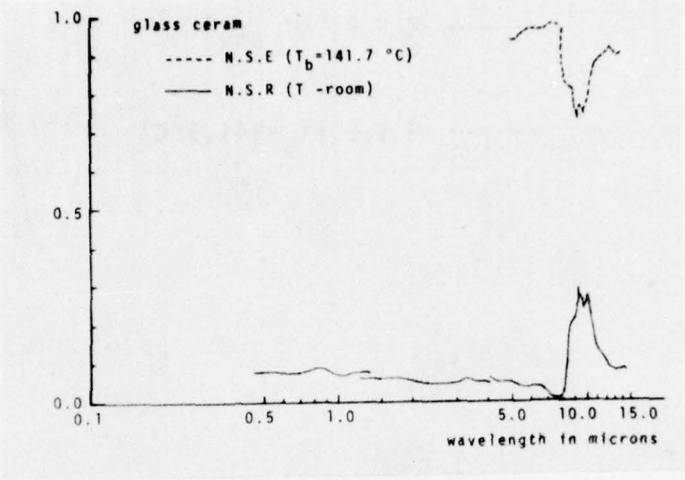

Fig. 2 The spectroscopic data of a glass ceramics.

The discontinuity of N.S.R. data at about 1.5 μm and 4.0 μm is due to the zero level shift of the servo amp. caused by the change of the diffraction gratings.

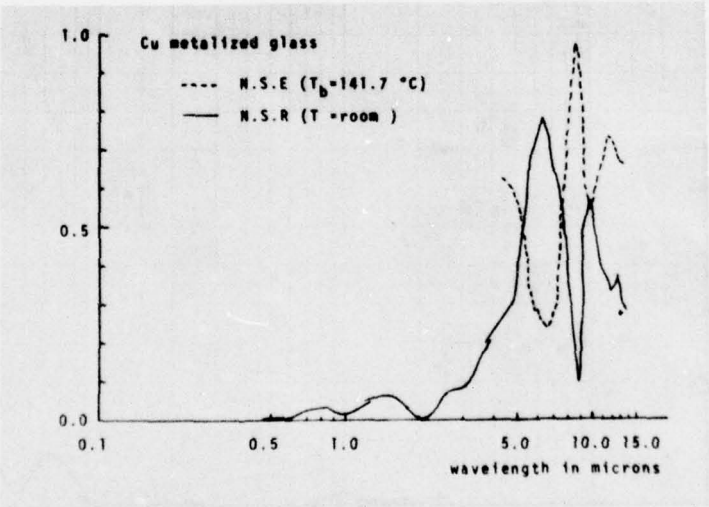

Fig. 3 The spectroscopic data of a metalized glass ceramics.

Strong absorption band at about 8.9 μm is observed.

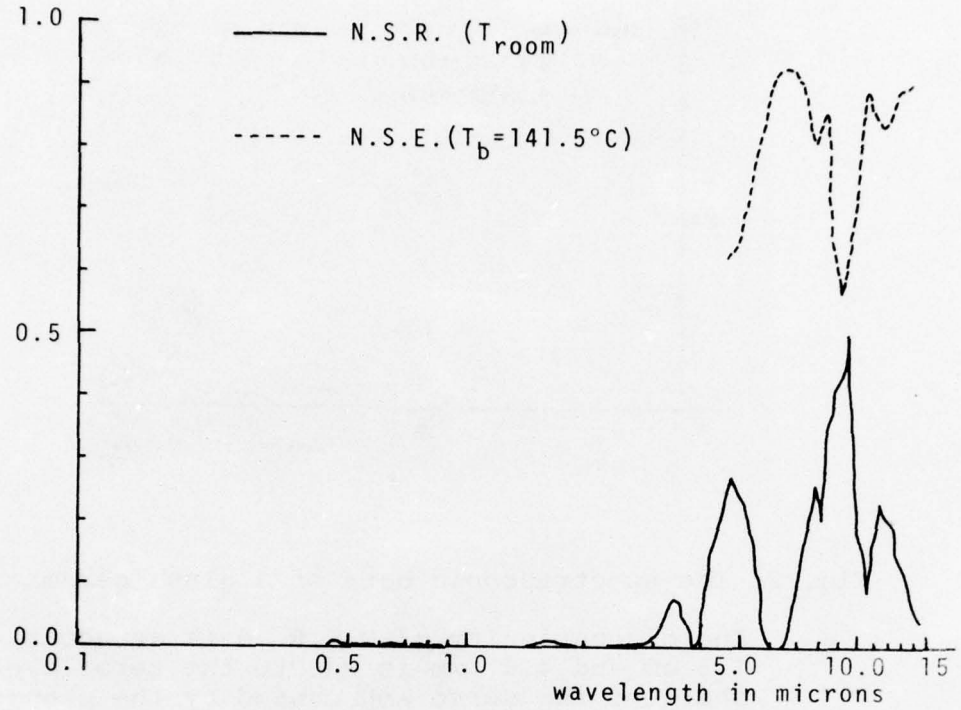

Fig. 4 The spectroscopic data of sample 4.

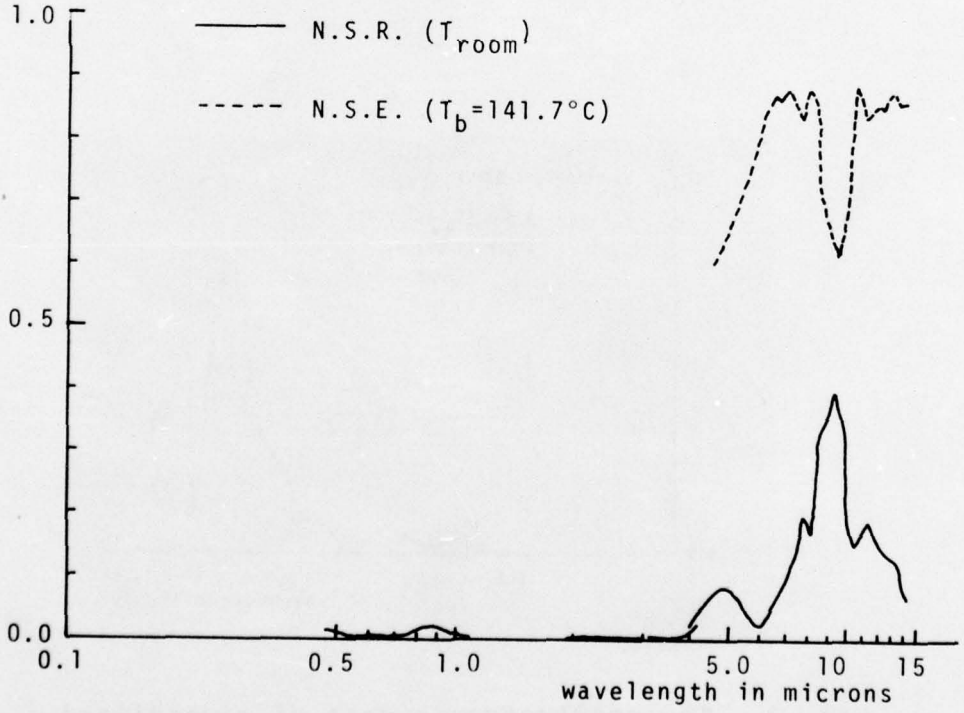

Fig. 5 The spectroscopic data of sample 5.

The peaks and troughs shown at the wavelength range of over 4.0 μm correspond exactly to those appeared in Fig. 4.

WA4-1

SELECTIVE ABSORPTION OF TUNGSTEN LAYER FABRICATED BY C.V.D. METHOD

S. Tanemura & T. Noguchi

Solar Research Laboratory
Government Industrial Research Institute, Nagoya, Japan

and

S. Umezu & T. Yoshiwa

Toho Metal Ltd., Moji Factory, Japan

1. The sample preparation

Tungsten has been vapour-deposited on graphite substrate by means of the hydrogen reduction of tungstenfluoride. The system temperature, the ratio of inlet H_2 gas to $WF_6$and reaction time in the process used were 600°C, 3.0 and 12 minutes respectively. The petrographic microscopy on the cross section of a sample shows that tungsten layer of 30 μm in thickness grew on the substrate. The surface topographs of the sample was shown in Fig. 1 by SEM image.

2. The normal spectral reflectance (N.S.R.) and normal spectral emittance (N.S.E.) measurements.

The new scanning spectrometer of a grating type have been designed for those purposes. The principle of the measurement is based on the double beam optical null method. The scanning wavelength covers from 0.40 μm to 15.0 μm. N.S.R. data of a specimen from room temperatures to 900°C in situ are attainable. The bolck diagram for this system is shown in Fig.2a. A N.S.E. of a specimen from 80°C to 900°C can be obtained by a usual method shown in Fig. 2b schematically. Both measurements can be carried out alternately by setting of the auxiliary optical system of a caset type indicated by the dotted lines in Fig. 2a and 2b respecively.

The temperatures of sample surface and black body furnace were controlled within an accuracy of about $\pm$ 0.5 % at about 140°C respectively. We adjust the black body temperature to sample surface temperature within an accuracy of $\pm$ 1 % in such a way that the heated standard specimen (the sample coated with 3M black paint with about 100 μm in thickness) has N.S.E. value reported by Hall [1] at 100°C. This might reduce the errors of a N.S.E. at the concerned wave length range down to $\pm$ 5 % in the present experiments.

3. Results and Discussion

In Fig. 3, the results for the graphite substrate are given. The N.S.R. obtained at 137.9°C coincides with that at 23°C. This indicats the optical properties of the sample are not affected by the temperature elevation within the present wavelength.

The shape of the N.S.R. curve does not reflect the surface roughness effect which is estimated by the factor $\exp[-\{4\pi\sigma/\lambda\}^2]$ in which roughness σ of about 1.0 μm is given from the surface topograph. The mutual coincidence between the N.S.R. and [1 - N.S.E.] is not satisfactory. The facts require the discussion of more precise geometry of the surface.

Tungsten layer contains no other metalic elements and only the surface layer with about 100 Å contains the WO_3 according to ESCA and Auger analysis. This WO_3 might reduce the N.S.R. in rather shorter wavelength range.

[1] W. Hall ; Thermal radiative properties Vol. 9 ed.Y.S. Toulkian et al, p536, Plenum Press, New York (1972)

Fig.1. Surface topograph of tugsten layer.

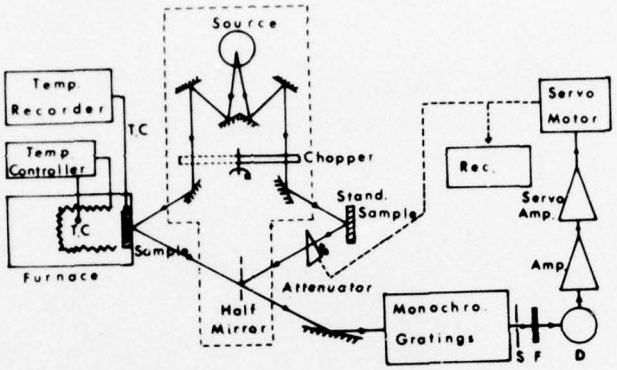

Fig. 2a The block diagram of reflectance measurement.

T.C.; thermocouple, S; slit, F; filter, D; detector of vacuum thermocouple, Amp; pre-amplifier and lcok-in amplifier, and Rec; recorder. Either Al coated or Al coated mirror was used as a standard sample. The incident angle is smaller than 5° in arc.

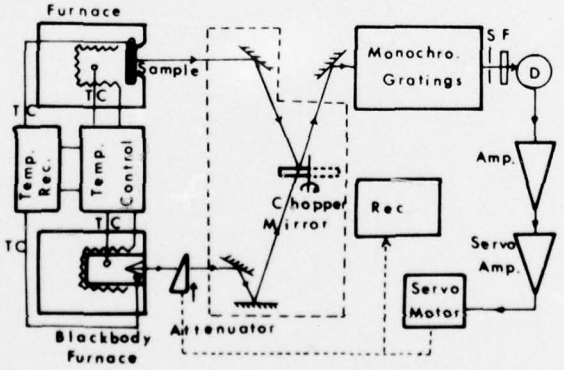

Fig. 2b The block diagram of emittance measurement

Abbreviations used here are explained in Fig. 2a. Precisely, the radiation energy emitted within the solid angle of 8×10^{-3} steradian is focussed on detector.

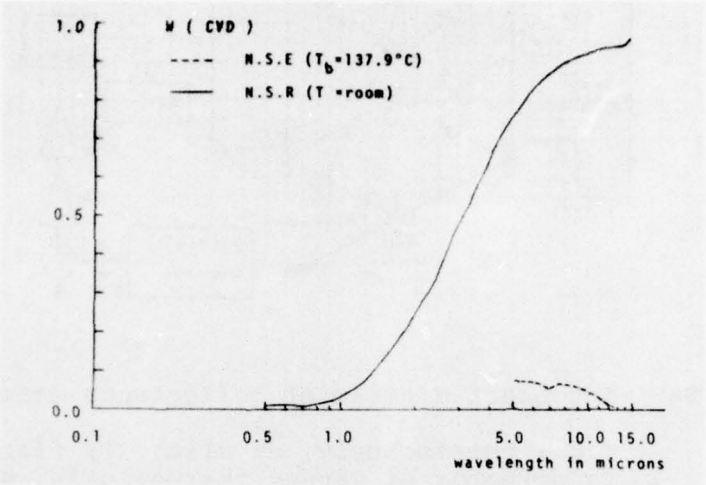

Fig. 3 The spectroscopic curves of the present sample.

NOTES

THE TOTAL HEMISPHERICAL EMISSIVITIES OF COPPER, ALUMINUM AND SILVER.

K.G. Ramanathan, San Ho Yen and Edward A. Estalote

Physics Department, University of New Orleans, New Orleans, La-70122.

By combining Planck's law of blackbody radiation with the Fresnel equations and the equation for the propagation of a plane electromagnetic wave in a non-ferromagnetic, homogenious conducting medium at $T^{o}K$, Davisson and Weeks[1] deduced for the total hemispherical emissivity ε_h, the equation

$$\varepsilon_h = 0.751\ (\rho T)^{\frac{1}{2}} - 0.632\ (\rho T) + 0.670\ (\rho T)^{3/2} - 0.607\ (\rho T),^{2} \qquad (1)$$

where the electrical resistivity $\rho = 1/\sigma$, is in ohm-cm. In Eq. (1), ohm's law $J = \sigma E$, for the current density in the metal, is assumed to be a point relation so that the absorption of energy from an incident electromagnetic field and its dissipation as heat in the conductor are assumed to be continuous processes. More recently, Parker and Abbott[2] modified this theory by taking into account the finite, non-zero relaxation time τ, of the conduction electrons in the metal and arrived at a general expression for ε_h, which is strongly dependent on a certain parameter $\underline{a} = 1.31 \times 10^{11}\ \tau T$, introduced into their theory. The particular values of ε_h for five different values of $\underline{a}$ are presented here.

For $\underline{a}$=0.0, $\varepsilon_h = 0.766\ (\rho T)^{\frac{1}{2}} - (0.309-0.0889 \log \rho T)\ \rho T - 0.0175(\rho T)^{3/2}$ (2a)

For $\underline{a}$=0.2, $\varepsilon_h = 0.534\ (\rho T)^{\frac{1}{2}} - (0.218-0.0411 \log \rho T)\ \rho T + 0.0141(\rho T)^{3/2}$ (2b)

For $\underline{a}$=0.5, $\varepsilon_h = 0.384\ (\rho T)^{\frac{1}{2}} - (0.172-0.0208 \log \rho T)\ \rho T + 0.0306(\rho T)^{3/2}$ (2c)

Foe $\underline{a}$=1.0, $\varepsilon_h = 0.281\ (\rho T)^{\frac{1}{2}} - (0.153-0.0109 \log \rho T)\ \rho T + 0.0461(\rho T)^{3/2}$ (2d)

For $\underline{a}$=1.5, $\varepsilon_h = 0.232\ (\rho T)^{\frac{1}{2}} - (0.148-0.0076 \log \rho T)\ \rho T + 0.0570(\rho T)^{3/2}$ (2e)

The experimental results of Parker and Abbott for the transition metals Nb, Mo, W and Ta were claimed by them to be in qualitative agreement with Eq. 1 and with Eq. 2a which correspond to τ=0, though their Eqs. 2 b, c, d and e corresponding to $\tau > 0$, predict lower values of ε_h.

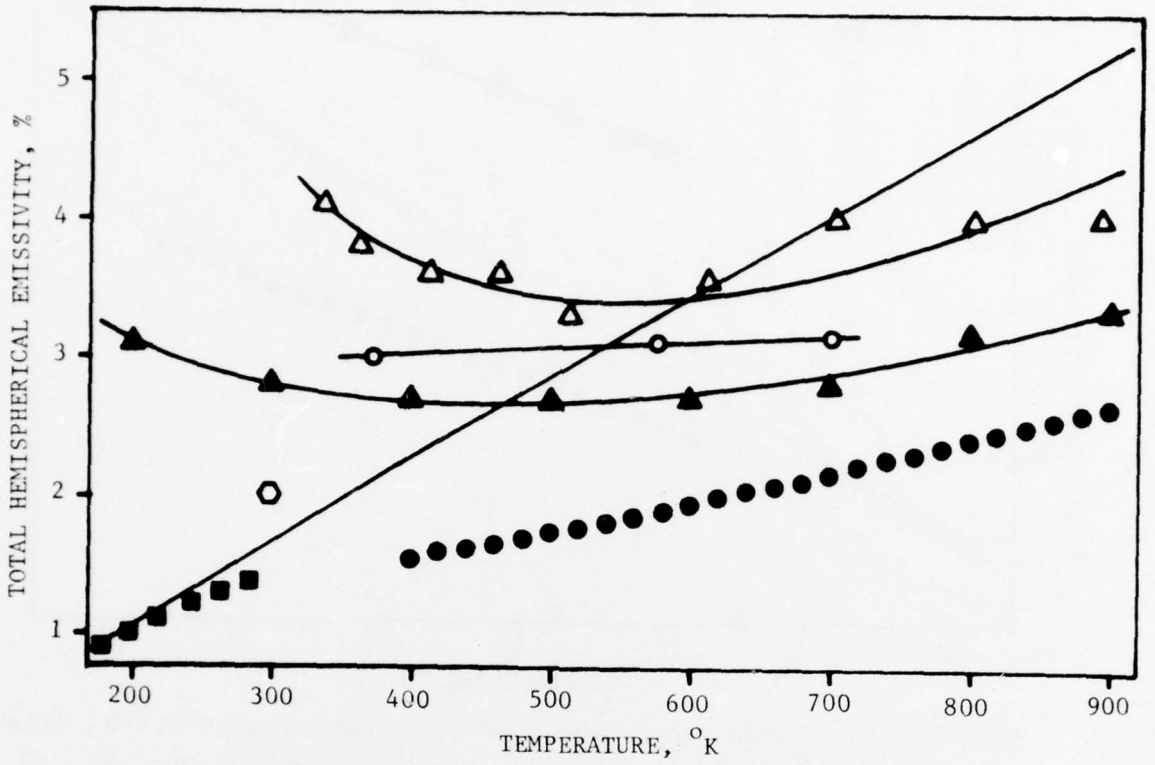

Fig. 1. ε_h vs T data for Copper: ● , Ramanathan and Yen;[3] ■ , Estalote and Ramanathan;[4] ——— , Davisson and Weeks,[1] Eq.1; —○— , —▲— , —△— and ⬡ , data points of previous workers, see Refs. 3 and 4 for details.

Presumably due to improper surface conditions and/or due to large unaccounted errors in measurements, the ε_h vs T curves of many of the past investigators are very much higher than those predicted by Eq. 1. This disparity between theory and experiment and the serious discord which exists among results of past investigators for any one metal, led the present writers[3,4] to carry out 5%-accurate measurements of ε_h of polished surfaces of 5N pure Cu, Al and Ag with a transient calorimetric technique. ε_h vs T data for electrolytically polished surfaces of Cu and Al, obtained in the range of 400 to 1100 K with a high temperature apparatus and in the range of 150 to 300 K with a specially designed low temperature apparatus are reproduced in Figs. 1 and 2 respectively. It is seen that our high and low temperature data fit together as well as

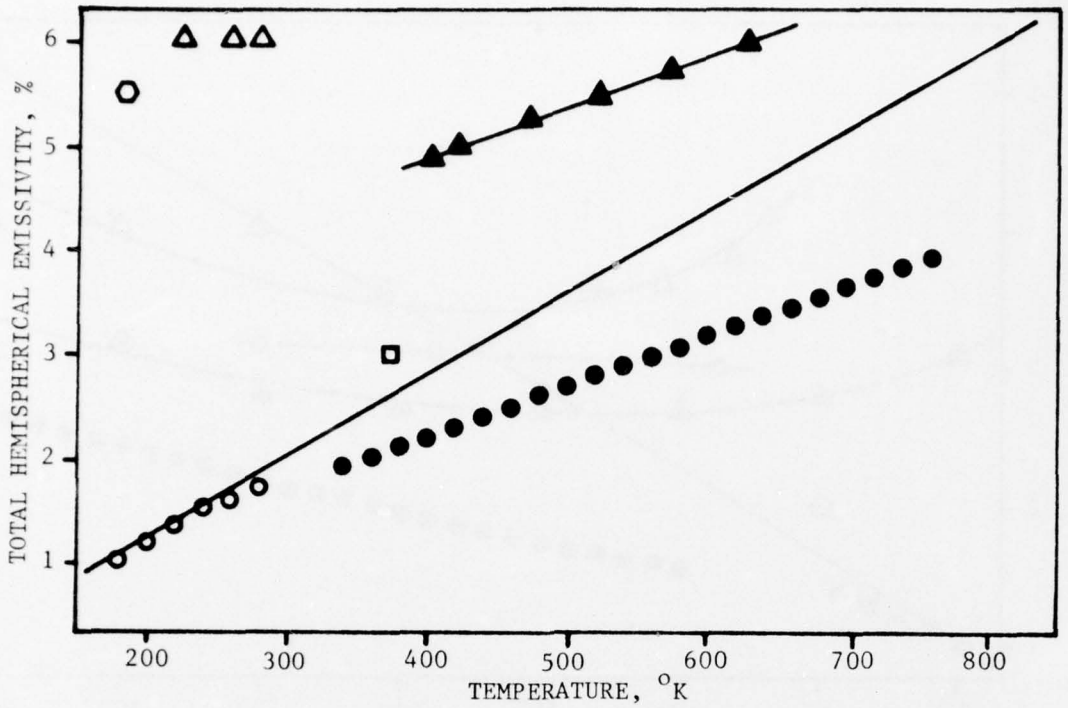

Fig. 2. ε_h vs T data for Aluminum: ● , Ramanathan and Yen;[3] ○ , Estalote and Ramanathan;[4] —— , Davisson and Weeks,[1] Eq. 1; △ , —▲—, □ and ⬡ , data points of past workers, see Refs. 3 and 4 for details.

may be expected. Data obtained for mechanically polished Ag with the high temperature apparatus are shown in Fig. 3. In all three figures our ε_h data are seen to be the lowest ever obtained. Furthermore, our data points at the highest temperatures are seen in all three figures, to be well below the continuous curves representing Eq. 1. However, this disparity is seen to decrease steadily with temperature. Our results for Cu, Al and Ag thus appear to lend support to the relaxation theory of Parker and Abbott.

The τ values calculated from our ε_h vs T data using the set of equations 2, a to e, are of the same order of magnitude as the τ values determined from the dc conductivity of the bulk metals using the relation $\sigma = ne^2\tau/m$, where n is the number density of conduction electrons, e is the electronic charge and m its mass. Therefore, it is believed that a detailed investigation of the

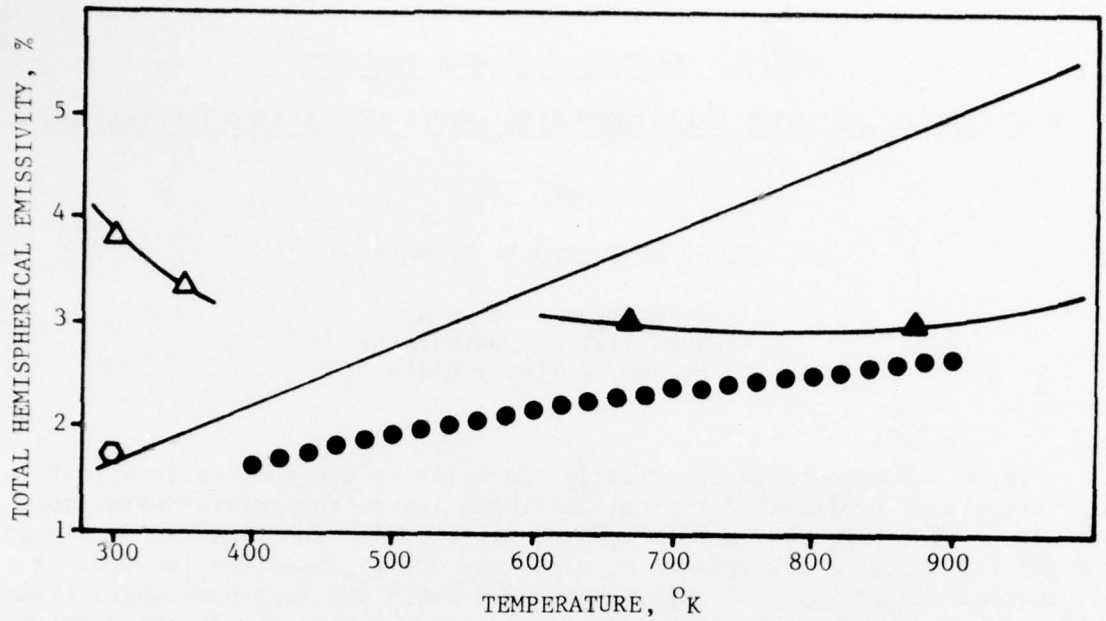

Fig. 3. ε_h vs T data for Silver: ● , Ramanathan and Yen;[3] ——— , Davisson and Weeks,[1] Eq. 1; ⬡ , —△— and —▲— , data points of previous workers, see Ref. 3 for details.

temperature variations of the total hemispherical and spectral emissivities of clean surfaces of very pure metals will be useful in elucidating the theory of the optical properties of good conductors.

REFERENCES

1. C. Davisson and J. R. Weeks, Jr., "The Relation between the Total Thermal Emissive Power of a Metal and Its Electrical Resistivity," J. Opt. Soc. Am. 8, 581-605 (1924).
2. W. J. Parker and G. L. Abbott, "Theoretical and Experimental Studies of the Total Emittance of Metals," Symposium on Thermal Radiation of Solids, edited by S. Katzoff (U.S. Government Printing Office, Washington D. C., NASA SP-55, 1965) pp. 11-28.
3. K. G. Ramanathan and S. H. Yen, "High Temperature Emissivities of Copper, Aluminum and Silver," J. Opt. Soc. Am. (in course of publication).
4. E. A. Estalote and K. G. Ramanathan, "The Low Temperature Emissivities of Copper and Aluminum," J. Opt. Soc. Am. (in course of publication).

INFRARED SPECTRAL EMITTANCE PROFILES OF SPECTRALLY SELECTIVE SOLAR ABSORBING LAYERS AT ELEVATED TEMPERATURES

by

D. E. Soule and D. W. Smith

Department of Physics
Western Illinois University
Macomb, Illinois 61455

A study was made to parametrically characterize the spectrally selective (SS) absorptance profiles of typical absorbing layers for solar-thermal conversion. A five-parameter modified Fermi distribution function was developed[1] to model the spectral absorptance α_λ profile. These parameters include: A the short-wavelength α_λ limit approaching 0.3 μm, B the long-wavelength limit approaching 40 μm, λ_o the half-height α_λ shoulder wavelength, TK the shoulder broadening factor and SK the skew factor. This model was applied to SS layers of several types:[2] interference multilayers Al-SiO-Al-SiO (ASAS) with the spectral reflectance ρ_λ measured by Hass et al,[3] MgF_2-Mo-CeO_2 (MMC) on Mo by Schmidt and Park[4] and Al_2O_3-Mo-Al_2O_3 (AMA) on Mo by Peterson and Ramsey;[5] an intrinsic bulk absorbing stack SiO_2-Si_3N_4-Si-Cr_2O_3-Ag-Cr_2O_3 (SCA) by Masterson and Seraphin[6,2]; and mixed-type absorbers chromium black (CrBk) on Al by McDonald[7] and nickel black (NiBk) by Streed.[8] Typical fits for α_λ are shown in Fig. 1. In the fitting process, A was adjusted with a weighted fit at the solar peak wavelength S, skewing was performed about λ_o and B, TK and SK were adjusted with a fit in the emission peak wavelength range E for typical solar absorber operating temperatures T_x. As a working measure for the degree of fit, the calculated thermal conversion efficiency predicted for the Fermi model typically agreed with that found for the original spectral data to within 1%.[1]

A major aim in this study was to determine the in situ spectral behavior of an absorbing SS layer in the IR emission range at elevated temperatures. Problems exist in the usual interpretation of the spectral reflectance data for the case of high reflectance, where $\rho_\lambda \to 1$, in converting to the spectral emittance $\varepsilon_\lambda = \alpha_\lambda = 1 - \rho_\lambda$ and in resolving hemispherical averaging.[9] Difficulties arise in measuring ρ_λ at an elevated T_x and in relating to the thermal, structural and environmental history of the SS layer. In addition, α_λ proved to be most sensitive to increasing temperature in the IR portion of the spectral profile for those SS layers studied, as demonstrated in Fig. 2 for SCA and MMC from 25° to about 500°C. Both show an increase in the IR ε_λ with temperature, dominated by the metallic substrate. The difference in the absorption mechanism is also apparent, where for MMC only the B parameter shifts with temperature, while for SCA both B and λ_o vary. Such shifts in the IR ε_λ significantly influence the net conversion efficiency at low and intermediate collector concentrations.

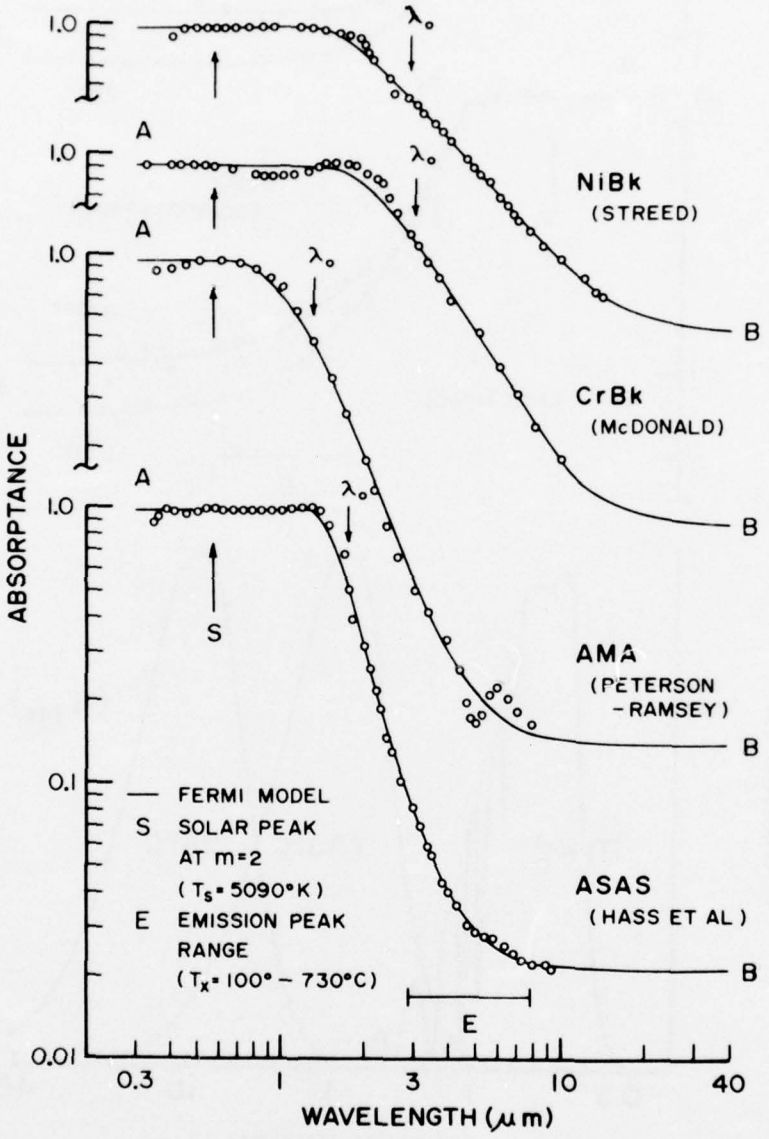

Figure 1. Fermi model fit to spectral absorptance for typical spectrally selective absorbing layers from spectral reflectance room temperature measurements.

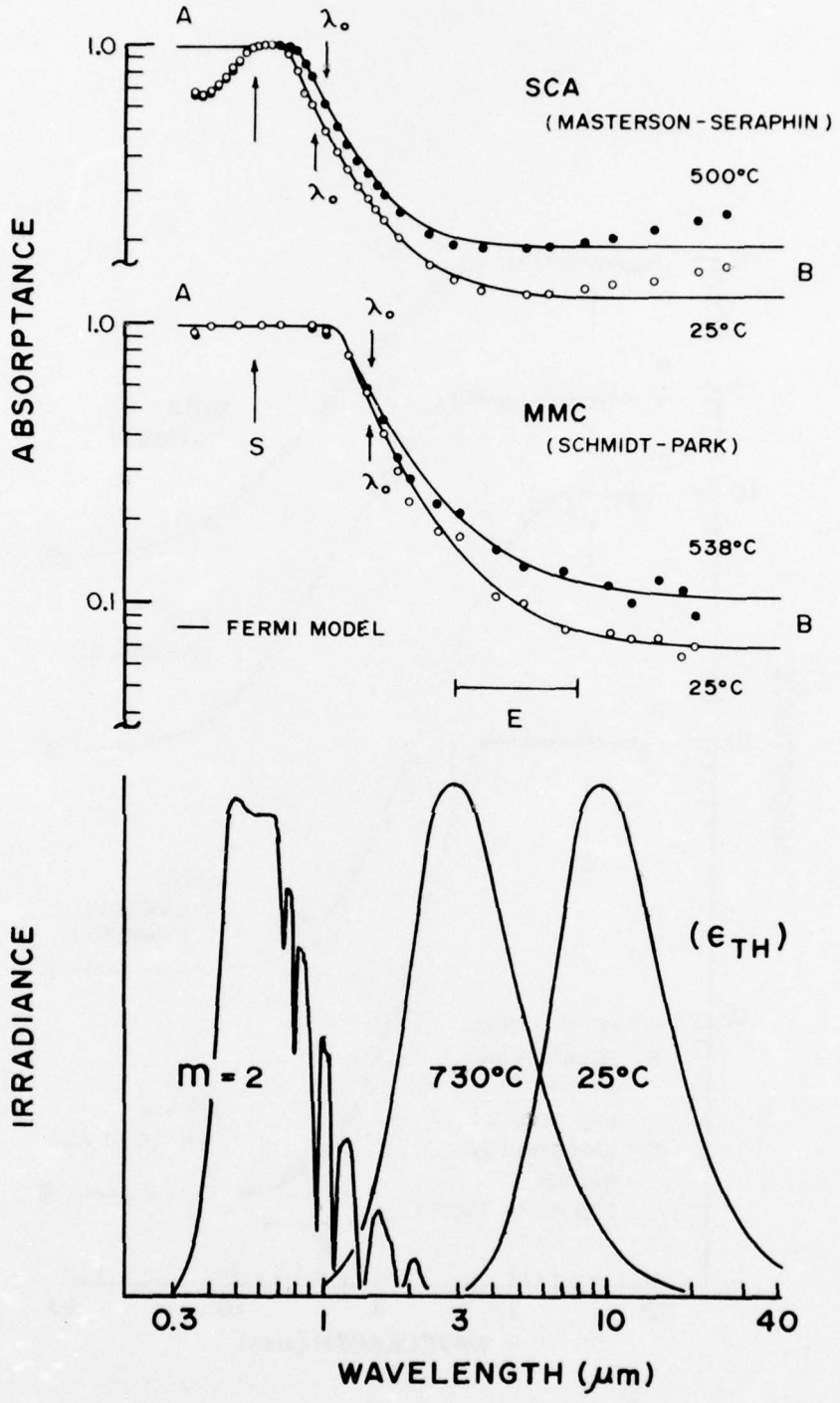

Figure 2. Temperature shift in the spectral absorptance profiles of spectrally selective absorbing layers with weighted fits at S and in E range. Interference fringes smoothed in SCA. Relevant spectral regions are given by the normalized solar spectrum and Planck emission spectra for measured hemispherical total emittance.

An alternative method is presented in this paper for defining the IR spectral absorptance profile. The hemispherical total emittance ε_{TH} was also measured here on the SS layer at T_X. Measurements were made calorimetrically at thermal equilibrium for temperatures up to 730°C. This approach represents more directly the thermal heat transfer extant in a solar conversion system. Figure 2 shows the relative positions of the Planck emission spectra P(T), along with the solar spectrum for air mass 2. Integration was performed for the emissive power loss to the environment at T_O,

$$\frac{C}{4} \int_{1\ \mu m}^{40\ \mu m} \varepsilon_H^* (\lambda, T_X) \left[P(T_X) - P(T_O) \right] d\lambda \ ,$$

where the effective spectral emittance ε_H^* is given by the Fermi model, as extrapolated from its fit in the solar absorption region. Iterative comparison with the measured ε_{TH} provided a thermal basis for scaling ρ_λ in the IR to produce the required ε_λ. The temperature dependence of the spectral emittance and a comparison between spectral profile methods will be discussed.

. . . . . .

1. D. E. Soule, J. H. Schnitzmeyer and W. R. McKie, Proc. Inter. Solar Energy Conf., Winnipeg, Canada, Aug. 15-20, 1976.

2. See B. O. Seraphin and A. B. Meinel, "Photothermal Solar Energy Conversion and the Optical Properties of Solids," Optical Properties of Solids--New Developments, North Holland Pub. (1975).

3. G. Hass, H. H. Schroeder and A. F. Turner, J. Opt. Soc. Am. 46, 31 (1956).

4. R. N. Schmidt and K. C. Park, Applied Optics 4, 917 (1965).

5. R. E. Peterson and J. W. Ramsey, J. Vac. Sci. Tech. 12, 174 (1975).

6. Private communication from K. D. Masterson. See also K. D. Masterson and R. C. Yoder, J. Opt. Soc. Am. 64, 1384 (1974).

7. G. E. McDonald, Solar Energy 17, 119 (1975).

8. E. R. Streed, Proc. Solar Heating and Cooling for Buildings Workshop, March 21-23 (1973) Washington, D.C. NSF/RANN Report, p. 26.

9. See J. P. Millard and E. R. Streed, Applied Optics 8, 1485 (1969).

AN INFRARED, HEMISPHERICAL REFLECTOMETER FOR CHARACTERIZING SELECTIVE SURFACES FOR SOLAR THERMAL ENERGY CONVERSION

Keith D. Masterson
Optical Sciences Center, University of Arizona
Tucson, Arizona 85721

In order to obtain reliable infrared spectral reflectance measurements from diffusely reflecting, spectrally selective surfaces of interest for solar thermal energy conversion, a new reflectometer configuration modified from designs by Dunn[1] and Blevin and Brown[2] is proposed. As shown below light from a monochromator is focused onto the sample which is placed at one focus of the collector (a section of a prolate ellipsoid of revolution having an eccentricity of 1/3). The sample surface is in a plane perpendicular to the axis of the ellipse. A flat mirror also in this plane relays the conjugate focus into the detector located at the intersection of the axis with the elliptical surface. This design has the advantage of a high signal-to-noise ratio with stronger signals than are available from infrared integrating spheres.[3,4] As in the Coblenze sphere[5] or hemi-ellipsoidal[6,7] configurations, specular optics are used. Therefore, an extremely wide spectral range of application is possible. One advantage over the hemi-ellipsoid is that neither the source optics nor the detector must have 180° fields. A detector with approximately a 90° field of view is adequate. By placing the detector above the sample surface obscuration of the paraxial rays by the sample and sample holder is avoided. However if the sample dimensions are larger than twice the detector dimensions some rays could be obscured. This is avoidable by enlarging the aperture in front of the detector and using a secondary concentrator such as a compound parabolic concentrator.[8] The input optics can be arranged to provide a variable angle of incidence.

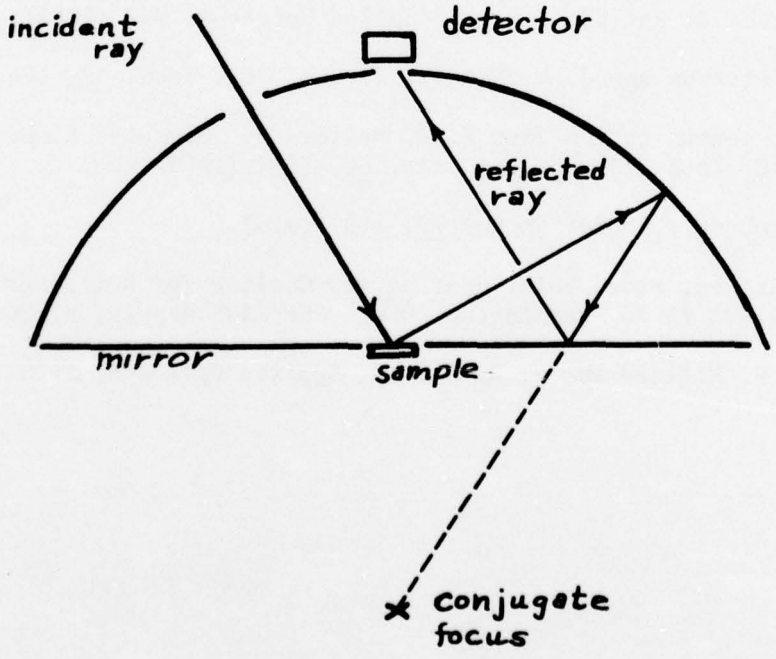

REFERENCES

1) S. T. Dunn, J. C. Richmond, and J. F. Parmer, J. Spacecr. Rockets 3, 961 (1966).
2) W. R. Blevin and W. J. Brown, Rev. Sci. Instrum., 42, 385 (1965).
3) B. W. Wood, et al., AIAA J. 9, 1338 (1971).
4) B. E. Wood, et al., AIAA J. 9, 1836 (1971).
5) W. W. Coblentz, Nat. Bur. Stand. U.S. Bull. 9, 283 (1913).
6) J. T. Neu, NASA CR-73193 (1968).
7) B. E. Wood, et al., Appl. Optics 15, 940 (1976).
8. H. Hinterberger and R. Winston, Rev. Sci. Instrum. 37, 1094 (1966).

THE STRUCTURAL COMPOSITION AND OPTICAL PROPERTIES OF GOOD SOLAR BLACKS: GOLD BLACK*

P. O'Neill, C. Doland and A. Ignatiev
Department of Physics
University of Houston
Houston, Texas 77004

Current emphasis in the utilization of solar energy has spurred interest in the investigation and understanding of the basic physical concepts underlying the absorption of solar radiation by a material. It is well known, that metals, semimetals and semiconductors are absorbers of solar radiation due to their high extinction coefficient (k), however, they are also good reflectors due to their high index of refraction (n). The net results for these systems is that the solar absorptance is small.

There are, however, materials defined as solar blacks that are highly absorbing in the solar spectrum. These materials, though generally stable only below 300°C, are believed to be metallic or semimetallic in nature and have $\alpha \approx 10^3$ cm^{-1} and $R \approx 1\%$. It has been previously reported[1] that such materials are particulate in nature with however few specifics given on the dependance of absorptance on particle size, particle packing density and absorbing layer thickness. We have undertaken a complete analysis of the dependance of optical absorptance on these parameters for a test solar black system: gold black. The information that we have obtained will be utilized in the development of a high-temperature stable solar black through the concept of modifying the surface of the material so as to obtain the optimal particulate properties for maximum solar radiation absorption.

Gold black films were deposited onto glass and metallic substrates by evaporation from a tungsten filament at between 0.5 and 10 torr of helium. The particulate nature of the films as well as their DC conductivity, absorp-

tion coefficient, and reflection coefficient were measured as a function of evaporation temperature and helium pressure. It was found that the films were in fact composed of loosely packed gold particles whose size increased from 40 to 200Å with increasing helium pressure. The packing fraction of the particles, however, decreased with increasing pressure from a value of about 0.03. The structural analysis including measurements of film thicknesses in the micron range was done with both scanning electron microscopy (SEM) and transmission electron microscopy (TEM).

Spectrophotometric techinques[2] were used to measure the reflectance and transmittance of the samples in the wavelength range of 0.35μ to 2.4μ.

The absorption coefficient was determined from the following expression using the measured transmittance and the thickness of the sample.

$$I = I_0 e^{-\alpha x}$$

where I_0 is the intensity of incident light at some wavelength λ, and I is the intensity at some distance x into the material.

It was found that the absorption coefficient is relatively wavelength independent and increases with increasing packing factor (decreasing particle size) with the highest value, $\alpha \simeq 1 \times 10^4$ cm^{-1} found for films with 70Å average particle size and 0.02 packing factor. The measured reflectance for such films was ~ 0.15% and relatively wavelength independant and mainly diffuse.

Theoretical analysis of the optical properties of a low density gold film including the effects of core electron polarization, plasma excitation and interband transitions was undertaken in order to correlate to experiment. The analysis resulted in the following reduced expressions for the optical properties:

$$n \simeq \sqrt{\varepsilon_1}$$

$$k \simeq \varepsilon_2/2\sqrt{\varepsilon_1}$$

where ε_1 and ε_2 are the real and imaginary parts of the dielectric constant of the material.

For a film of packing factor 0.02, the calculations have yielded $n \simeq 1.05$, and $k \simeq 0.06$. From $\alpha = {}^{4\pi k}/_{\lambda}$ we obtain $\alpha \simeq 0.85 \times 10^3$ cm^{-1} at 7000Å in good agreement with the experimental value of 1×10^3 cm^{-1}. The calculated reflectance for such a film is 0.14% in good agreement with the experimental value of 0.15%.

* Work supported by the University of Houston Solar Energy Laboratory.

1) Harris, L., The Optical Properties of Metal Blacks and Carbon Blacks, The Eppley Foundation for Research, Newport, R. I., 1967.
Harris, L., J. Opt. Soc. Am., 51, 80 (1961).

2) Wendlandt, W. W. and A. G. Hecht, Reflectance Spectroscopy; (J. Wiley & Sons, New York, 1966).

Optical Coatings for Solar Heating and Cooling

H.Y.B. Mar, R.E. Peterson and J.H. Lin

Honeywell, Inc.

Systems and Research Center

2600 Ridgway Parkway

Minneapolis, MN 55413

Solar collectors have been used for many years to heat water. The basic design of a solar collector for heating water or for heating and cooling buildings is similar. However, improved collector performance, which can be obtained through use of special coatings, is required for heating and cooling applications.

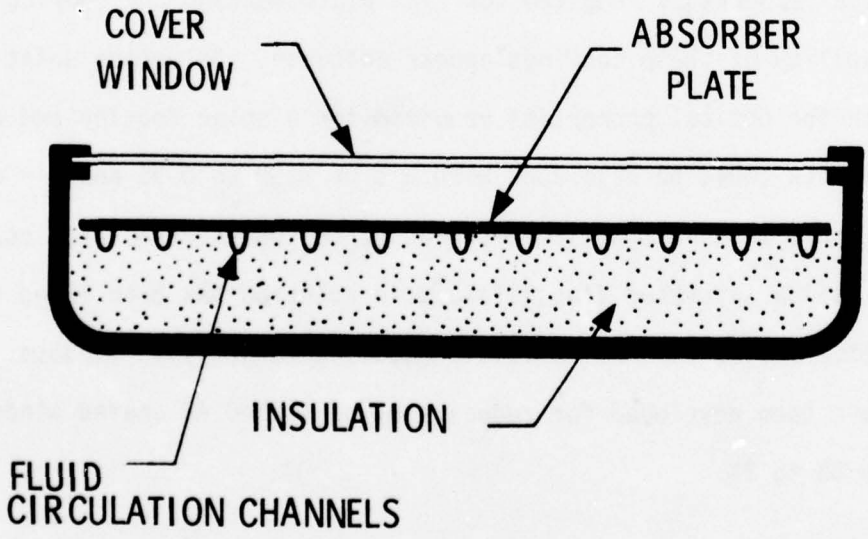

FIGURE I. CROSS-SECTION OF A FLAT PLATE SOLAR COLLECTOR

Figure 1 shows the cross-section of a simple solar energy collector often called a flat plate collector. The portions of the collector that require coatings are the absorber plate and the window cover. A selective solar absorber coating on the absorber plate allows efficient absorption and retention of incident solar energy. Such coatings are characterized by a high solar absorptance (α) and a low thermal emittance (ε). An antireflection coating on the cover window maximizes the solar energy transmitted to the absorber plate. A figure of merit for the antireflection coating is the total solar reflectance (R_S).

Table 1 summarizes the key features of several coatings that are currently being considered for use in flat plate solar collectors. Black chrome and black nickel are electroplated coatings that are very attractive as selective solar absorber coatings. Their technology is well established and they are relatively low cost coatings. Black chrome and black nickel coatings have been developed with the optical properties required for flat plate heating and cooling systems. Also the durability of these coatings appear adequate. Selective paint coatings currently lack the optical properties required for a solar heating and cooling system. If paints could be developed with α's of 0.90 to 0.95 and ε's of 0.10 to 0.15 they would be an attractive alternative to the electroplated coatings. Etching in a silica saturated fluosilicic acid solution has been found to be a cost effective method for antireflection coating large glass windows. Techniques have been developed for reducing R_S of etched AR coated windows from approximately 8% to 2%.

Table 1. Properties of Selected Solar Coatings

Type	α	ε ($100^{o}C$)	Estimated Materials Cost ($/ft^2)	Estimated Life (yrs)
Black Chrome	0.96	0.12	0.25	>15
Black Nickel	0.96	0.07	0.40	>2
Selective Paint	0.90	0.30	0.001	>15
Etched Anti-reflection	R_S = 0.02		0.01	>15

RECENT ADVANCES IN MEASUREMENT TECHNIQUES FOR SMALL ABSORPTION COEFFICIENTS

A. Hordvik

Rome Air Development Center
Deputy for Electronic Technology
Hanscom AFB, MA 01731

The development of high power lasers and fiber optics has created a need for low loss optical components which in turn have necessitated a variety of new techniques to be developed for measuring bulk and surface absorption in the 10^{-4} to 10^{-6} range. At the Conference on Optical Properties of Highly Transparent Solids, 3-5 February 1975, Skolnik [1] reviewed the state of the art at that time in particular as related to the measurement of bulk absorption. In the almost two years that have passed since that meeting several new methods have been developed. In particular, an effort has been made to find techniques capable of determining surface absorption and absorption in coatings. The measurement of surface absorption has become especially important with the realization that for a number of high quality optical materials surface absorption dominates bulk absorption at some high power laser wavelengths.

This paper reviews several new measurement techniques with emphasis on various laser calorimetric and photoacoustic methods which allow both bulk and surface absorption coefficients to be determined simultaneously. A description is also given of techniques suitable for measuring losses in coatings. Representative examples of measurements made using the different approaches are described, and the advantages and disadvantages of the various procedures are discussed. Estimates are made of the sensitivities that can be achieved with the different techniques. Finally, a description is given of a new a.c. interferometric technique for measuring very low bulk absorption.

References:

[1] L. Skolnik in "Optical Properties of Highly Transparent Solids", edited by S. S. Mitra and B. Bendow, p. 405 (Plenum Press, New York, N.Y., 1975).

PHOTOACOUSTIC SPECTROSCOPY:
A MEASUREMENT TECHNIQUE FOR LOW ABSORPTION COEFFICIENTS

H. S. Bennett and R. A. Forman

National Bureau of Standards, Washington, D.C. 20234

SUMMARY

We have presented earlier the theory of a photoacoustic gas cell[1] and have demonstrated that the photoacoustic gas cell has a sufficient number of parameters which we may vary experimentally to determine separately the surface and bulk absorption coefficients. We give here expressions for the acoustic stress which are valid at intermediate frequencies ω.

Figure 1 is a sketch of the photoacoustic gas cell for measuring absorption coefficients. A confined, non-absorbing gas at ambient pressure p_o fills the space inside the cell between the two windows which are made from a weakly absorbing material. The window thickness is $d = z_3 - z_2$ and the cell length is $\ell = 2z_2$. A collimated and modulated laser beam propagates in the z direction, has power W_ℓ and has angular modulation frequency ω. A pressure transducer located in the gas region at $|z| \leq z_2$ gives the acoustic stress amplitude. Because we neglect the flow of heat in all directions transverse to the z axis and assume that the laser beam has a uniform intensity profile, we reduce the problem to a one dimensional problem in the z direction.

Using the linearized hydrodynamic equations, we find that the acoustic stress simplifies considerably whenever the following set of inequalities are all satisfied: $\xi_a z_2 << 1$, $\xi_s d >> 1$ and $\xi_t z_2 >> 1$. The inverse of the wavelength of the acoustic behavior is $\xi_a = \omega/c_g$, where c_g is the speed of sound in the gas; the inverse of the thermal diffusion length in the windows is $\xi_s = (\omega/k_s)^{1/2}$, where k_s is the thermal diffusivity of the windows; and the inverse of the thermal diffusion length in the gas is $\xi_t = (\omega\gamma/k_g)^{1/2}$, where k_g is the thermal diffusivity in the gas and $\gamma = C_p/C_v$ is the ratio of the specific heat of the gas at constant pressure C_p to that at constant volume C_v. When $z_2 = 1.0$ cm and $d = 1.0$ cm, the intermediate frequency range for air (nitrogen) at standard temperature and pressure and for a representative laser glass becomes $3.31 \times 10^4 (\text{rad/s}) >> \omega >> 0.201$ (rad/s). For this intermediate range of frequencies the acoustic stress T_{zz} has the approximate form for $|z| \leq z_2$,

$$\frac{T_{zz}(z,\omega)}{p_o} \approx \frac{imI_o(k_s k_g \gamma)^{1/2}}{T_o K_s z_2 \omega} \{\alpha_s + \frac{(1-i)\alpha_B k_s^{1/2}}{(2\omega)^{1/2}}\} \times$$

$$\times \{1 + (K_g \gamma k_s / K_s k_g)^{1/2}\}, \qquad (1)$$

where m is the modulation depth of the laser beam, I_o is its intensity, α_s is the bulk absorption coefficient in inverse units of length, K_s is the thermal conductivity of the window and K_g is the thermal conductivity of the gas.

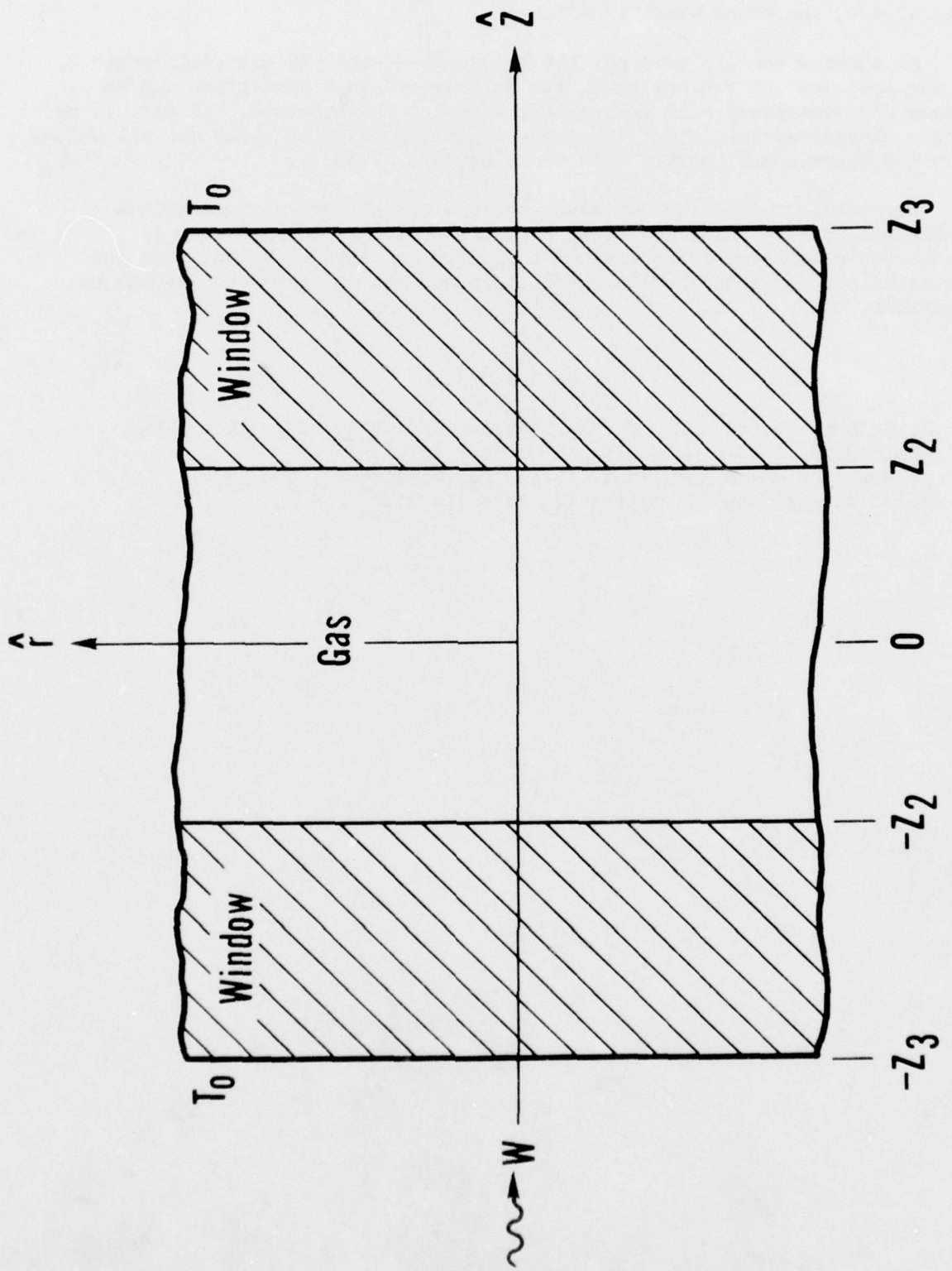

Fig. 1 Schematic of photoacoustic gas cell.

We observe that for the above intermediate frequency range, the acoustic stress is independent of z; is directly proportional to ω^{-1} when $\alpha_B = 0$; and is directly proportional to $\omega^{-3/2}$ when $\alpha_S = 0$. In addition, when $\alpha_B = 0$, the phase shift of the stress relative to the laser beam modulation is 90° and when $\alpha_S = 0$, the phase shift is 45°.

By varying the pressure p_o, the frequency ω, and the gas cell length ℓ, we may optimize the regions where the surface and bulk absorption can be determined separately with reasonable precision and accuracy. In Ref. 1, we give a closed expression for the acoustic stress which is valid for all values of ω and compare our results with those of Refs. 2 and 3.

Because this technique averages to some extent over any absorption inhomogeneities in the windows, we expect that localized absorbing or scattering centers could be less of a problem for this technique than for the calorimetric techniques in which the placement of thermocouples may be important.

References

1. H. S. Bennett and R. A. Forman, Applied Optics 15, 347 (1976); and Applied Optics (to be published October 1976).
2. A. Rosencwaig and A. Gersho, J. Applied Physics 47, 64 (1976).
3. J. G. Parker, Applied Optics 12, 2974 (1973).

ANALYSIS OF LASER CALORIMETRIC DATA

H. B. Rosenstock and M. Hass
Naval Research Laboratory
Washington, D.C. 20375

D. A. Gregory and J. A. Harrington
University of Alabama in Huntsville
Huntsville, Alabama 35807

Laser calorimetry is one of the most widely used methods for the determination of low absorption coefficients. However, the extraction of absorption coefficients of materials from the thermal rise curves obtained in laser calorimetry depends upon a knowledge of the time dependence of the temperature of a sample heated by a laser beam of known power. The general solution of heat equation for arbitrary geometries in the presence of both surface and bulk absorption is quite complex, but use of a long rod geometry introduces a number of simplifications in the analysis which will be discussed in detail. By means of this analysis, it becomes possible to deduce both the bulk and surface absorption in a single run.

Several features are generally expected in the relation between temperature and time measured near the center of the peripheral surface of a long cylinder heated along the central axis and at the end surfaces. These include: a constant temperature region (until the heat has had time to reach the

peripheral surface); a linear temperature increase (as long as heat flowing radially outward from the center arrives on the peripheral surface at a constant rate, unperturbed by heat transfer to the surroundings or end effects); a more rapid temperature increase, perhaps still linear in time, as heat flow from the end surfaces appears; a slower temperature rise once the surface temperature gets high enough that radiative or convective heat transfer to the surroundings can no longer be ignored; and, finally, a constant temperature when, in the steady state, the heat transferred to the environment equals the amount absorbed.

While the above features seem physically plausible enough, the details, and even the appearance of some of the distinct regions, depend sensitively on the quantitative values of parameters that are only qualitatively alluded to in the preceding: shape of the sample, position and magnitude of heat sources and measuring points, and relative values of the conductivity and heat transfer coefficients. The nature of this dependence is far from obvious by a glance at the solution of the heat equation for a particular situation, a solution that usually involves all these quantities in each term of a doubly infinite series in a complicated way.

Our purpose in this work is to determine quantitatively the physical conditions under which the correct solution of the heat equation can be approximately simplified to produce the simple

features that are intuitively expected. When this is legitimate it can be shown that some of the physical parameters can usually be more easily inferred than is possible by a full-scale analysis of the complete solution.

These results are illustrated by measurements and calculations of thermal rise curves encountered in studying laser window materials in the infrared. For the long rod geometry, a two-slope behavior in the thermal rise curve is found in accordance with intuitive expectations and the previous analysis. The first slope can be identified with bulk absorption alone and the second slope with the sum of surface and bulk absorption.

A NEW TECHNIQUE FOR MEASURING THE INFRARED ABSORPTION IN THIN FILM COATINGS*

James A. Harrington**, Morris Braunstein, and J. Earl Rudisill

Hughes Research Laboratories
Malibu, California 90265

Previous methods used to measure the optical absorption in transparent dielectric coatings on infrared laser window materials have generally relied on a comparison of the absorption in coated and uncoated substrates in order to obtain the absorption coefficient β_f of the coating. These methods have the disadvantage that one often obtains nearly identical absorption coefficients for both coated and uncoated substrates making extraction of β_f difficult or, at times, impossible. We have developed a technique to measure the absorption coefficient β_f directly without resorting to the need for independent measurements of both coated and uncoated substrates.

This new method involves the use of a long, rod-shaped sample with a low loss coating at one end. For a rod whose length is about 10 times greater than its radius, Hass[1] has shown that surface and bulk heat are separated in time in the heating-cooling curves obtained in conventional laser calorimetry. From these calorimetric data on long, rod-shaped samples it is then possible to measure directly the surface absorption alone and, therefore, the β_f of a low loss coating on one end of the bar.

We have measured the absorption coefficient in As_2S_3, CaF_2, ThF_4, and PbF_2 single layer films on a KCl substrate (2 x 2 x 13 cm) at 5.3 μm using this technique. The particular bar of single crystal KCl used in this study was RAP grown and exhibited extremely low bulk and surface absorption at both 10.6 and 5.3 μm. At 10.6 μm the KCl bar was essentially intrinsic (β=8 x 10^{-5} cm^{-1}) while at 5.3 μm measurements of bulk and surface absorption indicated immeasurably small surface absorption and bulk absorptions in the low 10^{-6} cm^{-1} range. Therefore, this bar is ideal for a substrate since effectively only the coating to be evaluated will contribute to the heating-cooling curve and measurement of the final slope in the heating curve will yield β_f. Typical heating-cooling curves will be presented and discussed in relation to thermocouple placement on the bar and β_f given for each film measured.

1 M. Hass, Proc. Fifth Laser Window Conference, Las Vegas, NV (1975)

* Sponsored by the Office of Naval Research and the Defense Advanced Research Projects Agency, DARPA support monitored by RADC/ETSO Hanscom Air Force Base, Massachusetts, 07131

** Permanent address: Physics Department, University of Alabama in Huntsville, Huntsville, Alabama 35807

NOTES

PARALLELICITY CRITERION FOR SAMPLES TO BE STUDIED USING FABRY-PEROT INTERFERENCES

Raoul Weil and Dalia Neshmit,
Physics Department and Solid State Institute
Technion, Israel Institute of Technology
Haifa, Israel

Properties of materials such as the temperature dependence of the index of refraction[1,2] and the piezo-optic coefficients[3] can be measured by shaping samples into Fabry-Perot Etalons. Coherent light is sent through the sample and reflections from the entrance and exit faces interfere in a mode depending on the optical length of the sample. For the reflectivity of the faces one depends usually on the difference in the index of refraction of the material and the surrounding air. The desired properties are measured by observing the shift of the interference peaks in response to an independent variable such as temperature or pressure.

For the measurement to be successful it is essential that there be good contrast between the interference maxima and minima. Parallelicity of the faces is one of the parameters that strongly affect the contrast. Maximum contrast is obtained with perfectly parallel faces. The question to which this paper addresses itself is what deviation from parallelicity is tolerable if a useful contrast between Fabry-Perot maxima and minima is to be obtained.

For the calculation a sample of the shape shown in Fig. 1 will be assumed. θ is the angle that defines the lack of parallelism between the input and exit faces. It will be seen that θ is only a fraction of a degree so that its extent is greatly exagerated in the figure for clarity. Perfect parallelicity is assumed along the x direction. The coherent beam, of vacuum wavelength λ_o, is assumed to be a plane wave of dimensions a and b in the x and y directions, respectively. The beam is assumed to impinge normally on the sample and to travel in the z direction. The shortest path of the beam through the sample is defined as ℓ_o The material is assumed to be perfectly transparent. In the calculation use will be made of eq. 6 of reference 4 which gives the electric field intensity E_T transmitted by a parallel faced

element of the sample of length $\ell = \ell_o + y\theta$:

$$E_T(y) = E_o\, t_{AR}\, t_{BR}\, (e^{-ik\ell} + r^2\, e^{-3ik\ell}), \qquad (1)$$

where E_o is the field strength in the incoming beam, t_{AR} and t_{BR} are the transmission coefficients of the input and exit faces of the sample, k is the wave vector ($k = \frac{2\pi n}{\lambda_o}$) and r the reflection coefficient of the sample surfaces. In equation 1 the terms of higher order than r^2 have been neglected. This is valid for reflection coefficients smaller than 0.5 where the neglected terms amount to less than 10% of the field. The intensity of the transmitted beam I_T will be:

$$I_T = a \int_o^b E_T(y) \cdot E_T^*(y)\, dy. \qquad (2)$$

$$I_T = a(E_o t_{AR} t_{BR})^2 \{b + \frac{r^2}{k\theta} [\sin 2k\,(\ell_o + b\theta) - \sin 2k\ell_o]\}\ . \qquad (3)$$

By differentiating I_T with respect to the angle $\psi = 2k\ell_o$ one can find $I_{T\text{-max}}$ and $I_{T\text{-min}}$. Their ratio will be:

$$\frac{I_{T\text{-min}}}{I_{T\text{-max}}} = \frac{1 - \frac{2r^2}{k\theta b} \sin k\theta b}{1 + \frac{2r^2}{k\theta b} \sin k\theta b} \qquad (4)$$

Fig. 2 is a plot of eq. (4) for the case of CdS at $\lambda_o = 10.3\ \mu m$. The absisa is given in units of mm-minutes. It is seen that for these conditions any lack of parallelicity greater than 7mm-minutes causes the contrast between $I_{T\text{-max}}$ and $I_{T\text{-min}}$ to be less than 10%, making precise measurements difficult. If the width of the beam is one mm, the I_{min}/I_{max} ratio is 0.7 when the angle between the faces is 4 min. For the same contrast a beam width of 2mm can only tolerate 2 min of an arc parallelicity deviation. It also follows from eq. 4 that if the wavelength is reduced say to 1μ, the allowable lack of parallelicity will drop to 0.4 min for a 1mm beam width and 0.7 contrast ratio.

References:

1) R. Weil, J. Appl. Phys., 40, 2857 (1969).
2) J.E. Kiefer and A. Yariv, Appl. Phys. Letters, 15, 26 (1969).
3) R. Weil, Proceedings International Symposium on CdTe, P. Siffert and A. Cornet eds., Strasbourg June 29-30, 1971.
4) R. Weil, J. Appl. Phys. 41, 3012, 1970.

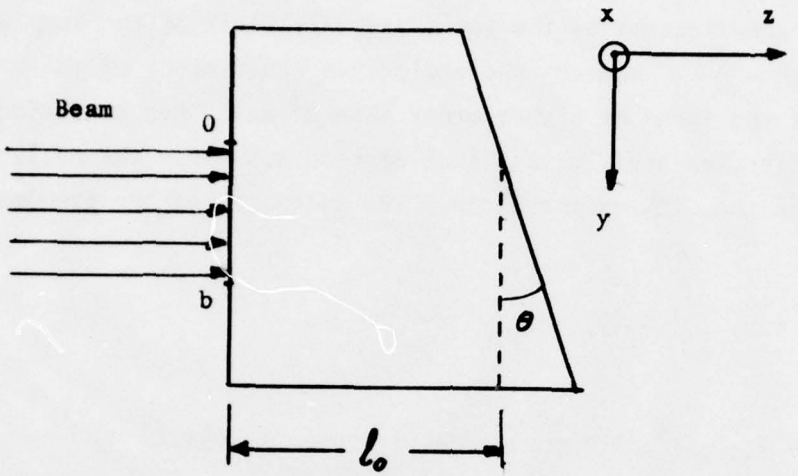

Fig. 1: Assumed Geometry

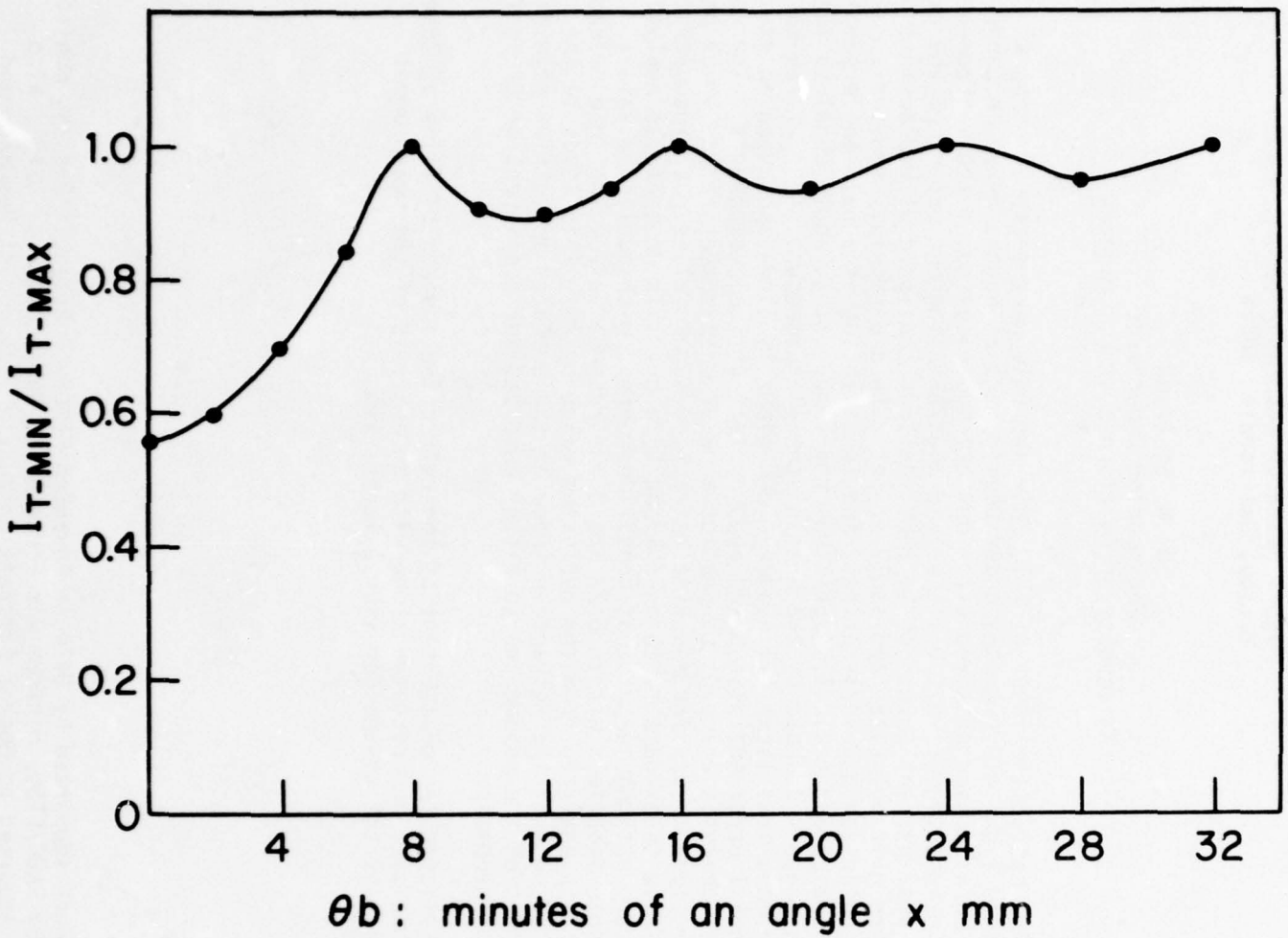

Fig 2: **Ratio of Minima to Maxima of Fabry - Perot Interferences as a function of Etalon parallelicity. The curve applies to CdS (n = 2.2) at 10.3 μm wavelength.**

10.6 μm ELLIPSOMETER MEASUREMENTS OF REFRACTIVE INDICES OF IR MATERIALS *

M. E. Pedinoff and M. Braunstein
Hughes Research Laboratories
Malibu, California 90265

O. M. Staffsud
Engineering Department
University of California at Los Angeles

The refractive index of KCl, ZnSe and CdTe were measured using a modulated light ellipsometer under development at Hughes Research Laboratories. These results were obtained after optical modification of the instrument[1] to eliminate signal instabilities and angular alignment errors of the order of several percent each. These modifications consisted of replacement of the wire grid polarizer and analyzer set with a Germanium Brewster's Angle polarizer and analyzer set, and installation of a half angle sample drive[2] which automatically positions the sample at an angle equal to half of the angle subtended by the arms of the ellipsometer. A brief review of the modulated light ellipsometer equations is given including an experimental error analysis based upon perfect optical components. The results of this analysis allow us to predict angular measurement ranges which produce the smallest errors for specific refractive index values. Ellipsometric refractive index data taken on KCl and CdTe crystals under these analytically predicted optimum measurement conditions agrees with published values for these materials within 0.7% and 0.03% respectively. The ZnSe refractive index data deviates from the published value by 2%. This leads to the speculation that the refractive index at the surface[3] may differ significantly from that of the volume due to either adsorbed surface layers or to surface damage phenomena.

Ellipsometer measurement of the refractive indices of films of ZnSe and ThF_4 will be presented along with an analysis of the measurement accuracy of the system for single layer films.

* Work supported by Defense Advanced Research Projects Agency, monitored by RADC/ETSO, Hanscom Air Force Base, Massachusetts, 07131; also supported by Hughes Aircraft Company's Independent Research and Development Projects.

References:

1. "S.D. Allen, A.I. Braunstein, M. Braunstein"
J. C. Cheng and L.A. Nafie, In Optical Properties of Highly Transparent Solids, S.S. Mitra and B. Bendow (Plenum Publishing Company, New York)

2. "E.G. Lluesma, C.A. Pela and I. Wilmanns", Surface Science Vol. 56 p. 189 1976

3. "M. Ohlidal, I. Ohlidal and F. Lukes", Surface Science Vol 55 pp 467 (1976)

A BRDF MEASURING INSTRUMENT

F. O. Bartell, A. G. DeBell, D. S. Goodman
J. E. Harvey, W. L. Wolfe

Optical Sciences Center
The University of Arizona
Tucson, Arizona 85721

An instrument has been built for measuring the bidirectional reflectance distribution function (BRDF)[1,2] for radiant energy reflected from surfaces. This instrument features wide ranges of measurement conditions and simple mechanical construction.

The reflection of electromagnetic radiation from surfaces is a subject of increasing theoretical and experimental interest, and the BRDF provides one of the best ways for describing the reflected energy. The BRDF is a function of four angular variables--the elevation and azimuth of both the incident and the reflected rays measured from the surface of the sample.

The instrument is shown in Figure 1, and it is called BRDFRI (BRDF Recording Instrument). The geometry of BRDFRI is based on the idea of one of the authors (D.S.G.), that the incident and reflected rays intersect at the sample, so these two lines define a plane; and this plane can always be kept horizontal. BRDFRI has been built with each source fixed except for provisions to accomodate polarization rotations. The detectors move only in a horizontal plane so there is no problem of spilling liquid coolants.

The samples are given three degrees of angular rotation to provide the angular motions that would otherwise be provided by more cumbersome motions of the source and detector.

For BRDFRI's operation, the angular positions of the source, detector and sample do not correspond to the four BRDF angles directly, but must be related to them by mathematical transformations. This requirement is met by choosing BRDF angles in advance and then calculating the corresponding instrument angles necessary for making the desired measurements. A better way to handle this angular transformation requirement is to provide real time computer control for BRDFRI, and we are in the process of setting up that capability. It will then be possible to command a sequence of measurements in BRDF angles; and then the computer control will perform the transformation to instrument angles, step the instrument through the desired positions, record the detector readings at each data point, process the data, and plot the results according to an appropriate format.

BRDFRI features include:

(1) Wide ranges of measurement conditions including variations in all four BRDF angles, and interchangeable sources and detectors.

(2) Simple mechanical construction with the capability for having several sources permanently installed and aligned, and detectors moving only in a horizontal plane.

(3) The capability for the rapid measurement of large amounts of data with computer control for programming experimental sequences; and real time processing and recording of BRDF data.

---

1. Fred E. Nicodemus, Appl. Opt. 4, 767 (1965).
2. F. E. Nicodemus, Appl. Opt. 9, 1474 (1970).

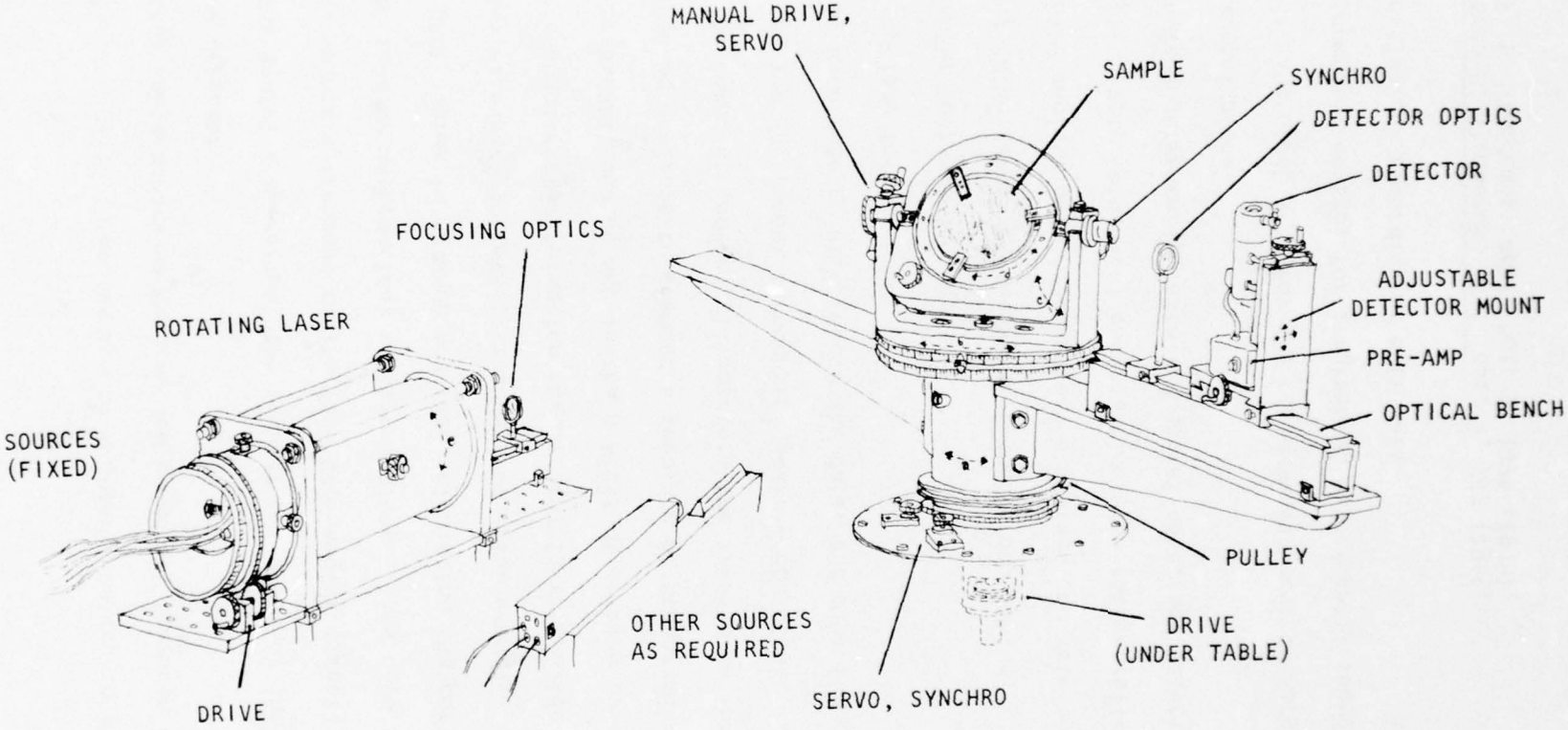

WD3-3

FIG. 1. BRDF RECORDING INSTRUMENT (BRDFRI).

TOPOGRAPHICAL INVESTIGATION OF THE VARIATIONS IN STOICHIOMETRY IN $Hg_{1-x}Cd_xTe$ USING ELECTROLYTE ELECTROREFLECTANCE

P.E.Vanier, Fred H. Pollak and Paul M. Raccah

Physics Department
Belfer Graduate School of Science
Yeshiva University
New York, N.Y. 10033

We have developed a unique approach for evaluating the topographical variations in stoichiometry across wafers of $Hg_{1-x}Cd_xTe$ utilizing electrolyte electroreflectance (EER). The method is non-destructive and can be employed at room temperature. The technique is sensitive enough to determine changes of composition $\Delta x \approx 0.002$ for samples in which $x \approx 0.2 - 0.3$ with a spatial resolution of about 150μ. This approach has a number of advantages over the microprobe technique.

The energy of features in the optical spectra of alloys of the type $A_{1-x}B_xC$ ($Hg_{1-x}Cd_xTe$, $Ga_{1-x}Al_xAs$, etc) depend on the composition, x, in a continuous way. Therefore, by measuring the changes in energy of a particular optical feature utilizing a small scanned light spot the variations in stoichiometry, Δx, can be determined across the face of such a material. EER is particularly suited to such an investigation since it yields a sharp optical structure at room temperature, can be performed on a free surface (i.e. nothing need be deposited on the sample surface to apply the electric field) and hence is non-destructive. The most convenient optical feature for our purposes is the E_1 peak since it gives the largest FER signal, is in the convenient 2 eV range and its dependence on composition is known.[1]

Standard EER was employed with an electrolyte consisting of 1 part

conc. HNO_3 to 5,000 parts methanol, by volume. Light from a monochromator was focused to a spot size of about 150μ on the sample by means of an f/1.8 camera lens. Spectra in the vicinity of E_1 were taken with the light spot on one portion of the sample, the sample was then moved by means of an X-Y stage and spectra taken in the new position. Step sizes were 200μ in the horizontal (X) direction and 400μ along the vertical (Y). The shift in the spectra was then correlated with the known composition dependence of E_1 in order to evaluate the change in composition, Δx. Samples were provided by the Santa Barbara Research Center.

Shown in Fig. 1 is a contour map of the variations in composition Δx of sample WK-2 (unannealed) as displayed by a Tektronix 4051 Basic Graphic System and reproduced by the hard copy unit. The contours

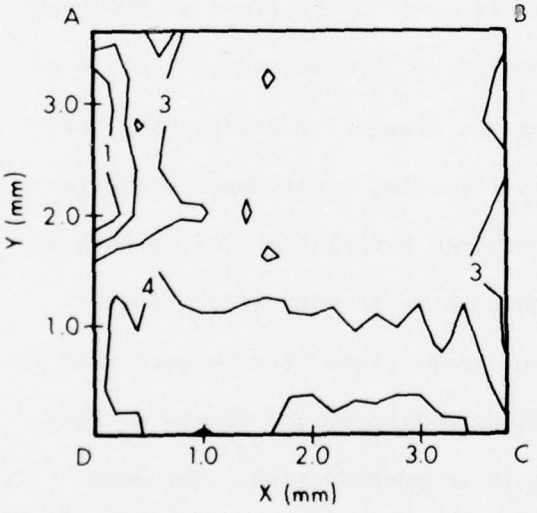

Fig. 1. Contour map of the variation in composition Δx of $Hg_{1-x}Cd_xTe$ sample WK-2 (unannealed). The nominal value of x is 0.21, and the contours are at intervals of $\Delta x = 0.005$.

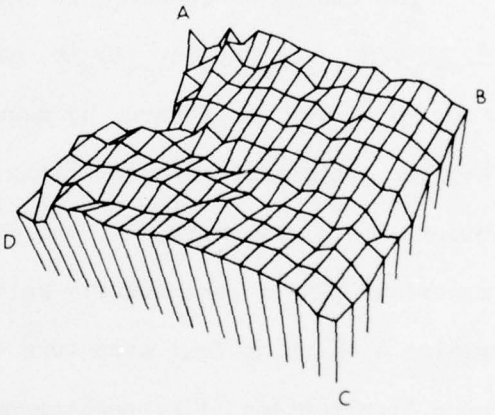

Fig. 2. Perspective drawing of 3-D representation of the same data used in Fig. 1.

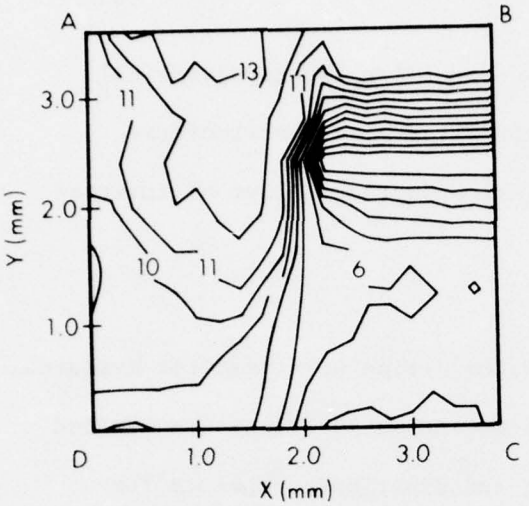

Fig. 3. Contour map of Δx for sample WK-4(annealed). The nominal value of x is 0.31 and the contour interval is $\Delta x = 0.005$

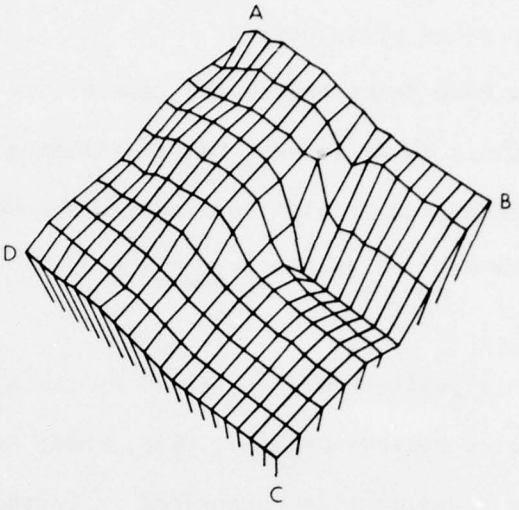

Fig. 4. Perspective drawing of 3-D representation of the same data used in Fig. 3

are at intervals of $\Delta x = 0.005$ and the and the nominal value of $x = 0.21$. The corners are labelled ABCD. In Fig. 2 we show a 3-dimensional projection of the contours of Fig. 1. also made by the Tektronix system. The sample is quite uniform in the upper right hand corner with a depression about midway along AD. The contour map of the variations in composition Δx of sample WK-4 (annealed) is displayed in Fig. 3 with contours at intervals of $\Delta x = 0.005$ and a nominal value of $x = 0.31$. The 3-dimensional projection of the contours of Fig. 3 are shown in Fig. 4. Figure 5 is the 3-dimension-

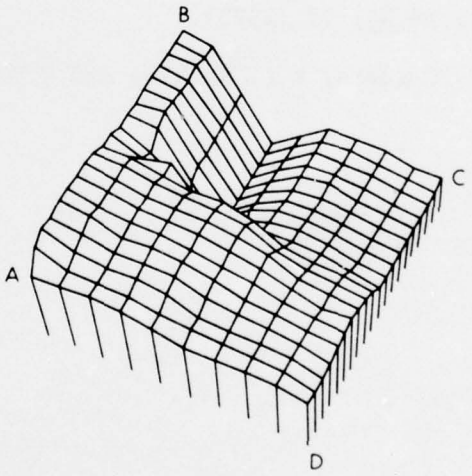

Fig. 5. The same data as in Fig.4, rotated 90 degrees.

al projection rotated by 90^{o} in relation to Fig. 4. The large depression in the upper right hand region of Fig. 3 is probably due to a grain boundary or other gross defect.

We have demonstrated the feasibility of determining the topographical variations in Δx in $Hg_{1-x}Cd_{x}Te$ utilizing electrolyte electroreflectance. This technique is also applicable to other semiconducting alloys of interest such as $Ga_{1-x}Al_{x}As$, $In\,As_{1-x}P_{x}$, etc.

This research was sponsored by the Air Force Office of Scientific Research, Air Force Systems Command, USAF, under Grant No. AFOSR-74-2714B. The United States Government is authorized to reproduce and distribute reprints for Governmental purposes notwithstanding any copyright notation hereon.

References

1. A. Moritani, K. Tanaguchi, C. Homaguchi, and J. Nakai, J. Phys. Soc. Japan 34, 79 (1973).
2. M. Cardona, K.L. Shaklee and F.H. Pollak 154, 696 (1967).

INFRARED TECHNIQUE FOR OBSERVATION OF SUPERCOOLING

Edward M. Alexander
Naval Research Laboratory
Washington, D.C. 20375

We are presenting here a technique for studying supercooling of materials in capillary tubes by measuring infrared emission as a probe for monitoring temperature. The phenomenon of supercooling is observed for liquids in narrow enclosures where the material remains liquid while cooling below its bulk melting point (T_m) until a nucleation center forms whereupon a significant fraction of the material suddenly solidifies resulting in a liquid-solid mixture at T_m.

Supercooling of a liquid in a capillary tube is traditionally studied by inserting a temperature sensor inside the tube. This has the disadvantage of placing a foreign body in the material under study which could act as a nucleation center or otherwise obscure the phenomenon. In addition, the sensor technique permits study of only a single point in the material and necessitates physically moving the sensor through the material to study a different part. Our infrared technique involves plotting the infrared emission as a function of time from the liquid, and thereby drawing a supercooling curve. This infrared technique avoids the difficulties of the temperature sensor method since nothing is being inserted in the material and different parts of the material can easily be studied by repositioning the capillary tube within the field of view of the infrared imager.

To demonstrate this system we chose to look at supercooling of Barium Hydroxide Octahydrate (BaOH) in a polyethylene capillary tube of inner and outer diameters .35 and .8 millimeters respectively. Polyethylene was chosen because it is reasonably transparent between 8 and 14 microns where these measurements were taken.

The infrared emission was monitored with a Barnes Infrared Microscanner operating between 8 and 14 microns. The instrument was used in a single line scan mode where a scan was taken across a line normal to the axis of the tube resulting in a display of infrared emission vs distance along a direction normal to the axis of the tube. The material temperature inside of the tube varies with its infrared emission and therefore with the amplitude of the display. This amplitude can be output as a voltage at the rear of the instrument. The voltage is fed into a box car integrator which is gated over a narrow region at the peak of the voltage scan corresponding to the center of the tube. The output from the box car integrator is then sent to a recorder where the radiation from the material is displayed as a function of time.

A typical cooling curve from this system is shown in Figure 1. The tube with the salt material inside was heated above the BaOH melting point (78°C) and then allowed to cool in air. The material supercooled below the melting point but at approximately 14 seconds suddenly partially froze with the temperature of the liquid solid mixture jumping to T_m. The salt remained at T_m until completely frozen and then cooled toward room temperature.

A method has therefore been demonstrated to monitor the supercooling processes without placing a foreign object in the liquid which could affect the experimental results.

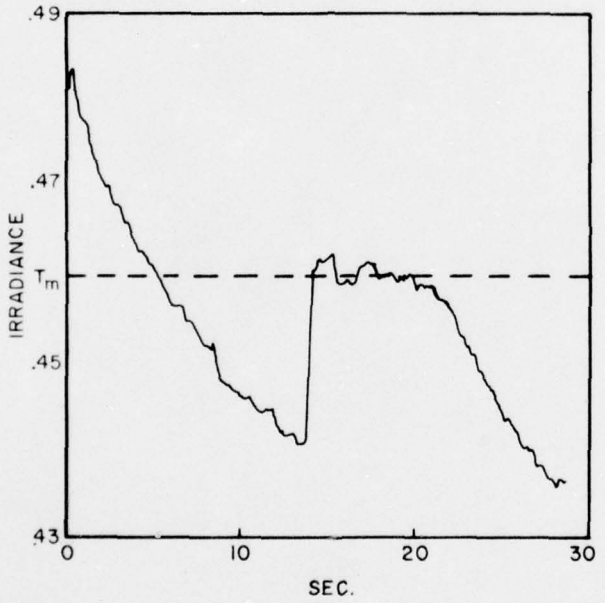

FIGURE 1-Cooling curve of BaOH displayed as infrared irradiance (in units of $mw/cm^2/ster$) as a function of time. The material cools below its normal melting point (indicated by the dotted line) and then suddenly partially freezes at 14 seconds' with its temperature jumping to T_m. It remains a liquid-solid mixture at the melting point until 21 seconds when it is completely frozen and then cools toward room temperature.

NOTES

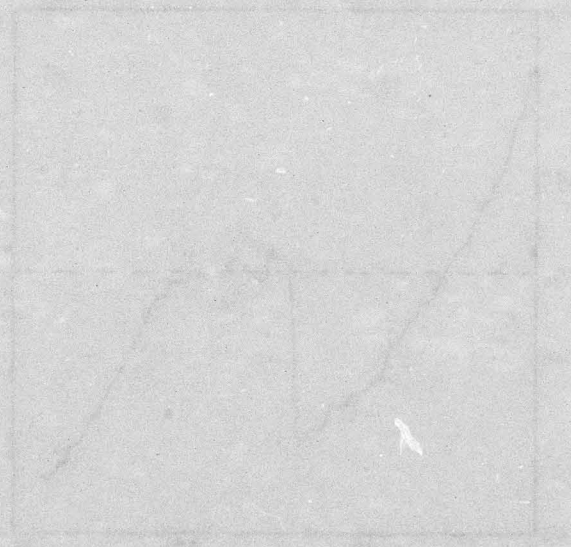

DETERMINATION OF THE OPTICAL PROPERTIES OF THIN FILMS

F. ABELES
Laboratoire d'Optique des Solides †
Université P. et M. Curie
75230 Paris Cedex 05
France

The determination of the optical properties of metals in the infrared is a problem which did not receive yet a satisfactory solution. This is due to their high reflectivity in this spectral region. We show here how one can take advantage of the attenuated total reflection (ATR) techniques in order to determine the optical constants of thin films (a few hundred ängstroms thick, i.e. having the bulk metal properties) or of bulk materials. For very thin films (thickness less or equal to 100 Å) other methods can be used, as, for instance, reflectance and transmittance in normal incidence. Problems related to the experimental techniques will be discussed and some experimental results indicated.

For low absorption materials, which are quasi-transparent in contradistinction to metals (which have also low absorption) ATR techniques can be efficiently used. The advantage of the method is that it avoids the usual reflectance and transmittance absolute measurements and are based on a kind of differential measurement, the accuracy of which is relatively high. The theoretical discussion will be followed by experimental results concerning the absorption edge of amorphous germanium films.

† Equipe de Recherche Associée au C.N.R.S.

Finally, the possibilities of detecting and measuring the optical characteristics of adsorbed layers on metal surfaces will be discussed. The point in case is that this method does not require nearly grazing incidence multiple reflections, but uses the modification of surface electromagnetic waves due to the presence of the adsorbed layers.

RETROREFLECTANCE MEASUREMENTS OF PHOTOMETRIC STANDARDS AND COATINGS - II

W. G. Egan and T. Hilgeman, Research Department
Grumman Aerospace Corporation
South Oyster Bay Road, Bethpage, New York 11714

An interesting infrared optical phenomenon has been observed, that of retroreflectance; this is the reflectance of a surface with illumination collimated and coincident with the observation direction. Observations between 0.6 and 1.105 μm have been made with low coherence (incandescent) illumination. Initial measurements were reported with a combined collimation and sensor acceptance angle of 1^{o} (Egan and Hilgeman, Appl. Opt.15, 1845 (1976)). The results indicated an opposition effect of approximately 1.5 for diffuse paints and photometric standards at normal incidence. The opposition effect is defined here as the ratio of the retroreflectance of a surface to the diffuse reflectance for the same surface at a 30^{o} scattering angle. Laser illumination at 0.6328 μm revealed up to an order of magnitude greater opposition effect for the same surfaces and sensor acceptance angle. An existing theoretical explanation was satisfactorily applied to the non-coherent opposition effect, but none existed for the laser effect.

We have subsequently made retroreflectance measurements on the same samples with a combined collimation and sensor acceptance angle of 0.1^{o} for a variation of incident angle between 0 and 60^{o} in the same wavelength range using the previously described techniques. The results indicate an additionally enhanced opposition effect with laser illumination for the smaller acceptance angle (0.1^{o}) over the larger (1^{o}). This oppposition effect is especially significant in photometric calibrations using laser illumination when observations are made close to the incident angle.

We have developed a theoretical analysis for the coherent radiation opposition effect based on an analogy with a diffraction grating. The fact that the opposition effect increases with decrease in sensor acceptance angle lends credence to an interferometic explanation. Also, since the observed enhancement of the opposition effect is stronger for the darker diffuse surfaces, the lack of multiple scattering by the surface in the retro direction must be a factor in the enhancement. These factors are included in the theory to be presented.

We are also investigating the wavelength dependence of the opposition effect at laser wavelengths of 1.152 and 3.391 μm, for the same samples, viewing geometries, and sensor acceptance angles in order to check the theoretical analysis.

Study of Optical Transitions in Disordered Thin Films of Ionic Compounds as a Function of Conditions of Preparation

A. Barrière, and A. Lachter,
Laboratoire de Recherches en Electrotechnique et Physique du Solide,
Université de Bordeaux I, 351, Cours de la Liberation, 33405 Talence
France

The AlF_3 and MgF_2 thin films are prepared by vacuum thermic evaporation and sublimation. The temperature of the substrate at the same moment of the deposition of the vapours and their velocity of condensation remain the principal parameters of the fabrication. They establish the state of crystallization of the layers (determined by X-Ray diffraction), the time of the preevaporation of the powder and the nature of the crubible on wich depends the composition of the samples (measured by retrodiffusion of α particles and α.X reactions).

In all our samples, we found some quantity of sodium. The presence of this element can be explained bya preferential evaporation, in the beginning of the fabrication, of some fluorine compounds contained in the basic powder. A preevaporation of the last one before the reception of the vapours permits a huge reduction of the Na/Mg or Al ratio.

The analysis shown, morever, in the layers, an absence of fluorine which follows the evolution of the sodium tenor. It is from these anion defeciencies that one can interpret the electric conduction under the initial vacuum.

On placing the samples in the atmosphere, we can observe an absorption of water, followed by a diffusion into the thin film. This mecanism corresponds to a filling up of the majority of the fluorine defeciencies by OH^- ions. This is detected by a study of the intramolecular vibrations of the system (Infra Red absorption). This process of distribution explains the electric stabilisation phenomena which occur on placing the films in the atmosphere. It can also explain the different conductivities observed in coming back in vacuum.

The several mecanisms of conduction considered, assume the existence of abundance of localised states (coulombien centres and traps). The characterization of these states has been made from the examining together, thermoluminescence of the thin films and thermally stimulated currents of the sandwiches metal-MgF_2 or AlF_3-metal.

This study shows, morever, that the short distance disorder which characterizes the materials in bulk is true in the thin films even in the case where they are strongly disordred. Then, one can consider some delocalisation of the carriers of the charges.

In a domain of incident radiations of energies of between 1,5 eV and 15 eV, a study of optical absorption as a function of the degree of crystallization and of the composition of the samples, shows that the ionic compounds studied can be discribed by a diagram of energy bands, alternatively allowed and forbidden. The notion of delocalisation of the carriers in the allowed bands can still be considered, even in the case where the materials present a strong degree of disorder. Elsewhere, this study gives rise the homogeneity of the films. In the basic matrice (MgF_2 or AlF_3), some inclusions of Na $MgF_{3-x}(OH)_x$ or Na $AlF_{4-x}(OH)_x$ coexist in state of mixture after the samples in the atmosphere.

Evaporation or sublimation from a tantalum crucible leads to some new TaO_2F inclusions.

The analysis of optical absorption spectra allows the characterization of fundamental transitions between the last occupied states of anions and the first empty states of cations of these materials. The latter have weak interactions between each other in the boundary zones.

Some important variations of the fundamental edge and the appearance of wide absorption tails are a consequence of increasing structural disorder, or of the number of the inclusions. These phenomenas can involve the creation of internal electric fields acting as a broadening of the states in the border of the allowed bands.

This study gives, at last, a qualitative representation of the distribution of the localised states in the forbidden gap. This result served as basis for the interpretation of the electric conduction mecanisms in the materials.

BIBLIOGRAPHIE

(1) A. Barrière - Thèse de doctorat es sciences - Bordeaux 1976.

(2) B. Saboya, J.F. Chemin, J. Roturier, - A. Barrière, Y. Danto et J. Salardenne - J. Phys. D. Appl. Phys. Vol 8 (1975) 1008.

(3) J. Salardenne, Y. Danto, A. Barrière - Ann. Chim. 10 (1975) 201.

(4) Y. Danto - Thèse de doctorat es sciences - Bordeaux (1976)

(5) A. Barrière, Y. Danto, J. Salardenne et A. Schallon - Thin Solid films 12 (1972) 539.

(6) A. Barrière, Y. Danto et J. Salardenne - Thin Solid Films 16 (1973) 513

(7) A. Barrière, Y. Danto et J. Salardenne - Thin Solid Films 26 (1973) 201

(8) A. Barrière, Y. Danto et J. Salardenne - Thin Solid Films 26 (1975) 273

(9) A. Barrière - Communication "Work Shop" - Montpellier - Sept (1976)

(10) A. Barrière - to be published in thin solid films - Sept (1976)

(11) A. Barrière - to be published in thin solid films - Sept (1976)

INFRARED IMPURITY AND FREE-CARRIER ABSORPTION IN SILICON-SILVER FILMS

S. O. Sari, P. Hollingsworth Smith and H. S. Gurev
Optical Sciences Center, University of Arizona, Tucson, Arizona 85721

SUMMARY

Electronic, vibrational, and impurity transitions, as well as free carrier absorption, can be studied optically in a semiconductor film on a metal substrate. We have examined a number of such film combinations produced by chemical-vapor deposition of silicon on evaporated silver surfaces. These silicon layers are disordered and have thicknesses varying between 0.5 μ and 5 μ. They have been investigated in a wavelength range of 0.3 μ to 15 μ. Below the fundamental absorption edge where silicon becomes relatively transparent, multiple-beam interference is observed. A typical spectrum is given in Fig. 1, which shows a sequence of reflectivity curves versus wavelength for silicon layers of increased thickness. Reflectivity minima belong to fringes of various orders. Near 9-μ in this reflectivity spectrum the depth of fringes increases and a splitting is observed within a given order. A detailed analysis shows that this behavior is due to the presence of an impurity transition which is coupled to electromagnetic normal modes of the silicon layer, i.e. a polariton in the film. It has been necessary to calculate the polarization in the film quantum mechanically, and we have included both oscillator damping and free carrier conductivity in our treatment. An exact expression for the film reflectivity is used as a basis for a detailed numerical comparison of a one oscillator model to reflectivity line shapes. A sequence containing a number of individual films yields good agreement in this comparison. This gives values for several silicon parameters whose meaning will be discussed. These measurements

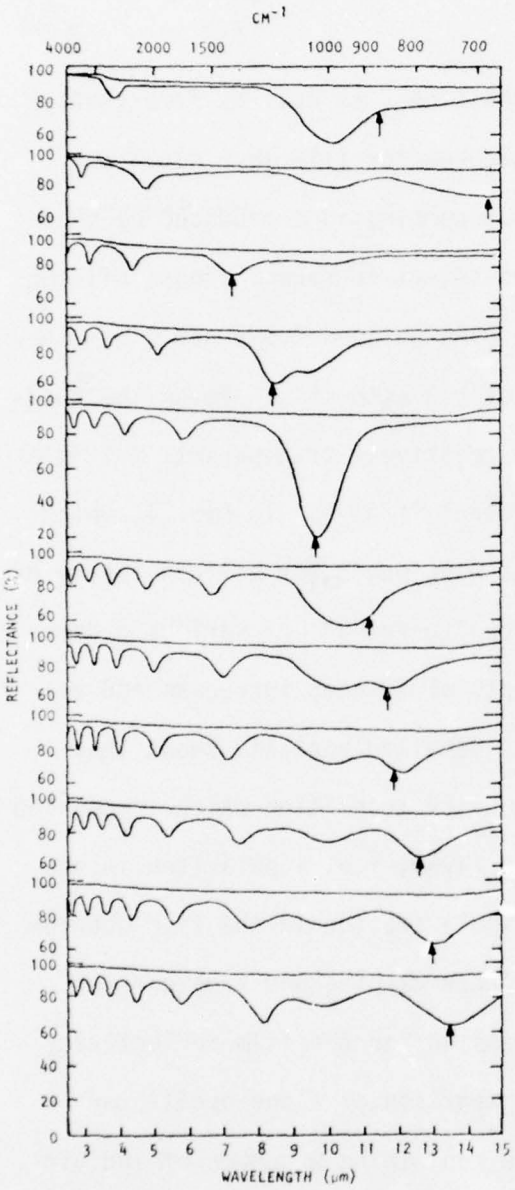

Fig. 1. *Infrared reflectivity* spectra versus wavelength for a sequence of silicon film layers of increasing thickness. A novel interferometric effect is seen near 9 μ, splitting a fringe in a given order. This behavior is explained by a simple polariton model discussed in the summary. Arrows in the figure show location of reflectivity minima near 9-μ which would be present in the absence of the impurity transition.

are compared to those in bulk crystals of silicon. The film conductivity determined in the present measurements is small though the free-carrier concentration is sizeable indicating disordered silicon in which the carriers have a very small mean-free path. The transition responsible for the 9-μ absorption is well-known and has been studied by Briggs, Fan, Kaiser and others. It is known to be due to an oxygen impurity in silicon. A number of interpretations have been proposed for explaining the nature of this transition. Comments will be made on these models in light of an observed anomaly in its oscillator strength.

SURFACE, GUIDED AND INTERFERENCE EM-WAVES IN ATTENUATED INTERNAL REFLECTION (AIR) PRISM SPECTROSCOPY*

A. Hjortsberg, W. P. Chen and E. Burstein
Department of Physics and the Laboratory for Research on the Structure of Matter, University of Pennsylvania, Philadelphia, Pa. 19174

Surface, guided and interference (Fabry-Perot) EM-waves occurring in three-media prism configurations are examined. It is shown that AIR-spectroscopy in which one or more of these modes are excited, gives enhancement of fields and increased interaction lengths at the interfaces of the specific prism configuration. As a probe of surface and thin film properties, AIR-spectroscopy can be more sensitive than spectroscopic techniques using volume EM-waves.

The surface, guided and interference EM-modes of the three-media configurations occur in different frequency and wave vector regions. A single prism is used for the excitation and detection of these modes in either the Kretschmann[1] prism-dielectric film-air structure (Fig. 1a) or the Otto[2] prism-air-dielectric configuration (Fig. 1b). The types of leaky modes that occur in the two configurations are shown in Fig. 2.

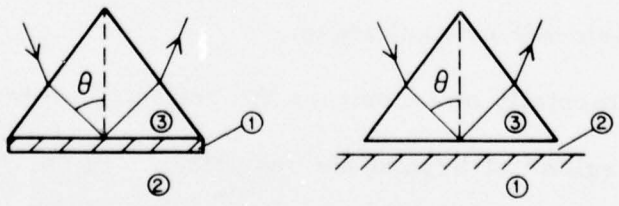

Fig. 1 Kretschmann and Otto three-media configurations used in AIR-spectroscopy, $\epsilon_3 > \epsilon_2 > 0$.

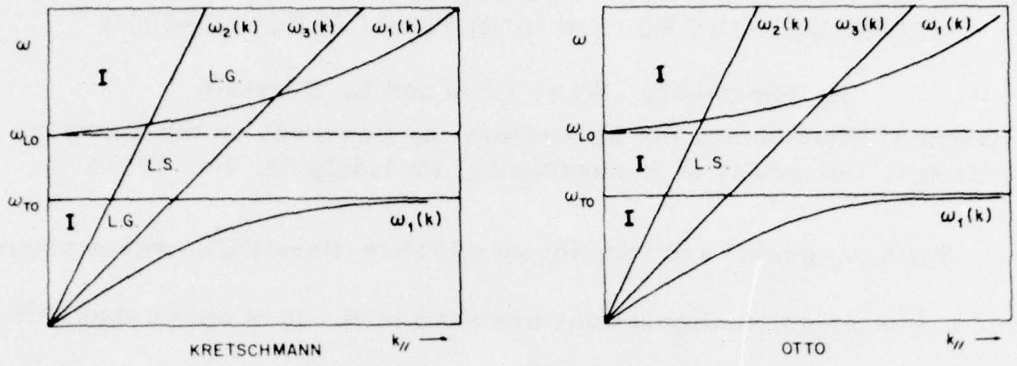

Fig. 2 Wavevector and frequency regions where leaky surface (LS), leaky guided (LG), and interference (I) EM-modes occur for the Kretschmann and Otto prism configurations. The ω_1, ω_2 and ω_3-lines represent the dispersion relation for volume EM-waves in the three media.

Excitation of the modes occurs when the wavevector parallel to the surface and the frequency of the volume EM-wave in the prism match those of the modes. This is in contrast to conventional spectroscopy in which only frequency is matched. The mode dispersion relation derived from AIR-spectroscopy as well as the excitation resonance width and magnitude can then provide more detailed information about the involved media. AIR-spectroscopy goes beyond attenuated total reflection (ATR) spectroscopy in that one makes use of the excitation of modes at angles of incidence below as well as above the prism-air critical angle.

Experimentally one monitors the reflected intensity either from the "excitation region" or beyond the "excitation region," whereas it arises from radiative decay of the free-running wave.[3] Data is obtained either as a function of incident angle at fixed frequency, or from fixed angle frequency scans. Various examples of the use of surface, guided and interference

modes in AIR prism configurations for the investigation of thin films, surfaces and interfaces will be given.

References

* Research supported by the U. S. Office of Naval Research and the National Science Foundation.

1. E. Kretschmann, Z. Physik 241, 313 (1971).

2. A. Otto, Z. Physik 216, 398 (1968).

3. W. P. Chen, G. Ritchie and E. Burstein (to be published).

EVALUATION OF THIN FILM COATINGS BY ATTENUATED TOTAL REFLECTION*

R.T. Holm, E.D. Palik and J.W. Gibson
Naval Research Laboratory, Washington, D.C. 20375

and

M. Braunstein and B. Garcia
Hughes Research Laboratory, Malibu, CA 90265

We have made a number of calculations of attenuated-total-reflection (ATR) spectra of thin films on a bulk substrate in order to determine the optimum conditions under which ATR should be done to determine the film absorption constant. While real anitreflection (AR) coatings typically consist of two or more films of appropriate indices of refraction and thicknesses, we start first with one film on a substrate. Depending on the magnitudes of the indices of refraction of the two materials, interesting ATR effects occur for both s- and p-polarized radiation as a function of the angle of incidence inside the bulk. In some cases, as the angle of incidence increases the evanescent wave switches from the film-air interface to the substrate-film interface. Interference fringes in the film appear which depend on the absorption constant of the film and are not present if there is no absorption. In a typical ATR experiment a trapezoid of the substrate material is used to obtain multiple reflections, often as many as fifty. Our calculations indicate that in an optimum case of a ThF_4 film 2 μm thick on a ZnSe trapezoid with 50 reflections, with the internal angle 31.5^{o}, with s-polarization at a wavelength of 3.8 μm and a peak absorption constant of 10 cm^{-1}, the ATR is 0.25. For an absorption band with a peak absorption constant of 1 cm^{-1}, the ATR scales to 0.85, still a large effect.

*Supported in part by ONR Material Sciences Division and DARPA monitored by RADC/ET.

Plans are underway to measure the OH and CH vibration bands at 2.9 μm and 3.4 μm in single films of ZnSe and ThF_4 on CaF_2 trapezoids in an attempt to determine the absorption constant quantitatively. The main problem so far has been to achieve a clean trapezoid surface free of measurable OH and CH with the present sensitivity of the experiment. Plasma cleaning, vacuum baking and ultrasonic cleaning have been tried but residual absorption as large as 5% for OH and 2% for CH is still present on the trapezoids. Once this contamination is minimized, absorption in films laid down on heated and unheated substrates will be studied. While the main thrust of the present effort is to produce films with minimal absorption at 2.9 and 3.4 μm, the sensitivity of the experiment also allows us to search for vibration bands of other contaminants.

Calculations for a double layer AR coating indicate that it is probably not feasible to determine the individual absorption losses of each film in the double layer. This can better by done on the single films as evaporated on individual substrates. However, the total absorption in a double layer could be determined. The double-layer calculations also indicate interesting resonance-like losses in the film layers as the internal angle of incidence is increased. The resonances are extremely sharp in angle ($< 0.5^{o}$) and depend on the various parameters of the two films and the substrate. For a film of intermediate index on a film of low index on a substrate of high index, these ATR losses represent the launching of a guided wave in the outer intermediate-index film in a manner analogous to intergrated optics techniques.

We thank M. Hass for helpful discussions.

TEMPERATURE DEPENDENCE OF THIN FILM POLARIZER

by

D. W. Ricks, S. Seitel, and E. A. Teppo
Naval Weapons Center
China Lake, CA 93555

The recently developed thin film dielectric polarizer (TFDP) is efficient and resistant to damage at high power levels. By coating a glass substrate with layers of dielectric materials of alternately high and low index of refraction, manufacturers have achieved 99% or better polarization efficiency and damage thresholds of more than 20 GW/cm^2. The trend today is away from the limited supply of expensive crystal polarizers and toward the less expensive TFDP.

Figure (1) shows reflected "p" polarization as a function as incident angle for two separate TFDPs. It will be noted that the "p" polarization curve has a definite minimum reflectance which we call "R_{min}" at the "polarizing angle". The problem with TFDPs is that due to the steepness of the "p" polarization curve, the performance of the TFDP is often very sensitive to small changes in the polarizing angle or in R_{min}. We tested six (6) TFDPs, two off-the-shelf samples fom each of three manufacturers. We found that every TFDP exhibited both temporary and long-term changes in the "p" reflectance curves as a result of a change in ambient temperature. The temporary change was a decrease in the polarizing angle with an increase in temperature; the values were 1.7 mrad/1° C, 1.3 mrad/° C and 0.65 mrad/1° C for the three manufacturers.

There were two long-term changes in the "p" reflectance curves due to temperature cycling. The first of these was an increase in R_{min} as shown in figure (2) for one sample. Also shown in the figure is the second long-term change, a residual polarizing angle shift upward after a return to room temperature. This shift was observed in all TFDPs tested.

The temporary change is probably due to a change with temperature in the index of refraction and thickness of the thin film materials. The second type of change is longer lasting, less predictable, and could be accelerated by the application of heat. Military systems using TFDPs typically undergo temperature cycling during acceptance testing and this may significantly vary the performance of the optical system. Though the sample

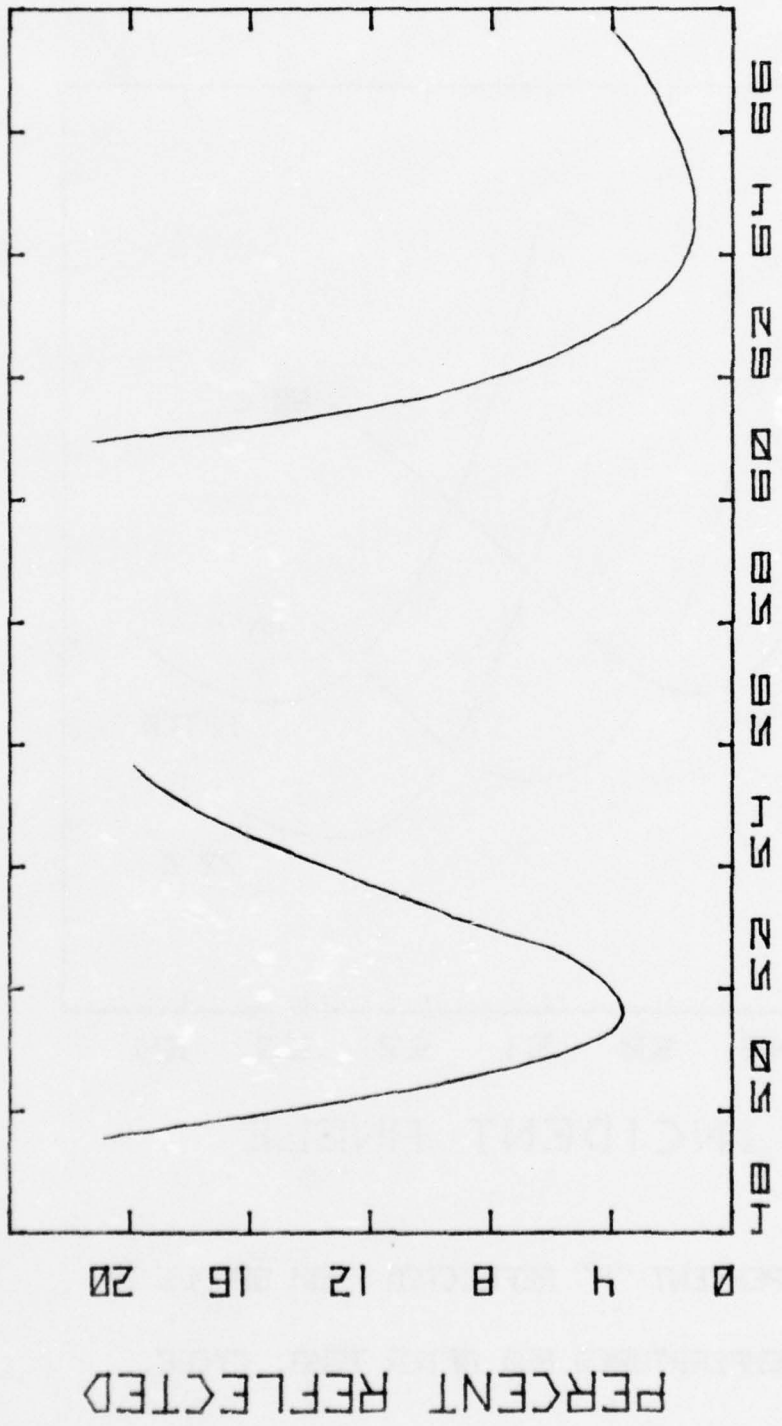

FIGURE 1. PERCENT "p" REFLECTED FROM TWO TFDPS. SPECIFIED 53±2° AND 59±2°; $R_{MIN} \leq 0.5\%$.

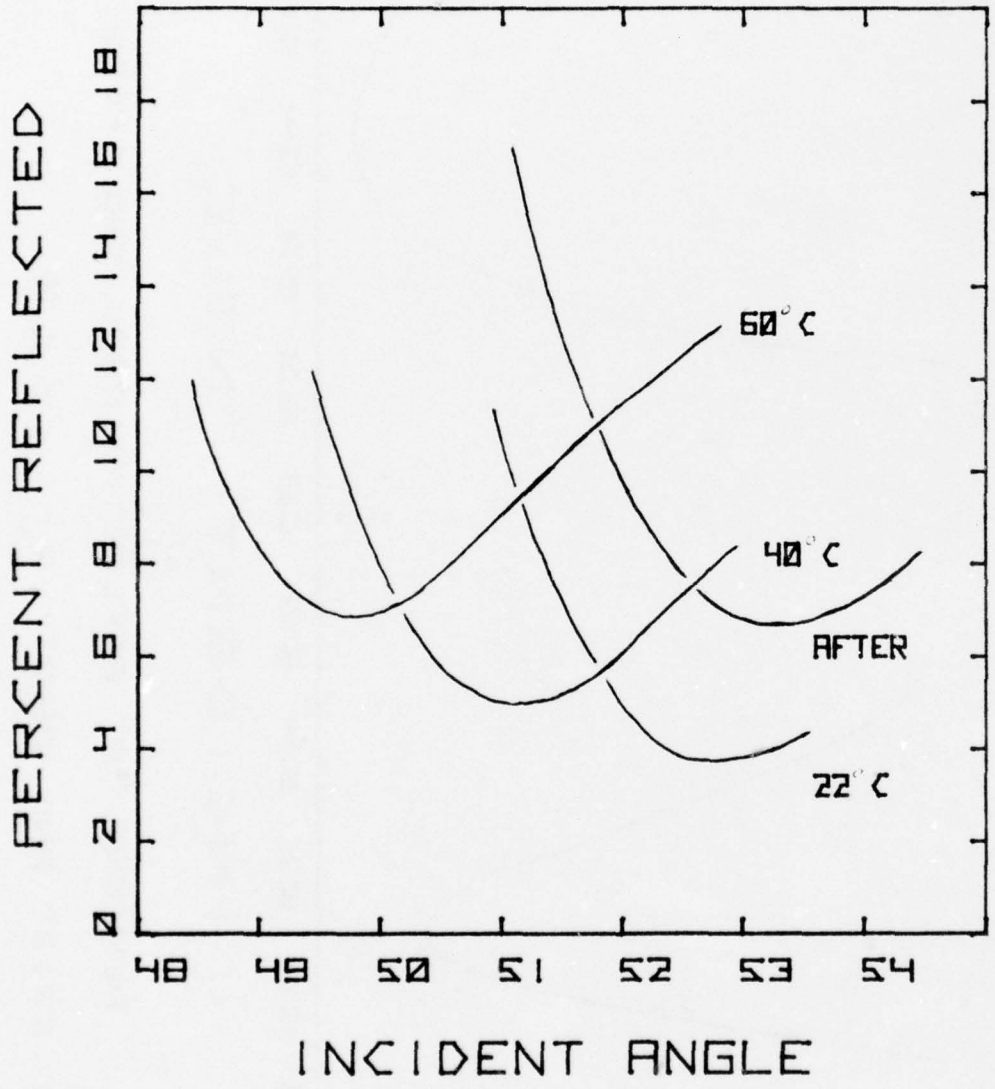

FIGURE 2. PERCENT "P" REFLECTED FROM SAMPLE 3A AT VARIOUS TEMPERATURES AND AFTER TEMP. CYCLE.

size was small it is fair to say that reproducibility is still a significant problem and thermally dependent properties of the TFDP restrict the use of this new component.

INFRARED LIGHT SCATTERING FROM SURFACES COVERED WITH MULTIPLE DIELECTRIC OVERLAYERS

J. M. Elson
Michelson Laboratories, Naval Weapons Center
China Lake, California 93555

In order to improve the performance of infrared optical systems, it is important to understand the sources and/or properties of scattered light emanating from various types of surfaces. Considering surface irregularities as a primary cause of scattering, we have developed a vector perturbation theory designed to predict the distribution of scattered light from surfaces with dielectric coatings. Dielectric layers may function as reflectance enhancing multilayer stacks or protective coatings. We also note here that first order scattering depends on the surface topographical characteristics and other factors such as dielectric permittivities, incident energy, and angles of incidence and scattering. These two areas are independent and in this discussion we consider only the latter dependence. We note, however, that the surface characteristics have a profound effect upon the scattering properties of a given surface.

It is interesting to note that for multilayer stacks on gratings theoretical results predict vastly different diffraction properties depending on the type of grating profile structure involved. Two grating profile structures are considered. First, the grating substrate profile is assumed to permeate the entire dielectric stack, i.e., each interface present in the dielectric stack is assumed to replicate the substrate profile. Second, the substrate is assumed smooth as are all succeeding dielectric layers with the grating profile in the outermost layer only. The first case is predicted to provide a much more stable diffraction pattern for layers having quarter-wave optical

thickness. Relatively small changes in layer thicknesses (e.g., thermal expansion or fabrication errors) are predicted to cause negligible changes in the diffraction pattern for this case (not so for the second case). It is also predicted that the angle between the plane of incidence and the direction of the grating grooves is a convenient parameter to control the polarization ratio in the diffracted orders. This may be useful to create a reflection grating/beam sampler which is independent of the incident polarization.

RESIDUAL ABSORPTION IN INFRARED MATERIALS

M. Hass
Naval Research Laboratory
Washington, D.C. 20375

B. Bendow
Rome Air Development Center
Hanscom AFB, MA 01731

During the past few years, great strides in both the measurement and understanding of the origin of residual absorption in infrared materials have occurred. This has come about largely as a result of the need for highly transparent infrared windows for high energy lasers, although prospects for IR integrated optics and fiber optics have also served as motivations.

Common infrared window materials are ionic crystals such as the alkali halides, alkaline earth and fluorides, and semiconductors such as III-V's and II-V's. They are characterized by a highly transparent region (absorption $\lesssim 10^{-3}$ cm^{-1}) between the reststrahlen band at long wavelengths (associated with lattice motion) and the fundamental absorption edge at short wavelengths (associated with electronic motion). In practice, of course, the choice of a particular infrared window depends not only upon its absorption coefficient in the region of interest, but also upon its mechanical thermal, environmental and other properties. Also, considerable variations in the apparent residual absorption coefficient are observed in the transparent region due to

absorption and scattering by impurities, imperfections, and surfaces. Nevertheless, an extensive body of experimental data has been amassed, especially with respect to the region of the lattice tail, in a wide variety of materials. This data is found to display clear trends with respect to the magnitude as well as the temperature and frequency dependence of the absorption in the transparent regime. One finds, in most cases, a relatively smoothly varying lattice tail spectrum as a function of frequency in ionic solids, while semiconductors display structure on the lattice tail. The classification and interpretation of the observed trends has aided in distinguishing intrinsic from extrinsic features in spectra, and in deducing the limiting, intrinsic absorption properties of infrared window materials. Advances in measurement techniques have enabled the separation of surface and bulk contributions to absorption and data of this sort are now available for a large number of materials at many frequencies throughout the transparent regime. The effects of impurities on the absorption in actual materials has also been investigated for a variety of cases.

A substantial theoretical effort has been directed at identifying the principal mechanisms determining residual lattice absorption in transparent solids. Both mechanical and electrical anharmonicity can contribute to the absorption, although their relative roles in specific cases remains controversial. Nevertheless, our theoretical understanding of many-phonon absorption

has advanced sufficiently to account successfully for many aspects of the frequency and temperature dependence of a variety of infrared materials. Recent investigations have also improved our understanding of the structural features in both ionic and semiconducting materials.

The close involvement of both theory and experiment in unraveling the origins of the residual absorption in infrared materials has led to very significant advances in the past few years and may be expected to continue in the future.

MECHANISMS FOR PRODUCING LATTICE ABSORPTION: ONE OR TWO?

Herbert B. Rosenstock
Naval Research Laboratory
Washington, D C. 20375

Conventional wisdom proclaims that under certain conditions a model crystal absorbs light only at one (or at most a few) frequencies. These are called the "limiting", or "Reststrahl" or "TO" frequencies. They are infinitely sharp, and their position and intensity are independent of temperature. The conditions under which this is true are said to be two:

(A) No anharmonicity (i.e., the potential function is quadratic in the ionic displacements or, equivalently, the ionic displacements are linear in the interionic forces); and

(B) No non-linear moment (i.e. the electric dipole moment is linear in the ionic displacements).

We shall refer to a crystal in which both (A) and (B) are satisfied, and which therefore exhibits absorption at the reststrahl frequencies only, as a "linear" crystal. When the crystal is not linear - i.e. when either (A) or (B) are untrue - absorption can arise that is not sharp, far from reststrahl frequencies, or temperature-dependent. Such absorption is in fact observed. The question therefore arises whether this is "due to" violation of (A) or (B) - that is, due to anharmonicity or due to a nonlinear electric moment. Mathematically we can use the formulation of Szigeti[1].

$$V = \frac{1}{2}\sum_i \omega_i^2 Q_i^2 + \sum_i \sum_j \sum_k b_{ijk} Q_i Q_j Q_k$$

for the potential and

$$P = \alpha_o Q_o + \sum_i \sum_j \beta_{ij} Q_i Q_j$$

for the dipole moment. The Q_i are the normal coordinates (orthonormal combinations of the atomic displacements), Q_o is the reststrahl oscillator, the b_{ijk} the anharmonic coefficients and the β_{ij} the coefficients for the nonlinear moment. The crystal is "linear" by our definition if both the b's and the ß's vanish.

It seems plausible that mechanisms described by mathematical expressions as similar as these two should be physically related. Others have also attempted to compute[1] effects jointly caused by both mechanisms, showing that both quantities are related to the matrix elements of the Hamiltonian.[2] Recently, Boyer[3] et al. noted that both mechanisms are a consequence of charge overlap, and their distinction thus conventional, or traditional in nature. Our purpose here is to examine the physical basis of both in order to ascertain what their relationship is. We find that a non-linear electric moment invariably implies existence of anharmonicity; conversely, anharmonicity implies a non-linear moment whenever extended, rather than only point, charges exist in the lattice. Implications for attempts to separate the two mechanisms experimentally[4] will be discussed.

References

1. "Lattice Dynamics", R.F. Wallis, editor (Pergamon, 1965). B. Sziegeti, p. 405.

2. J.S. Langer, A.A. Maradudin and R.F. Wallis, in Ref. 1, p. 411.

3. L.L. Boyer, J.A. Harrington, M. Hass, H.B. Rosenstock, Phys. Rev. B11, 1665 (1975).

4. R. Hellwarth and M. Mangir, Phys. Rev. B10, 1635 (1974).

TEMPERATURE DEPENDENCE OF MULTIPHONON ABSORPTION IN ZINC SELENIDE

P. A. Miles
Raytheon Company
Bedford, Massachusetts

Previous attempts to observe the temperature dependence of intrinsic multiphonon absorption in ZnSe at 10.6μm have failed mainly due to its masking by extrinsic impurity absorptions and partly to a failure to separate bulk and surface components. The development in late 1975 of higher purity zinc selenide made by chemical vapor deposition has reduced the extrinsic component by an order of magnitude and allows the intrinsic component to be observed. Calorimetry was carried out in a conventional vacuum calorimeter using a 20 watt CO_2 laser on two separate rectangular bar samples of nominal length 1 cm and 4 cms. The samples were heated by pressing a flat wire heating coil against one of the flat lateral surfaces. The gross temperature was sensed by a chromel-alumel thermocouple and increased in 20° steps between 20°C and 300°C. At each ambient level, temperature stability was achieved by manual variation of a stabilized a.c. source using the high sensitivity calorimeter thermocouple circuit itself as an indicator. In all cases temperature drift over a two minute interval preceding laser turn-on was kept to less than 5 per cent of the expected temperature change during a two minute laser heating period. The resultant ballistic thermal characteristics were analyzed using both slope and peak methods to establish consistency.

The overall absorption of the 4 cm sample increased by a factor of 3 over the range 20°-300°C. Unexpected variations in the slope of this curve only became intelligible when compared with the corresponding 1 cm sample data. Taken together these curves were used to separate the temperature variations of surface and bulk absorptions. Surface losses showed a monotonic increase over the range 20°-80°C, an abrupt drop between 120 and 180°C to a steady level between 180°-240°C, about one half its original

value, and a fast monotonic rise between 240°and 300°C. This profile suggests the evaporation or dissolution of a surface contaminant at temperatures about 120°C, followed eventually by the thermal activation of a remaining surface specie.

The remaining bulk absorption characteristic now shows a smooth monotonic increase. Its interpretation in terms of a residual extrinsic component and an intrinsic multiphonon component is still somewhat ambiguous, however. An extrapolation to 10.6μm of the multiphonon spectrum observed at wavelengths beyond 11μm suggests a 10.6μm value of 2×10^{-4} cm^{-1} at 20°C, made up of 4 and 5 phonon processes. Current high order phonon theory predicts a temperature variation between T^4 and T^5, reduced by a factor that accounts for the reduction of phonon frequency with increasing temperature. Indeed, the present experimental data, together with the value 2×10^{-4} cm^{-1} at 20°C are consistent with such a variation up to 170°C, but only if it is assumed that the remaining 2×10^{-4} cm^{-1} extrinsic component drops off rapidly at temperatures between 20° and 120°C. In any case, the observed rate of increase at temperatures between 170°C and 300°C is too low to fit the predicted function. This indicates either a more rapid decrease in phonon frequency than expected, or the influence of a specific phonon spectral feature.

IMPURITY ABSORPTION IN CVD ZnSe

Herbert G. Lipson
Deputy for Electronic Technology (RADC)
Hanscom AFB, MA 01731

In this work Fourier transmission spectroscopy and laser calorimetry measurements are used to determine the presence and strength of impurity bands in CVD ZnSe samples. As ZnSe is a prime candidate for high power laser windows at the 10.6μm CO_2 wavelength and a possible choice for the shorter CO and chemical laser wavelengths, it is important to establish the level of impurity absorption between 2.5 and 12μm (4000 to 833 cm^{-1}).

Samples which were state-of-the-art over two years ago show a number of bands between 2500 and 833 cm^{-1}. Our measurements indicate that the strongest peaks in this material occur at about 1630 and 1190 cm^{-1}. We find that a contribution from an impurity band in the vicinity of 1000 cm^{-1} increases the 10.6μm (943 cm^{-1}) absorption to the 3 to 5 x 10^{-3} cm^{-1} level.

The temperature dependence of ZnSe absorption between 295 and 570°K was determined over the 500 to 1000 cm^{-1} range by transmission spectroscopy measurements on a sample whose room temperature absorption spectrum is shown in Figure 1. This sample, characteristic of relatively recent state-of-the-art ZnSe, had an absorption of 2.3 x 10^{-3} cm^{-1} at 943 cm^{-1}, as measured by laser calorimetry. Impurity absorption between 1800 and 800 cm^{-1} is shown in the insert.

Absorption values below 5 x 10^{-3} determined from transmission spectroscopy are subject to error in estimating the background level, but the presence of band peaks can be established. As can be seen in Figure 1, impurity band tails at the higher frequencies still increase the minimum absorption to a higher level than expected from extrapolation of the multiphonon peak in the vicinity of 800 cm^{-1}. The impurity bands do not broaden appreciably at higher temperatures and make little further contribution to intrinsic multiphonon absorption at elevated temperatures. The multiphonon contribution to absorption at 943 cm^{-1}, as determined from theoretical calculations is estimated to be ~10^{-4} cm^{-1}.

Present state-of-the-art ZnSe has absorption at 943 cm^{-1} of 4 to 8 x 10^{-4} cm^{-1}, close to the predicted intrinsic level. Low level absorption bands at 1630 and 1200 cm^{-1} have been detected by transmission spectroscopy in ZnSe, whose absorption at 943 cm^{-1} was found to be 8 x 10^{-4} cm^{-1} by laser calorimetry. While transmission techniques cannot be used to accurately determine absorption levels in this range, bands in the vicinity of 1000 cm^{-1} associated with those observed at 1630 and 1200 cm^{-1} in samples with higher impurity concentrations may still be present and contribute to absorption at 943 cm^{-1}. The band at 1630 cm^{-1} extends to the CO laser region and is responsible for the larger absorption value, 5 x 10^{-3} cm^{-1} measured in the frequency range for this sample.

While most of the impurity bands shown in Figure 1 are present in the bulk, the small band at 1545 cm^{-1}, is a result of a surface

condition. This band was considerably reduced after heating the sample in air during absorption temperature dependence measurements. Its peak absorption is found to increase after a sample is left in air and can be removed by cleaning the sample in acetone. The largest contribution to absorption at 943 cm^{-1} in the most recently produced CVD ZnSe has been attributed to surface losses.

In summary, tails of weak impurity bands detected by Fourier transmission spectroscopy have been seen to contribute to absorption at high energy laser frequencies and may be responsible for measured values higher than those estimated from intrinsic absorption.

AD-A037 737 OPTICAL SOCIETY OF AMERICA WASHINGTON D C F/G 20/6
OPTICAL PHENOMENA IN INFRARED MATERIALS.(U)
1976
AF-AFOSR-3061-76
UNCLASSIFIED AFOSR-TR-77-0163 NL

2 OF 3
AD A037737

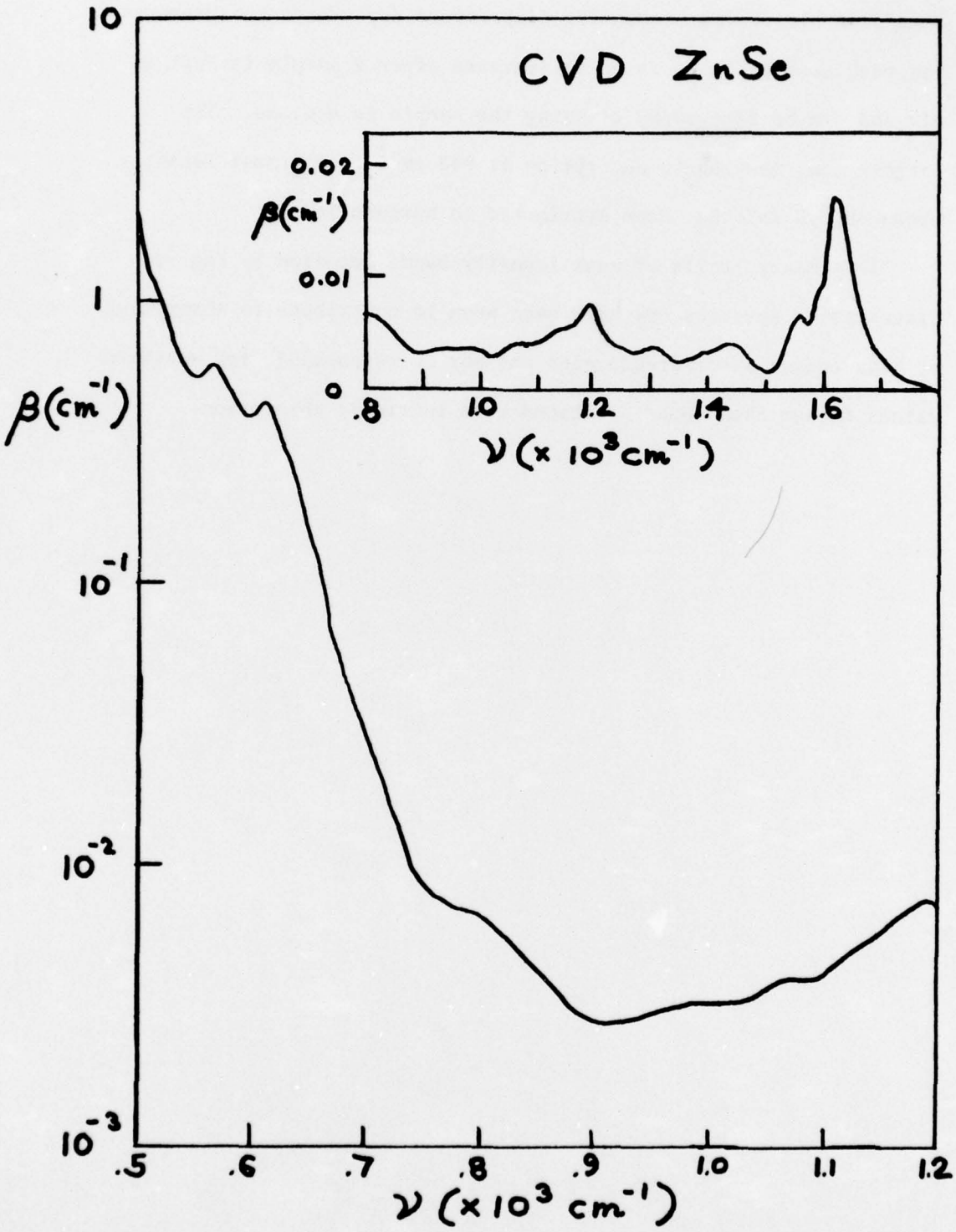

Figure 1. Multiphonon and impurity absorption in CVD ZnSe from transmission spectra ($\beta_{10.6\mu m} = 2.3 \times 10^{-3}$ cm^{-1}, determined from laser calorimetry).

NOTES

INFRARED ABSORPTION IN GERMANIUM AND SILICON*

Don A. Gregory and James A. Harrington
University of Alabama in Huntsville
Huntsville, Alabama 35807

and

Marvin Hass
Naval Research Laboratory
Washington, D. C. 20375

The infrared absorption associated with carriers in germanium and silicon may cause thermal blooming when these materials are used as infrared laser windows. It is important, therefore, to make a detailed study of how carrier absorption depends on sample doping, temperature and frequency in order to obtain improved window materials for 3 to 10 μm infrared lasers. In this investigation, we report our measurements on the frequency and temperature dependence of the absorption coefficient in germanium and silicon and compare these results with a simple calculation based on carrier absorption.

The dominant carrier absorption in the near infrared (3 to 10 μm) can be associated with either free electrons or intravalence band holes. In calculating the infrared absorption in germanium, Bishop and Gibson[1] expressed the absorption coefficient β (T) in terms of the lattice absorption β_{latt}, the electron and hole concentrations $N_e(T)$ and $N_h(T)$, and the electron and hole cross sections $\sigma_e(T)$ and $\sigma_h(T)$ by the expression,

$$\beta(T) = \beta_{latt} + N_e(T)\sigma_e(T) + N_h(T)\sigma_h(T).$$

The lattice absorption β_{latt} can be assumed to be effectively temperature independent compared to the other factors and to a first approximation the cross sections σ are also assumed to be temperature independent. The population factors N, however, are strongly temperature dependent. Using this approach and values of cross sections obtained from measurements on heavily doped material, it is possible to calculate the infrared absorption coefficient at all wavelengths and temperatures.

One interesting result of this calculation is that for germanium, at least, there is an optimal doping level for maximum transmission at any wavelength. This has been studied at 10.6μm in previous work[1] but not at other important laser wavelengths.

The results of our calculations are compared with infrared absorption measurements obtained by laser calorimetry on samples of germanium of various doping levels. The results to date indicate that the simple theory is adequate although there are some small deviations which suggest that temperature dependent cross sections should be employed. For silicon, our calcula-

tion predicts that this material should be extremely transparent in the 3μm region. Our measurements of the absorption coefficient for the ultrapure silicon are indeed very low but there still appears to be some residual absorption of as yet unknown origin.

* Research supported by DARPA

[1] P. J. Gibson and A. F. Gibson, Appl. Optics 12, 2549 (1973).

FREQUENCY AND TEMPERATURE DEPENDENCE OF RESIDUAL LATTICE ABSORPTION IN SEMICONDUCTING CRYSTALS

Bernard Bendow and Herbert G. Lipson
Deputy for Electronic Technology (RADC)
Hanscom AFB, MA 01731

Stanford P. Yukon*
Parke Mathematical Laboratories
Carlisle, MA 01741

The purpose of the present work is to further our understanding of the nature of the multiphonon absorption which limits the infrared transparency of wide-gap semiconductors. The multiphonon spectra in semiconductors differ widely from those in most ionic crystals; they display substantial structure, deviating from the smooth exponential frequency behavior characterizing ionic solids. Also, anharmonic effects are less pronounced, so that structure persists into higher temperature spectra. It appeared desirable to obtain sufficient measurements to confirm these trends and to provide a theoretical basis for interpreting them. Moreover, it was desired to identify in which frequency and temperature ranges intrinsic behavior was manifested by state of the art samples of various semiconducting materials.

Our measurements, which were taken on a Fourier spectrometer and were also corroborated in certain regimes by calorimetric, emittance and photoacoustic measurements, indicate that structure persists into

---

* Research supported by Deputy for Electronic Technology (RADC), under Contract No. F19628-71-C-0142.

the multiphonon regime of ZnSe, Si, and GaAs, even at elevated temperatures (~500°K). At frequencies higher than ~$10^3 cm^{-1}$ in ZnSe and GaAs, and ~2 x $10^3 cm^{-1}$ in Si, the observed behavior appears to be extrinsic. Measurements were conducted on ZnS as well, but our samples appeared to be dominated by extrinsic effects over much of the region of interest.

The theoretical model invoked to interpret the results emphasizes the influence of the many-phonon density of states on the spectra. We find that this model is indeed successful in accounting for many features of the observed spectra, implying that the density of states, as opposed to $\underset{\sim}{k}$-selection rules, is the dominant influence determining the behavior displayed by the spectra. The model incorporates both nonlinear moments and anharmonicity, and thus allows one to investigate the effects of both of these mechanisms on the multiphonon behavior. Although one cannot unambiguously establish the precise mix of the two by analyzing observed spectra, nevertheless, one can deduce ranges for the moment and potential parameters which are consistent with the data. Thus, multiphonon measurements provide insight into the microscopic parameters governing the absorption processes in semiconducting crystals.

BULK AND SURFACE CALORIMETRIC MEASUREMENTS AT CO WAVELENGTHS *

S.D. Allen and J.E. Rudisill

Hughes Research Laboratories
Malibu, California

Laser calorimetry was utilized to measure the bulk and surface absorption coefficients of a series of long, thin bars by the M. Hass [1] technique. The lower limit of the apparatus for measuring absorption coefficient was determined by measuring a high quality bar of RAP grown KCl. The bulk absorption coefficient of this KCl bar at 10.6 μm is 6×10^{-5} cm^{-1}, a value which is essentially the intrinsic limit of the material as predicted by extrapolation of the multiphonon absorption edge [2]. The same exponential curve predicts an intrinsic absorption coefficient of 7×10^{-13} cm^{-1} at 5.3 μm. As it is not possible to measure absorption coefficients this small with standard calorimetric procedures, the measured absorption coefficient (assuming surface and specific impurity absorptions are absent or of similar magnitude as the bulk absorption) provides an error range for the calorimeter apparatus.

The optical absorption of RAP KCl grown in three different atmospheres - N_2/CCl_4, He/CCl_4, and $He/CO_2/CCl_4$ - was compared. Other materials measured include KCl doped with 1.75% RbCl (single crystal and press forged), SrF_2 (single crystal and cast), CaF_2 (cast), and CVD ZnSe. All samples were polished and surface finished by the current state of the art techniques.[3] Thermocouple attachment was made at three different places on the bar (front edge, middle and back edge) as a check on surface absorption and scattering. Ag or Al mirrors were evaporated onto the bars prior to thermocouple attachment to minimize direct scattering to the thermocouple.

The calorimeter head used in these experiments is made from standard glass pipe parts and is pumped by sorption pumps to eliminate any contamination of optical surfaces by oil. The laser is a cooled (0°C), 2 meter himiconfocal cavity, 10 watt cw device the output of which is focussed with an antireflection coated CaF_2 lens to a spot size of approximately 1mm at the center of the sample. The output power is distributed over 9 lines in the 5.25 μm to 5.5 μm region with most of the intensity in the 5.3 μm and 5.5 μm lines. The spectral intensity distribution of the laser has been quantitatively measured. The specification of the spectral distribution is important as preliminary results at the University of Dayton Research Institute [4] seem to indicate that some discrepancies in reported data at CO wavelengths lie in the differences in output wavelengths.

References:

1. M. Hass, J.W. Davisson, H.B. Rosenstock and J. Babiskin, Fourth Annual Conference on IR Laser Window Materials, 1974.

2. T.F. Deutsch, J. Phys. Chem. Solids, 34, 2091 (1973).

3. M. Braunstein and J.E. Rudisill, Fourth Annual Conf. on IR Laser Window Materials, 1974.
M. Braunstein, Third Annual Conf. on IR Laser Window Materials, 1973.

4. J. Johnston and G. Boner, UDRI, personal communication.

* Work was sponsored by the Defense Advanced Research Projects Agency; monitored by RADC/ETSO Hanscom Air Force Base, Massachusetts 07131

SURFACE AND BULK ABSORPTION IN HF/DF LASER WINDOW MATERIALS

A. Hordvik and L. Skolnik

Rome Air Development Center
Deputy for Electronic Technology
Hanscom AFB, MA 01731

We report measurements of both surface and bulk absorption at HF and DF laser wavelengths of a number of prospective high power laser window materials. Samples measured include LiF, MgF_2, CaF_2, SrF_2, BaF_2, ZnSe, Si, GaAs, MgO, and Al_2O_3. Both surface and bulk absorption losses are determined simultaneously utilizing a new photoacoustic technique. A chopped laser beam is incident on the sample, and the generated acoustic wave whose amplitude is proportional to the absorbed laser energy is synchronously detected with a piezoelectric transponder attached to the material. The transponder output is measured as a function of distance between transponder and beam, thus generating a curve of output response versus position of the incident laser beam. Since response curves for pure surface absorption and pure bulk absorption have entirely different functional dependences, it is possible to separate the composite curve into its surface and bulk contributions. In this manner, surface and bulk losses are measured simultaneously and nondestructively on the same sample. This photoacoustic technique has an additional advantage over conventional laser calorimetry in that it is an a.c. rather than a d.c. measurement so that extremely small laser powers may be utilized to determine low absorption coefficients. Typically, laser powers of 100 mw are sufficient to measure losses in the 10^{-5} cm^{-1} range.

Results indicate that losses dominate the absorption at mid-IR wavelengths for most of the samples tested. However, at HF laser wavelengths the bulk absorption coefficients of Si and Al_2O_3 (1.2×10^{-4} cm^{-1} and 2×10^{-4} cm^{-1} respectively) rank lower than even the fluorides which currently have bulk losses on the order of $\sim 3 \times 10^{-4}$ cm^{-1}. Therefore, while our results indicate that state-of-the-art silicon and aluminum oxide have bulk absorption coefficients close to their predicted intrinsic (multiphonon) limit, bulk absorption losses for currently available alkaline earth fluorides are probably still dominated by extrinsic (impurity) processes. Further, if surface losses in Al_2O_3 can be significantly reduced, this material would become an excellent candidate for a high power HF laser window.

MIXED FLUORIDES FOR MID-IR LASER WINDOWS

J. J. Martin*
Dept. of Physics, Oklahoma State Univ.
Stillwater, OK 74074

Herbert G. Lipson, Bernard Bendow and Audun Hordvik
Deputy for Electronic Tech., Rome Air Development Center
Hanscom AFB, MA 01731

Shashanka S. Mitra**
Dept. of Electrical Engineering, Univ. of Rhode Island
Kingston, RI 02881

We report investigations of crystal growth and infrared optical evaluation of mixed fluorides, including $KMgF_3$, $RbMgF_3$ and $KZnF_3$. Single crystals of the latter, which have the Perovskite structure, were grown by the Bridgeman method, utilizing the system described by Butler (Ph.D. Thesis, O.S.U., 1972, unpublished). We have also pulled crystals of $KMgF_3$ and $RbMgF_3$, using a modification of a puller for KCl, which has a graphite radiation shield and a special thermocouple added to allow operation at higher temperature. Various details of the crystal growth process will be discussed.

The infrared absorption of the grown crystals of $KMgF_3$, $RbMgF_3$ and $KZnF_3$ was measured by Fourier spectroscopy and photoacoustic calorimetry, at room temperature, in the frequency range 800-1800 cm^{-1}. In the range of higher absorptions ($\gtrsim 10^{-2}$ cm^{-1}) we obtain a characteristicly smooth, exponential-like variation of absorption with increasing frequency, although $KZnF_3$ does show enhancement suggestive of extrinsic effects, towards higher frequencies. The exponential decrease and absence of marked structure are features familiar from alkali-halide and alkaline earth fluoride spectra measured previously, and are believed to be a result of the dominance of anharmonic broadening and the lack of structure in the lattice density of

*Supported by Deputy for Electronic Tech., RADC, under contract F19628-76-C-0176.
**Supported by Deputy for Electronic Tech., RADC, under contract F19628-75-C-0163.

states. The magnitude and rate of decline for $KMgF_3$ and $RbMgF_3$ are nearly the same, implying that the Mg-F bond is the principal influence on the multiphonon spectrum. This is also supported by the similarity of these spectra to that of MgF_2, although the rate of decrease in the mixed fluorides is slightly slower than for MgF_2, and the overall magnitude is from 50% to 20% smaller in the range investigated.

NOTES

FAR-IR PHOTOCONDUCTIVITY IN SILICON DOPED WITH SHALLOW DONOR IMPURITIES

P. Norton*
Bell Telephone Laboratories
Murray Hill, New Jersey 07974

The photoconductive response from silicon doped with shallow impurities such as phosphorus has a spectral response with many interesting features, as shown in Fig. 1. The large peak and fine structure observed in the 250 - 450 cm^{-1} region are due to the photon interactions with neutral donor impurities which have energy states similar to those of hydrogen with a Rydberg smaller by a factor of 430. The details of these states have been studied extensively, beginning in the early 1950's. The broad response at frequencies below 200 cm^{-1} was only first observed in 1971 by Gershenzon et al[1] using backward wave oscillator tubes. This response is due to the photo-excitation of electrons off of negatively-charged impurity atoms, with similarities to the negative ion state of hydrogen. The existence of negative ion states for the shallow, hydrogenic impurities was predicted in 1953[2], but not confirmed experimentally

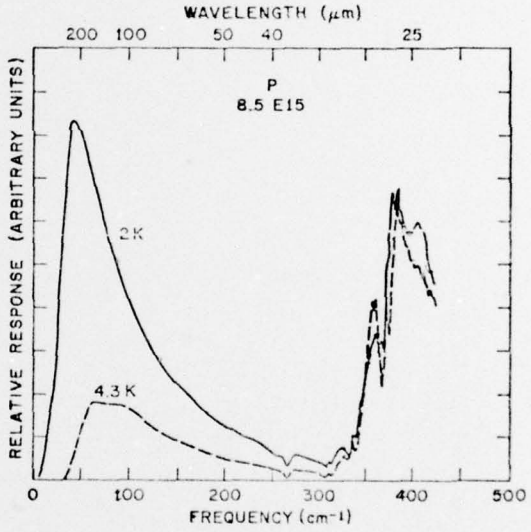

Fig. 1. Spectral response from silicon doped with P impurities, relative to a germanium bolometer, taken at two temperatures in the far infrared.

until 1967 in a study of bandgap photoluminescence by Dean et al.[3] The properties of these negative ion states have recently been investigated in some detail.[4-6] This paper will review the properties of these negative ion states, in their isolated condition, and the interactions they have with each other, together with describing the performance of a detector for the far infrared based upon these quantum levels.

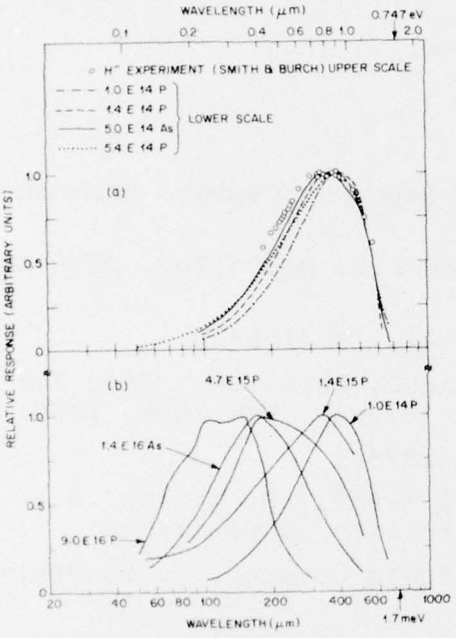

Fig. 2. (a) Spectral response from lightly-doped samples; (b) shifted response observed as doping concentration is increased.

The spectral response of several lightly-doped samples are shown in Fig. 2(a) in comparison to the photodetachment cross section measured for H^- by Smith and Burch.[7] The atomic result is shown shifted by the ratio of m^*/ε^2 as predicted by the effective mass theory. The agreement is very good as can be seen.

As the impurity concentration is increased above $10^{15}cm^{-3}$, the tails of the negative donor ion states begin to overlap, causing the formation of a band of energy levels. This band forms at a donor concentration of about 3×10^{15} cm^{-3}, and has been called the upper Hubbard band.[8] The upper Hubbard band is more formally described as forming from the states having two electrons per site, and this band together with the lower Hubbard band eventually overlap each other at a donor concentration of about $3\times10^{18}cm^{-3}$.

The weak binding energy of the negative donor ion states provide convenient quantum levels for a far-infrared photoconductive detector.[4,5] At 118.8 μm the quantum efficiency of a device based upon these levels has been measured using a pulsed submillimeter laser. The quantum efficiency was found to be between 1 and 5%. The response speed of the device is on the order of 1 nsec. As a heterodyne detector present results give noise equivalent powers near 10^{-16} W/Hz and improved design should permit operation near 4×10^{-19} W/Hz.

References

* Present address: Honeywell Corporate Research Center, Bloomington Minnesota 55420.

1. E.M. Gershenzon, G.N. Gol'tsman, and A.P. Mel'nikov, JETP Lett. 14, 185 (1971).

2. A.I. Ansel'm, Zh. Eksp. Teor. Fiz. 24, 83 (1953).

3. P.J. Dean, J.R. Haynes, and W.F. Flood, Phys. Rev. 161, 711 (1967); Localized Excitations in Solids (Plenum, New York, 1968).

4. P. Norton, J. Appl. Phys. 47, 308 (1976).

5. P. Norton, Phys. Rev. Lett. 37, 164 (1976); P. Norton, R. Slusher and M.D. Sturge, Appl. Phys. Lett., to be published.

6. M. Taniguchi and S. Narita, Solid State Commun., to be published.

7. S.J. Smith and D.S. Burch, Phys. Rev. 116, 1125 (1959).

8. A recent review of the subject matter relating to the Hubbard band model has been given by N.F. Mott in Metal-Insulator Transitions, (Taylor and Francis, Ltd., London, 1974).

Mercury Cadmium Selenide Infrared Detector Materials, C. J. Summers, D. A. Nelson, and C. R. Whitsett, Research Laboratories, McDonnell Douglas Corporation, St. Louis, Missouri 63166

$Hg_{1-x}Cd_xSe$ alloys with x-values between zero and 0.77 form a completely miscible series of solid solutions with the zincblende crystal structure[1]. Low x-value alloys are semimetallic and have negative energy gaps; high x-value alloys are semiconductors and have direct positive energy gaps. This variable energy-gap alloy system is being developed as an infrared detector material whose wavelength of peak response can be varied by controlling the alloy composition and with potential use as a spin-flip-Raman-laser material whose energy can be adjusted to coincide with laser pump frequencies to maximize efficiency and tuning range.

Crystals for electrical characterization, optical absorption studies, and photoconductivity measurements were grown by both the Bridgman and quench-anneal methods from melts with x-values between 0.16 and 0.44. Bridgman-grown ingots exhibit good single-crystal properties and cross-sectional composition uniformity. The longitudinal compositional gradients and crystal quality obtained in Bridgman-grown ingots is found to be dependent on growth conditions in agreement with the predictions of crystal growth theory and the phase diagram determined for this system[2,3]. Solid-state recrystallized ingots show compositional uniformity, but are polycrystalline.

Optical absorption studies at temperatures between 5-300 K have been analyzed to determine the dependence of the energy gap on alloy composition and temperature[3,4]. For compositions below $x = 0.55$, the energy gap increases with increasing temperature, and for compositions greater than $x = 0.55$ the energy gap decreases with increasing temperature. A functional relationship has been established for these energy-gap dependences on alloy composition and temperature which can be used to estimate performance in device applications.

As grown HgCdSe alloys are n-type with electron concentrations between 5×10^{16}-3×10^{17} cm^{-3}. The 300 K mobility increases from 800 $cm^2/V.s$ for $x = 0.68$ to 10 000 $cm^2/V.s$ for $x = 0.1$[4]. The mobility also increases with decreasing temperature and values of 230 000 $cm^2/V.s$ have been obtained at 50 K for low x-value samples. Dynamic-vacuum annealing is found to reduce the electron concentration to the low 10^{14} cm^{-3} range, but compensating centers are introduced which limit the electron mobility.

Photoconductivity measurements have been made on alloys with x-values between 0.25 and 0.54 at temperatures of 300, 77 and 5 K[3,4]. At temperatures below 80 K, minority-carrier trapping results in an enhancement of the photoconductive responsivity. These results demonstrate the potential of this alloy system as a high-responsivity, high-detectivity, infrared-detector material for wavelengths between 1.5-6 μm.

1. A. Kalb and V. Leute, Phys. Stat. Sol. 5, K199 (1971).
2. D. A. Nelson, C. J. Summers and C. R. Whitsett, Phase Diagram and Crystal Growth of Pseudobinary HgSe-CdSe Alloys. 18th Annual Conference of the Electronics Materials Committee (TMS/AIME), Salt Lake City, Utah, June 1976.
3. C. R. Whitsett, C. J. Summers, J. G. Broerman and D. A. Nelson, Development of the HgCdSe Alloy System for Infrared Sensor Applications, AFML-TR-76-112 (1976).
4. C. R. Whitsett, J. G. Broerman, D. A. Nelson and C. J. Summers Preparation and Characterization of HgCdSe Alloys, Final Report ONR Contract N00014-74-C-0318, (1976).

THALLIUM SELENIDE INFRARED DETECTOR*

P. S. Nayar and W. O. Hamilton
Department of Physics and Astronomy
Louisiana State University
Baton Rouge, Louisiana 70803

There has been considerable interest in new materials for broad band infrared detectors. Some results of a new infrared bolometer detector were published elsewhere[1,2]. In this paper we show that the detector speed and response can be increased without affecting the NEP, by suitable choice of the operating parameters and design of the optical system.

EXPERIMENTAL

The essential features of the experimental arrangement is shown in Fig. 1. The light pipe consists of a polished stainless steel pipe and cone made of copper. The bolometer element is p-type thallium selenide (TlSe) single crystal. It has dimensions of 3mm x 1mm x 0.18 mm. Gold wires of 0.12 mm diameter were welded to the ends and also the ends were coated with indium solder. Two copper leads soldered to the gold wires were heat sunk to the two helium wells soldered to the top flange of the vacuum can.

RESULTS AND DISCUSSION

The temperature dependence of the bolometer resistance between 1.5 and 4.2 K is shown in Fig. 2. This could be fitted to the empirical relation

$$R = R_o(T_o/T)^A \qquad (1)$$

where R is the resistance at temperature T and R_o is the resistance at temperature T_o. The value of the exponent A comes out to the 4. A detailed analysis of the bolometer characteristics is given elsewhere[1].

*Work supported by Air Force Office of Scientific Research under Grant No. AFOSR-71-2054.

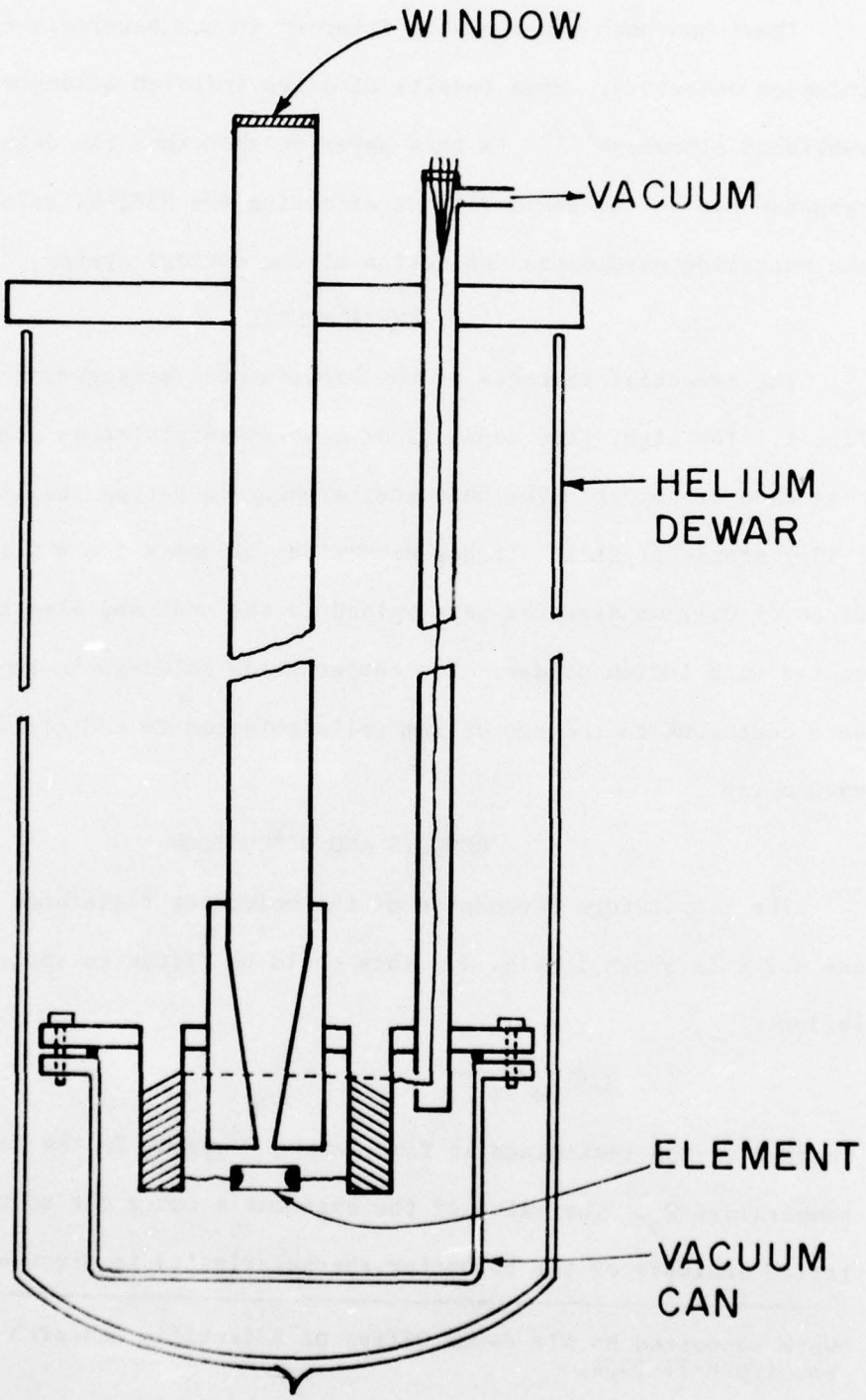
WINDOW
VACUUM
HELIUM
DEWAR
ELEMENT
VACUUM
CAN

The maximum responsivity (S_{max}) is given by[1]

$$|S_{max}| = 0.7(R_o/T_o G)^{\frac{1}{2}} \tag{2}$$

where G is the thermal conductance between the bolometer and the bath and is given by

$$G = P/(T-T_o) \tag{3}$$

where P is the power dissipated in the bolometer due to the constant current bias, T is the temperature of the bolometer and T_o is the temperature of the bath. T can be determined using the curve in Fig. 2 and the current voltage curve shown in Fig. 3. The response time (τ) is given by

$$\tau = 0.7\ (C/G) \tag{4}$$

where C is the heat capacity of the element.

The usefulness of a radiation detector is determined by its ability to detect the minimum value of the signal power, referred as the Noise Equivalent Power (NEP). The total noise power for a cooled bolometer in a unit bandwidth centered around an angular frequency $\omega < 1/\tau$ can be written as[3]

$$(NEP)^2 = \frac{4kT_o R_o}{(S_{max})^2} + 4kT_o^2 G + \frac{CI^{\alpha}}{\omega^{\beta} S_{max}^2} + 8\sigma\epsilon\, a\, T_R^5 \sin^2(\theta/2) \tag{5}$$

where k is the Boltzmann's constant, C,α and β are constants, I is the bias current, σ is Stefan-Boltzmann constant, T_R is the temperature of the background viewed through a solid angle θ, a is the area of the detector and ϵ is the emissivity. The first term in (5) is the Johnson noise associated with the bolometer resistance. The second term is the phonon noise power due to the statistical fluctuation of the bolometer bath temperature. The third term summarises the possible contributions from current noise and those arising from crystal imperfections. Since we use a very low current (10^{-7} amp) this term is neglected. The last term arises from the statistical

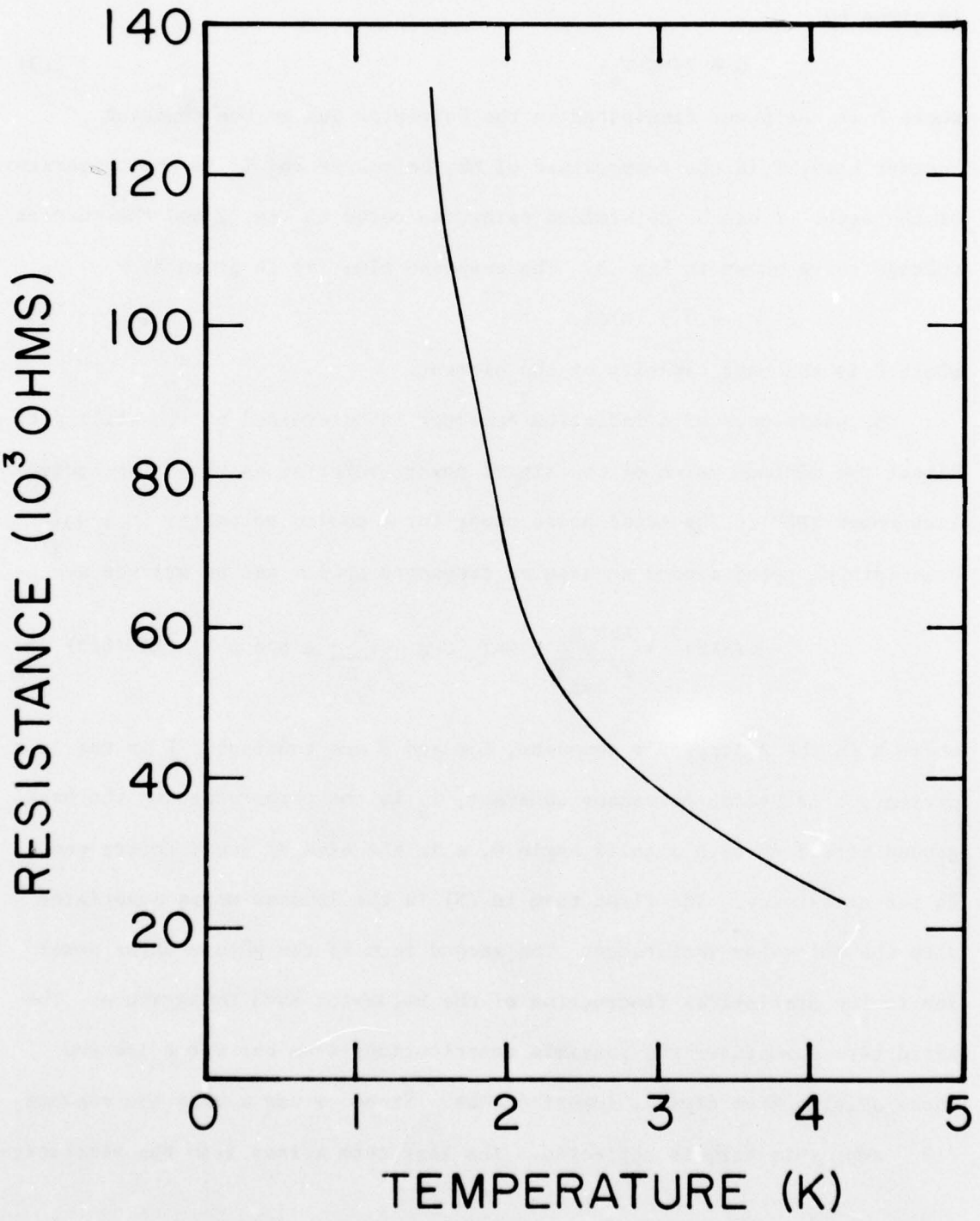
140
120
100
80
60
40
20
RESISTANCE (10^3 OHMS)
0
1
2
3
4
5
TEMPERATURE (K)

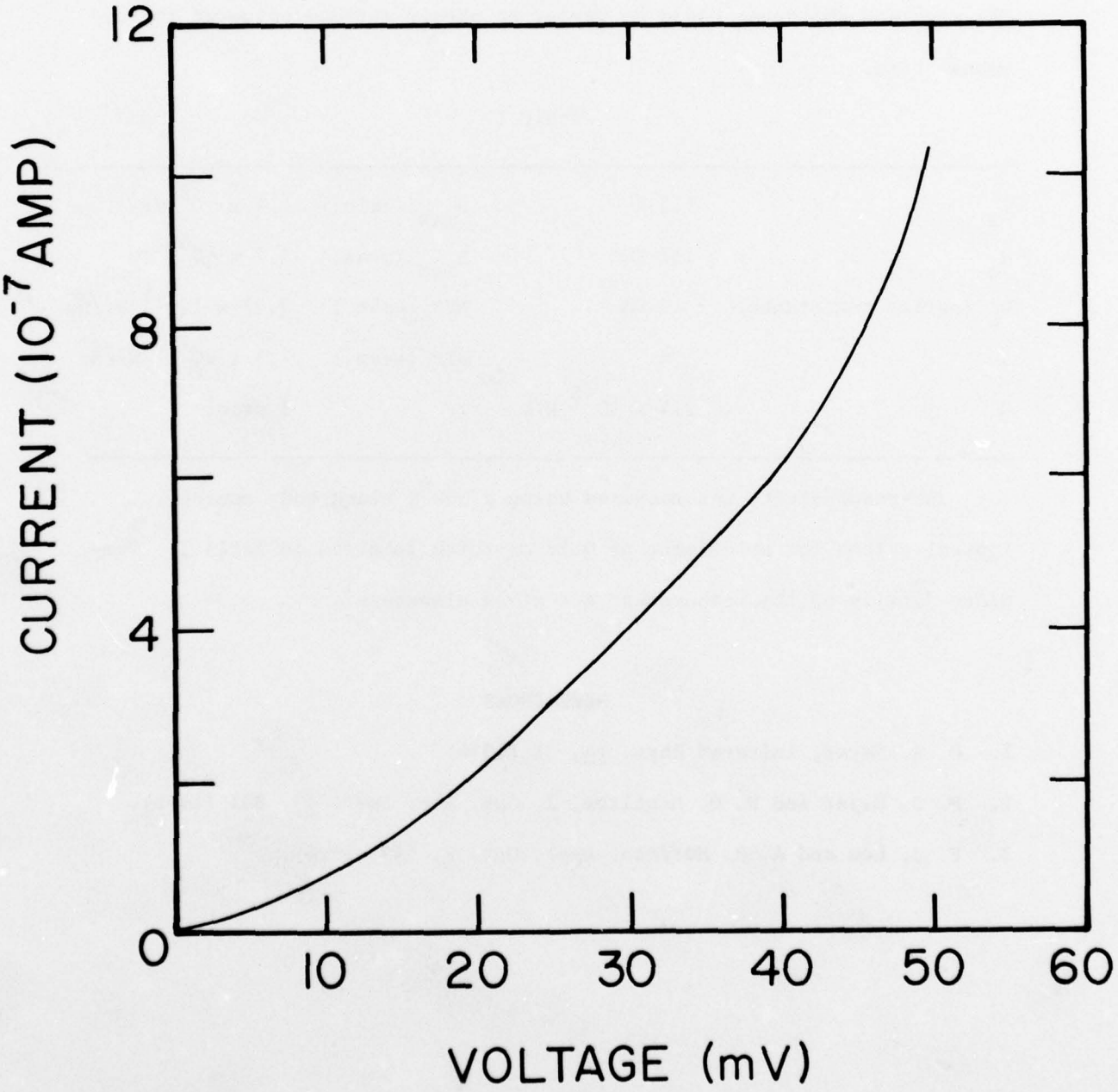
12
8
4
0
CURRENT (10^{-7} AMP)
10
20
30
40
50
60
VOLTAGE (mV)

fluctuations in the background radiation.

The first three terms in (5) constitute the inherent noise power of the detector. This can be evaluated separately using (2) for S_{max}

$$(NEP)_{bol} \simeq 4T_o (kG)^{\frac{1}{2}} \qquad (6)$$

Thus, the inherent noise power depends on the bath temperature and the thermal conductance only. For a given NEP (6) gives suitable values of G. The area and thickness could be varied to obtain minimum value of the response time.

Table I

T_o	1.5 K	S_{max} (calc.)	1.4×10^{6} V/W
R_o	137 KΩ	S_{max} (meas.)	1.2×10^{6} V/W
R_L (series resistance)	10 MΩ	NEP (calc.)	3.47×10^{-15} W/$\sqrt{\text{Hz}}$
A	4	NEP (meas.)	7.3×10^{-15} W/$\sqrt{\text{Hz}}$
G	2.4×10^{-8} W/K	τ	3 msec.

The responsivity was measured using a 500°K black body source[1]. Typical values for an element of 0.18 mm thick is given in Table I. Complete details of the measurement are given elsewhere[1].

REFERENCES

1. P. S. Nayar, Infrared Phys. 14, 31 (1974).

2. P. S. Nayar and W. O. Hamilton, J. Opt. Soc. Amer. 65, 831 (1975).

3. F. J. Low and A. R. Hoffman. Appl. Opt. 2, 649 (1964).

STRUCTURAL AND IR PROPERTIES OF $Pb_{1-x}Hg_xS$ THIN FILMS

N. C. Sharma, D. K. Pandya, H. K. Sehgal, and K. L. Chopra
Department of Physics
Indian Institute of Technology, Delhi
New Delhi-110029, India

Electron diffraction studies carried on thin films of PbS-HgS, prepared by the solution growth technique developed by us, suggest the formation of a uniphase ternary alloy with an f.c.c. symmetry. The lattice parameter of the alloy films can be made to increase or decrease with increasing concentrations of Hg depending on the choice of growth conditions. In case of films where the lattice constant increases with Hg concentration, the optical absorption edge shifts continuously towards higher energies. On the other hand, the band edge is displaced towards lower energies in the films for which the lattice parameter decreases with increasing Hg concentration.

Mercury sulphide is known to exist in two forms: the trigonal α-HgS (E_g=2 eV) which is stable at room temperature, and the zinc-blende β-HgS (E_g=0.1 eV at room temperature) which is stable above 280° C. Similarity in the structures and the lattice parameters of PbS and β-HgS and the known relaxation of the solubility conditions during atom-by-atom condensation process characteristic thin film growth suggests the possibility of formation of uniphase alloys of PbS with both α- and β-HgS.

The observed consistency in the shift of the optical absorption edge towards higher or lower energies and the measured variations in the lattice parameters with increase of Hg concentrations in the films indicate the formation of a uniphase $Pb_{1-x}Hg_xS$ system. By varying the concentration of Hg in the films and by stabilizing the phases formed due to alloying of PbS with (β-HgS) or (α-HgS), the band gap could be varied continuously from 0.1 eV to 2.0 eV.

One thus obtains a versatile material of variable optical gap for use in detectors in the near to far (≃10μm) infrared. Photoconductive IR detectors prepared from this material give a $D^* \simeq 10^{10}$ cm $Hertz^{1/2}$ $Watt^{-1}$. The peak response of the detectors could be shifted by changing the Hg concentrations in the films.

LIGHT SCATTERING FROM SURFACES OF INFRARED OPTICAL COMPONENTS

H. E. Bennett, J. M. Bennett, J. M. Elson and D. L. Decker
Michelson Laboratories, Naval Weapons Center
China Lake, California 93555

Under most circumstances the fraction of light scattered by optical components used at infrared wavelengths is much less than would be expected in visible and ultraviolet regions of the spectrum. In many applications, however, the amount of scattered light which can be tolerated in the infrared is extremely small so that an understanding of its origin and means for controlling it become essential. In the visible and ultraviolet most of the scattered light from well polished optical components arises from microirregularities only a few tens of angstroms in height. Total integrated scattering (TIS) from these microirregularities is well described by a simple scalar scattering theory based on the Kirchhoff approximation. Experimental studies of surface height distribution functions for optical surfaces show them to be Gaussian in nearly all cases. The TIS can then be calculated when only the rms height of the microirregularities is known. Conversely the surface microroughness can be determined from TIS measurements.

Directional scattering, often identified with the Bidirectional Reflectance Distribution Function (BRDF), requires knowledge of the surface autocovariance function as well as the height distribution function. Vector scattering theory, which is not based on the Kirchhoff approximation, describes directional scattering most accurately, but discrepancies between theory and experiment still exist.

At infrared wavelengths microirregularity scattering decreases rapidly in magnitude and larger macroirregularities such as surface particulates, scratches and other surface defects become relatively more important. Particulate and

defect scattering centers are assumed to be uncorrelated so that the amplitude of light scattered from these centers is simply the sum of the amplitudes scattered from each. Scattering of this type is approximately described by dipole scattering theory. The forward scattering from the surfaces of transparent media is predicted by this theory to be slightly greater than backscattering when the scattering centers are comparable to the wavelength. This behavior is observed experimentally in the near infrared. Forward and backscattering approach each other at longer wavelengths. Surprisingly, scattering levels for infrared windows may still sometimes be described over extended wavelength regions by an exponential which depends inversely on the square of the wavelength. Volume scattering as well as surface scattering may play a role in such cases.

Scattering from MIL-STD type scratches typically behaves as predicted by geometrical optics and shows little wavelength dependence in the visible and near infrared. A resonance would be expected to occur, however, when the scratch width becomes comparable to the wavelength. An increase in scattered light is sometimes found in the near infrared and may be caused by a similar resonance when the wavelength of the light is approximately equal to the diameter of dust particles on the surface. When illuminated by intense laser radiation, dipole resonances from surface imperfections can cause standing waves to be set up which are sufficiently strong to cause permanent ripples to appear in the component surface, probably because of differential joule heating.

More complicated than the case of individual incoherent scattering centers is the case of correlated scattering (diffraction) such as is found in gratings and other repetitive surfaces. The intensity of diffracted light in this case depends on the height, shape, and spacing of the surface grooves.

When low efficiency reflection gratings are overcoated with dielectric layers, theoretical studies predict that complicated interference patterns will dominate the diffracted orders. For dielectric layers of quarter-wave optical thickness, these effects will be minimized if the groove shape is replicated at every interface of the dielectric stack. In addition to being useful in the design of low efficiency diffraction gratings, this theory may also be of use in connection with diffuse scattering from multilayer stacks and for infrared optics produced by diamond point turning and then overcoated with a multilayer dielectric film. The scattered light levels observed in the best cases for diamond turned optical surfaces are remarkably low, and the absence of polishing defects and scratches make this technique very attractive for producing superior low scatter infrared optics.

SURFACE EVALUATION TECHNIQUES AND SURFACE STATISTICS FOR INFRARED OPTICAL MATERIALS

Jean M. Bennett
Michelson Laboratories, Naval Weapons Center
China Lake, California 93555

In order to obtain optimum performance from infrared optical systems, it is important that the surface finish on the optical elements be adequate. Surface microroughness, particulates, and isolated scratches and digs will produce scattering and may increase absorption, both of which can adversely affect the performance of an optical system. Particulates on or embedded in an optical surface can also lower the laser damage threshold of the component. In order to detect and minimize these effects, it is necessary to have adequate means to characterize optical surfaces. Techniques used at Michelson Laboratory for surface characterization include Nomarski and stereoelectron microscopy, Fizeau and FECO interferometry, stylus surface profilometry, ellipsometry, and Auger spectroscopy, as well as instruments for measuring scattered light and for quantitatively comparing scratches and digs on surfaces to standard scratches and digs.

According to most classical scattering theories, total integrated scatter in the infrared and visible spectral regions depends in part on the height distribution function of the surface, while the angular dependence of the scattering partly depends on the Fourier transform of the autocovariance function. The FECO Scanning Interferometer and Talystep surface profiling instrument both are capable of obtaining surface height data from which the statistical properties of optical surfaces can be evaluated. These properties include rms roughness, rms slope, height and slope distribution functions, and autocovariance function. The instruments have sensitivities to height variations of less than 10 Å with lateral resolutions on the order of a micron.

Information on heights and slopes of features whose lateral dimensions are in the submicron range is obtained by stereoelectron microscopy on surface replicas.

We have measured surface statistics for infrared mirror substrates (molybdenum, copper, fused quartz, etc.) and infrared window materials (calcium fluoride, magnesium fluoride, potassium chloride, and others). In general the height and slope distribution functions for all materials are very good Gaussians if an adequate statistical sample is taken. However, if the surface is deeply scratched, as is typical for some polished alkali halide surfaces for example, the height distribution function may have proportionately too many points on the tails to be strictly Gaussian (corresponding to deep scratches and large asperities). The initial portions of the autocovariance functions are mostly exponential, and none are Gaussian. Typical examples of surface statistics are shown in Figs. 1 and 2.

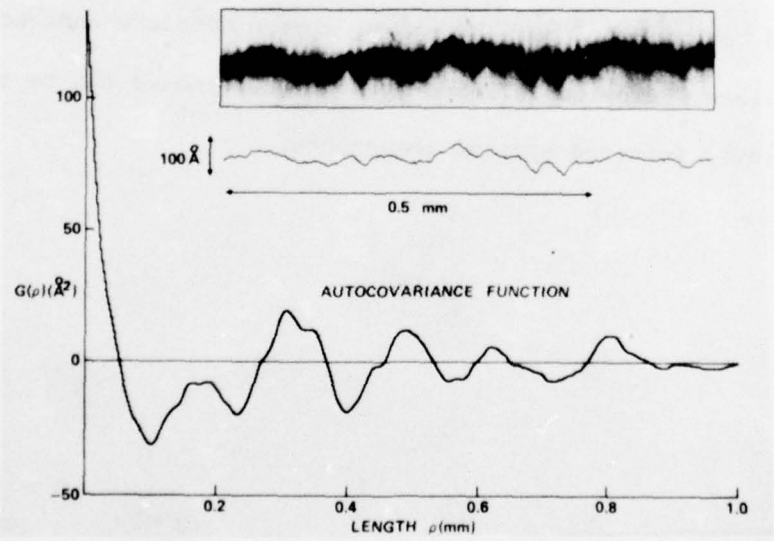

Fig. 1. FECO interferogram, surface profile, and autocovariance function for a single point diamond machined copper surface. Data average of 10 scans. The roughness measured visually from the width of the interference fringe was 22.5 Å rms.

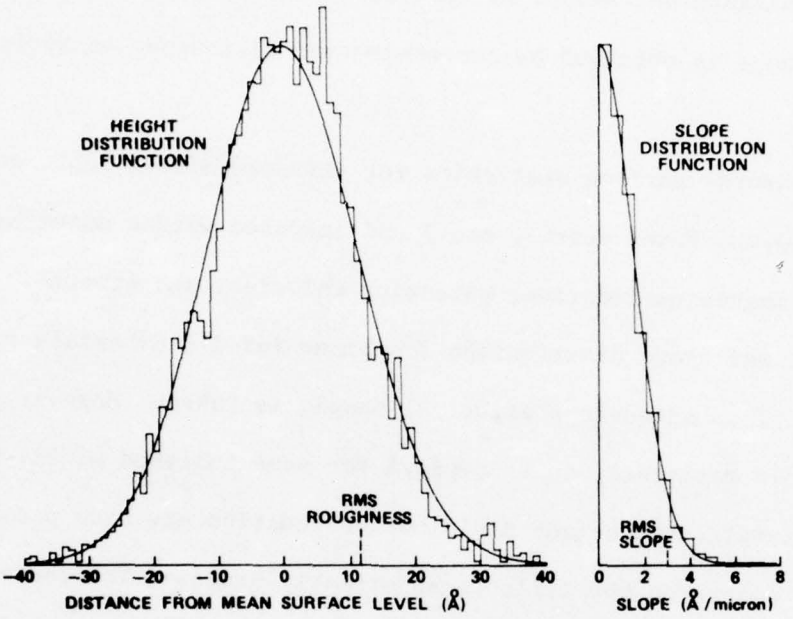

Fig. 2. Height and slope distribution functions for the same machined copper surface.

By incorporating the surface statistical data with data on particulates, surface defects and surface contamination layers obtained using the various instruments and techniques described above, a more complete understanding of the role of surface finish on infrared optical performance can be achieved leading to improved infrared optical components.

SCATTERING PROPERTIES OF OPTICAL SURFACES AND BAFFLE MATERIALS FOR INFRARED SYSTEMS

J. E. Harvey, J. A. Gunderson, R. V. Shack, and W. L. Wolfe

Optical Sciences Center
The University of Arizona
Tucson, Arizona 85721

The relationship between surface micro-roughness and radiant energy scattering plays an important role in many areas of technical interest. These include the cost versus performance trade-offs in the fabrication of optical surfaces, design considerations for stray light rejection systems, evaluation of machined metal mirrors for high energy laser applications, laser radar backscatter signature programs, and a host of other applications requiring extensive scattering data.

A theory of surface scattering has been formulated by utilizing the same Fourier techniques that have proven so successful in the area of image formation. An analytical expression has been obtained for a surface transfer function which relates the surface micro-roughness to the scattered distribution of radiation from that surface. For a large class of well-behaved surfaces it is therefore possible to describe this transfer function in terms of *only* the rms surface roughness and the surface auto-covariance function. This theory provides a straightforward solution to the inverse scattering problem (i.e., determining the relevant surface characteristics from scattered light measurements). Once the surface characteristics are known, the same theory provides an equally simple method of predicting the wavelength dependence of the scattered light distribution. Furthermore, the mere

existence of such a transfer function implies a *shift-invariant* scattering function which does not change shape with the angle of the incident beam. This is a rather significant development which has profound implifications regarding the quantity of data required to completely characterize the scattering properties of a surface.

Experimental verification of the inverse scattering problem and the shift-invariant scattering function has been successfully demonstrated for *smooth* surfaces ($\sigma << \lambda$), and the predictions of the scattering behavior as a function of wavelength have been shown to be accurate for wavelength changes over a limited spectral range. The light scattering properties of *rough* (diffusely reflecting) optical surfaces do not exhibit the shift-invariant behavior predicted by the simple theory. However, a more general theoretical treatment results in an infinite family of transfer functions which are required to completely characterize the scattering properties of a rough surface. The results of experimental measurements on several baffle materials exhibiting wide variations in scattered light behavior are presented and discussed in the context of these theoretical developments.

THE RELATIONSHIP BETWEEN SURFACE SCATTERING AND MICROTOPOGRAPHIC FEATURES

E. L. Church, H. A. Jenkinson, and J. M. Zavada
Pitman-Dunn Laboratory
Frankford Arsenal
Philadelphia, Pennsylvania 19137

Residual surface roughness can degrade the performance of optical and infrared components by leading to detrimental scattering effects and increased damage sensitivity. The vertical scale of such roughness is generally much smaller than the wavelength of visible light, which makes accurate microtopographic data difficult to obtain. Differential scattering measurements are particularly useful for this purpose since they are non-contact and constitute a functional test of surface quality. Also, with aid of a suitable scattering formalism, such data may be mapped into the power spectral density of the surface roughness, or equivalently, its autocovariance function.[1] These data may be viewed phenomenologically. Here, however, we seek further insight into the relationship between surface scattering and microtopographic features by calculating the scattering expected from surfaces consisting of a smooth plane marred by a number of defects. Various pits, bosses, grooves, and ridges are considered, both randomly and regularly distributed over the surface. The inverse problem of deriving effective surface contours from measured power spectral data is also considered. Results are illustrated with measurements of various diamond-turned and conventionally polished surfaces.[2]

[1]E. L. Church and J. M. Zavada, Appl. Opt. 14, 1788 (1975).

[2]E. L. Church and H. A. Jenkinson, J. Opt. Soc. Am. 65, 1216A (1975).

INFRA-RED OPTICAL REFLECTIVITY OF LIQUID METALS

Edward Siegel

Public Service Electric and Gas Company
Energy Laboratory
200 Boyden Avenue, Maplewood, N. J.

We utilize the concept of electron-phonon dominated optical conductivity and the Drude theory of optical properties of metals, as applied by Ujihara,[1] and the theory of melting in simple metals of Omini,[2] based on the Percus-Yevick[3] collective coordinate (liquid phonon) theory of simple liquids, to calculate the optical reflectivity in a variety of liquid metals. We compare the reflectivity of the metals treated by Ujihara, and extended by Siegel[4] (Ag, Au, Al, Cu, Fe, Ni, Co) at their melting temperatures in the solid and liquid phases to determine if the change in phonon spectrum and electron-phonon collision frequency in the solid to the Percus-Yevick "liquid phonon spectrum" and electron-liquid phonon collision frequency in the liquid affects the optical properties. Later we extend the calculations of reflectivity in the liquid metals beyond their melting temperatures. This is a valid criterion of whether the Percus-Yevick liquid phonon approach to electron-disorder scattering in liquid metals is applicable in evaluating the high frequency, optical properties of liquid metals, since we can readily determine of the calculated melting entropy of Ujihara corresponds to an expected change in the optical conductivity, dielectric constant and reflectivity. Extension to reflectivity as a function of laser power, and the possibility of non-linear infra-red reflectivity are discussed.

1. K. Ujihara, J. Appl. Phys. 43, 5, 2376 (1972)
2. M. Omini, Phil. Mag. 26, 2, 287 (1972)
3. J. K. Percus and G. T. Yevick, Phys. Rev. 110, 1 (1958)
4. E. Siegel - to be published.

NOTES

SURFACE CHEMISTRY AND ABSORPTANCE OF CaF_2 AND SrF_2 AT DF AND CO WAVELENGTHS*

P. KRAATZ AND S. J. HOLMES

NORTHROP CORPORATION
Northrop Research and Technology Center
Hawthorne, California 90250

ABSTRACT

The relative importance of bulk and surface contributions to absorptance in transmitting optics at DF and CO wavelengths has recently been discussed, with the observation that the surface contribution may be as much as 15 times that of the bulk.[1] The nature of changes in surface absorption and surface chemistry associated with such processes as cleaning with organic solvents or vacuum glow discharge have not been fully explained.[1,2] To elucidate some aspects of these problems, we report results of some investigations employing Auger electron spectroscopy (AES) in conjunction with DF and CO laser calorimetry. It has been found that exposure of CaF_2 and SrF_2 to vacuum glow discharge produces an initial, dramatic reduction in IR absorptance, followed by an increase to an absorptance exceeding that of the solvent-cleaned sample, within 24 hours in the ambient atmosphere. The latter effect is not reversible by solvent cleaning or repeating the glow discharge. Implications of these and other results are discussed in the light of surface states and the elemental composition of surfaces revealed by AES.

---

1. Rowe, J. M., Kraatz, P., and Holmes, S. J., "Calorimetric Absorptance Measurements of CaF_2 and SrF_2 at DF and CO Wavelengths," Proc. Eighth Symposium on Optical Materials for High Power Lasers, NBS, Boulder, Colorado, (1976).

2. Kraatz, P., Holmes, S. J., and Klugman, A., "Absorptance of Coated Alkaline Earth Fluoride Windows at CO Laser Wavelengths." Proc. Fifth Conf. on IR Laser Window Materials, DARPA, 1975.

---

*Work supported by Contract No. N00123-76-C-1321

RESIDUAL ABSORPTION IN HF AND DF LASER WINDOW MATERIALS FROM CONTAMINATION BY CARBONACEOUS AND OTHER IMPURITIES*

Philipp H. Klein

U.S. Naval Research Laboratory
Washington, DC 20375

Residual absorption in materials for infrared laser windows and coatings can be increased more than an order of magnitude by undetected impurities. As little as one absorbing molecule or ion in 10^8 (or even 10^{10}) molecules of optical material (0.01 ppmA) can result in bulk absorption coefficients of 10^{-4} cm^{-1} or more.

Experimental determination of such small absorption coefficients is exacting. Reported values may therefore err by an order of magnitude. Nevertheless, apparent extrinsic absorption has recently been noted at 2.7 and 3.8 μm in specimens of alkali halides and alkaline-earth fluorides whose absorption coefficients at 1.06 and 5.3 μm were approximately 10^{-5} cm^{-1} (1).

It has been suggested (1) that OH and CH impurities may be responsible for the "extra" absorption at 2.7 and 3.8 μm. We note that the carbonyl halides ($COCl_2$, COF_2, etc.), carbon suboxide (C_3O_2), bicarbonate ion (HCO_3^-), carbonate ion $CO_3^=$), and formate ion (HCO_2^-) all have strong absorption bands in the 2600-3700-cm^{-1} region.

Every one of these substances contains carbon-oxygen bonds. We estimate that as little as 10^{-6} mole of any one of these absorbers in 1 mole of matrix (1 ppmA) can produce 10^{-4} cm^{-1} of absorption at 2.7 or 3.8 μm. (Nitrates, nitrites, and interstitial water are equally effective.) Our estimates were performed by the method used by Duthler at 10.6 μm (2).

We have also calculated equilibrium constants for many of the purification reactions used in preparation of these halide materials. At the temperatures used for preparation of potassium

*Work supported in part by Defense Advanced Research Projects Agency.

chloride and bromide, carbon tetrahalides (CCl_4, CF_4) readily react with hydroxyl impurities to produce CO_2, CO, or even C_3O_2. Similar calculations for the higher temperatures used for growth of alkaline-earth fluorides show a somewhat lesser tendency for formation of these gases. Incorporation of these products by their solution in growing crystals could explain the extrinsic absorption at the HF and DF wavelengths.

In contrast, our calculations show that pure hydrogen halides (HF, HCl, HBr) do not produce any carbonaceous contamination. They are less effective for removal of OH^- impurities than are the carbon tetrahalides, especially at higher temperatures. They also introduce problems of equipment durability. Nevertheless, careful selection of materials of construction for purification and growth apparatus does make possible the use of hydrogen halides for purification of window materials for use at 2.7 and 3.8 μm. If excessive absorption in current materials continues to present problems, processing with hydrogen halides in carbon-free equipment may be warranted.

References

1. M. Hass, J. A. Harrington, D. A. Gregory, and J. W. Davisson, Appl. Phys. Letters 28, 610 (1976).
2. C. J. Duthler, J. Appl. Phys. 45, 2668 (1974).

REFRACTIVE PROPERTIES OF INFRARED LASER WINDOW MATERIALS*

Marilyn Dodge

Optical Physics Division, Institute for Basic Standards

National Bureau of Standards, Washington, D.C. 20234

The increased use of high-power infrared lasers has resulted in a need for improved transparent component materials to be used in large, high-resolution optical systems. As a result, new materials have been developed and new techniques developed for the manufacture of heretofore commonly used IR materials such as the alkali halides and the alkaline earth fluorides.

Optical distortion as a result of temperature gradients can occur in transparent or semi-transparent components of high-power laser systems at powers below that which would be required to melt or fracture the component.[1] Knowledge of the refractive index, n, and its temperature dependence, dn/dT, of a candidate material to be used in a high-power laser system is necessary before the amount of optical distortion which might occur can be predicted. The study of these parameters is a part of an optical materials characterization program[2] which is currently in progress at NBS.

The refractive index has been determined for chemical vapor deposited (CVD) zinc selenide, potassium chloride made by reactive atmosphere processing (RAP), potassium chloride doped with potassium iodide, and hot-forged calcium fluoride. Measurements were made from 0.25 μm in the ultraviolet to the infrared transmission cutoff by means of the minimum-deviation method on a precision spectrometer at two temperatures, near 20°C and 34°C. Each set of data was fitted to a

three term Sellmeier-type dispersion equation of the form $n^2-1 = \sum_j \frac{A_j\lambda^2}{\left[\lambda^2-\lambda_j^2\right]}$.

This equation permits interpolation of index values over the wavelength range of measured values within several parts in 10^5. The data obtained at the two temperatures for each specimen were used to calculate $\Delta n/\Delta T(°C)^{-1}$ as a function of wavelength. The refractive index values and temperature coefficients of index for these samples will be compared with literature values.

*This work was supported in part by the Defense Advanced Research Projects Agency.

[1]Sparks, M., J. Appl. Phys. 42, 5029 (1971).

[2]Feldman, A., Malitson, I., Horowitz, D., Waxler, R. M. and Dodge, M., "Laser Induced Damage in Optical Materials: 1974," NBS Special Publication 414, p. 141, U.S. Govt. Printing Office, Wash. (1974).

THE PHOTOELASTIC CONSTANTS OF POTASSIUM CHLORIDE AT 10.6 μm*

Albert Feldman, Deane Horowitz, and Roy M. Waxler
Institute for Materials Research
National Bureau of Standards
Washington, D. C. 20234

The piezo-optic constants are needed to predict the distortion of optical components subjected to high power laser radiation. Thus, even though the absorption coefficients may be extremely small, the residual absorption in a component may produce a significant temperature rise. In general, the temperature distribution will be nonuniform, hence, radiation propagating through the component will experience a wavefront distortion which, if sufficiently severe, may render the component unusable in diffraction limited operations. Theoretical analyses show that optical distortion will depend on several factors, one of which is the change of refractive index due to thermally induced stresses. Thus, it is important to measure piezo-optic constants.

We have measured all the piezo-optic constants at 10.6 μm of reactive processed (RAP) KCl and KCl doped nominally with 1% KI (KCl:KI). The results we have obtained are shown in Table I. The coefficients q_{11} and q_{12} describe absolute changes of refractive index with stress, whereas $q_{11}-q_{12}$ and q_{44} describe stress-induced birefringence. Within experimental error, we observe no differences in the piezo-optic constants of the two materials.

Table I. Piezo-Optic Constants of KCl at 10.6 μm in Units of 10^{-12} m^2/N.

Material	q_{11}	q_{12}	q_{44}	$q_{11}-q_{12}$
RAP KCl	4.3 ± .3	2.8 ± .3	-3.4 ± .4	1.8 ± .4
KCl:KI	4.2 ± .2	2.5 ± .2	-3.6 ± .3	1.8 ± .2

The absolute piezo-optic constants q_{11} and q_{12}, are measured by a null interferometric technique[1], in which the stress-induced optic path change in a specimen is compensated by a calibrated optic path change in a reference specimen of Ge. The relative piezo-optic constants $q_{11}-q_{12}$ and q_{44} are determined by a technique employing a Ge compensator whose function is equivalent to a Babinet-Soleil compensator.

In Table II, we present the elasto-optic constants of RAP KCl calculated from piezo-optic measurements at 10.6 μm and near 600 nm. Also shown in the table are theoretical values calculated by Bendow, *et al.*[2] The values near 600 nm are considered to contain only an electronic contribution, whereas the

values at 10.6 μm contain both an electronic and a lattice contribution. The theoretical model predicts a dispersion in all the coefficients from the visible to 10.6 μm, whereas the experimental values of p_{11} and p_{12} suggest a negligible dispersion. Moreover, the dispersion of the experimental value of p_{44} appears to be of opposite sign to the theoretically predicted dispersion.

Table II. Experimental and Theoretical Elasto-Optic Constants of KCl.

	Theory			Experiment		
	p_{11}	p_{12}	p_{44}	p_{11}	p_{12}	p_{44}
Electronic	.182	.134	-.026	.21	.15	-.029
10.6 μm	.232	.116	-.040	.20	.15	-.023

*Research supported in part by the Defence Advanced Research Projects Agency.

[1]A. Feldman, R. M. Waxler, and D. Horowitz, "Measuring Photoelastic and Elastic Constants of Transparent Materials by Application of Static Stress," in Optical Properties of Highly Transparent Solids, edited by S. S. Mitra and B. Bendow (Plenum Publishing Corp., New York, 1975) pp. 514.

[2]B. Bendow, P. D. Gianino, Y. F. Tsay, and S. S. Mitra, Appl. Optics 13, 2382 (1974).

ABSORBING PRECIPITATES IN CADMIUM TELLURIDE: ESTIMATES FOR CATASTROPHIC LASER-DAMAGE THRESHOLDS

Herbert S. Bennett

National Bureau of Standards, Washington, D. C. 20234

and

Cyrus D. Cantrell

Los Alamos Scientific Laboratory, Los Alamos, New Mexico 87544

SUMMARY

Cubic CdTe is a promising infrared material for laser optics. Absorption sites such as Te, In_2Te_3, and CdT_2 are present in CdTe samples[1] and may absorb sufficient radiation from an incident laser beam to produce deleterious stresses within the CdTe host. In this paper, we estimate the stresses which occur near such localized absorption sites and the thresholds for thermal extrinsic damage to occur. Applying the linear-uncoupled-quasistatic thermal elastic theory to absorbing polycrystalline aggregates in CdTe, we have derived expressions for the stress tensor components as functions of the laser power and pulse width and of the size, optical, thermal, and mechanical properties of the absorption sites and host.[2]

To illustrate numerical predictions, we compute the thermal stresses near polycrystalline Te absorption sites in the size range from 0.1 μm to over 10 μm. Our calculations indicate that the heating of such Te precipitates, when subjected to laser beams with 100 MW/cm^2 power densities and with 200 ns or 500 ns pulse widths, may produce thermal stresses which are comparable to or exceed the fracture strength of CdTe. The optical, thermal, and mechanical properties of the host material dominate in determining the maximum tensile stresses near absorbing sites. Hence, we expect that, even though the quantitative predictions will differ among In_2Te_3, and $CdCl_2$ precipitates, all such absorbing sites in the above mentioned size range, when subjected to the above mentioned laser beams, may produce thermal stresses which are comparable to or exceed the fracture strength of CdTe.

Using a value for the absorptance of the absorbing precipitate equal to one, we give in Fig. 1, the calculated maximum tensile stress $\sigma_{\theta\theta}(max)$ as a function of the size r_0 of the absorbing precipitate. The laser power density is F_p = 100 MW/cm^2, and the + and ⊙ denote data points for laser pulse widths of respectively 200 ns and 500 ns. The stress components in the host CdTe are proportional to the Young's modulus of the host in the direction of the stress E_{ijk}. The minimum value of the Young's modulus for single crystal CdTe is $E_{100}^{min} = 2.61 \times 10^{10}$ N/m^2. The measured fracture strength[3] of CdTe lies between 1.38×10^7 N/m^2 and 2.75×10^7 N/m^2 and hence is denoted approximately by the dashed line of $(E_{100}^{min}/1000)$ in Fig. 1.

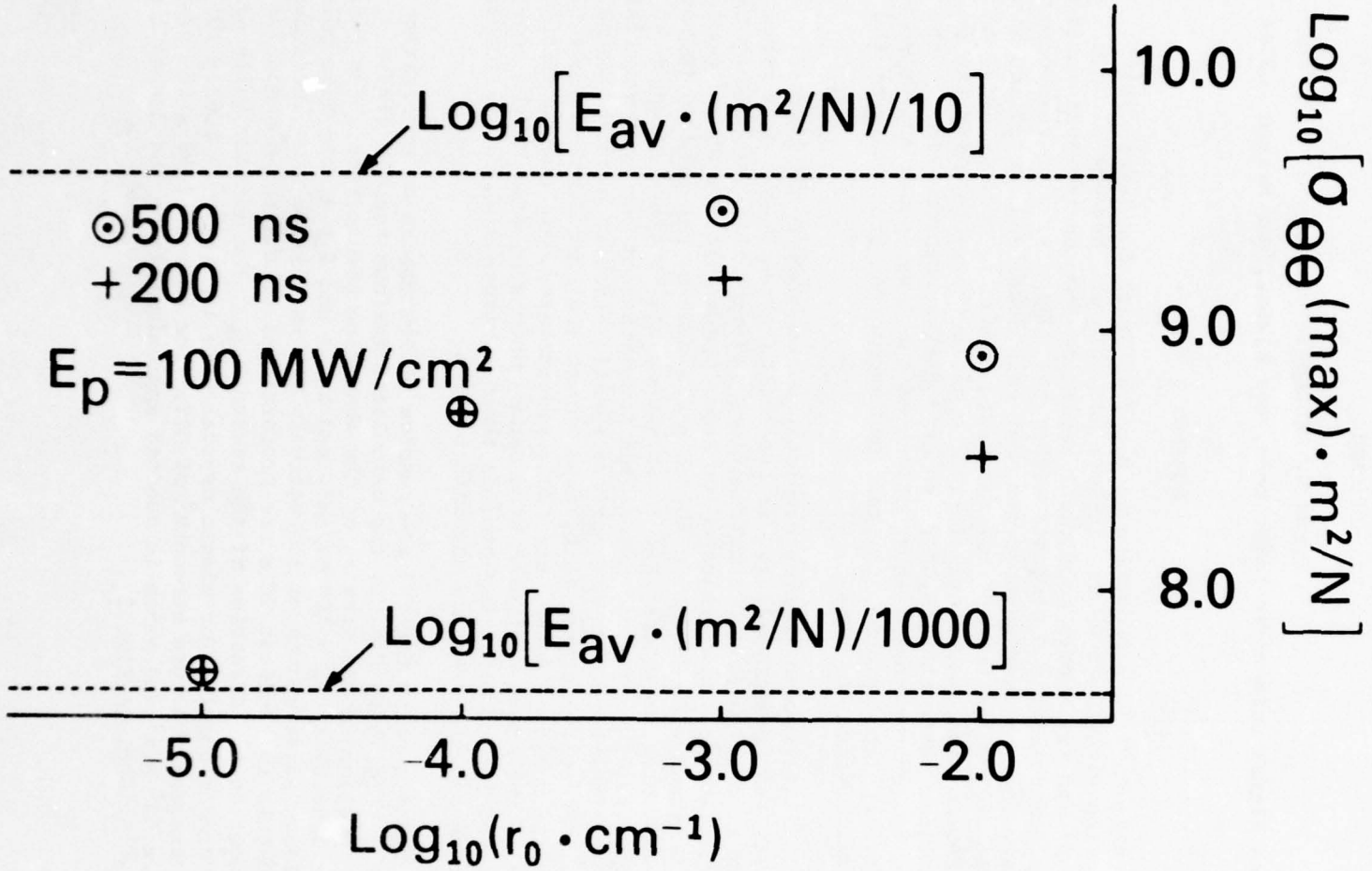

FIGURE 1. MAXIMUM TENSILE STRESS AS A FUNCTION OF ABSORBING SITE SIZE.

From these data, we then show that precipitates in the size range from 10^{-5} cm to over 10^{-2} cm have a high probability to produce catastrophic damage in the CdTe host crystals when subjected to laser power densities of the order of 100 MW/cm^2 for 200 ns to 500 ns.

In view of the above conclusions, researchers have some options. They may increase the size of the infrared optics and reduce the power density in them; they may devise ways to reduce all potentially damaging precipitates to tolerable sizes; and they may encourage the materials scientists to develop new alternative infrared materials with improved figures of merit when compared with presently available materials such as CdTe.

References

1. T. J. Magee et al., Phys. Status Solidi A 27, 557 (1975).
2. H. S. Bennett and C. D. Cantrell, to be published.
3. G. E. Kuhl, in *Proceedings of the Conference on High Power Laser Window Materials, Oct. 30 - Nov. 1, 1973*, edited by C. A. Pitha, U.S.A.F. Cambridge Research Laboratory Technical Report TR-73-0372, Vol. II, p. 607.

PULSE LASER DAMAGE IN INFRARED MATERIALS

Michael Bass
Center for Laser Studies
University of Southern California
Los Angeles, California 90007

The phenomenon whereby intense beams of laser light cause catastrophic damage to both transmissive and reflective optical components has been a major impediment to the development of more powerful laser systems. In general the designer has tried to deal with this problem by improving the quality of the materials used in the components, by improving surface finishing techniques, and by assuring that certain maximum flux densities are not exceeded. These efforts have lead to infrared optics which work in high power systems but which are very large and therefore very expensive.

Studies of the mechanisms whereby the components damage have been performed in order to provide the designers with the necessary data and to suggest means whereby materials might be improved. A summary of the reported damage fluxes at 10.6 μm shows the following state-of-the-art capabilities:

1. Most good dielectric coatings can reliably withstand at most 0.5 GW/cm^2.
2. An etched and buffed surface of an alkali halide can withstand a flux of $\sim \frac{1}{2}$ that of good bulk material. Conventionally polished alkali halides can withstand no more than 1/10 the bulk breakdown flux.
3. Bulk damage to good NaCl occurs at ~10 GW/cm^2 and may be caused by electron avalanche breakdown. KCl can be obtained

from commercial sources which damages at fluxes as high as 7 GW/cm^2 or as low as 0.35 GW/cm^2. The lower values occur in samples having many inclusions.

4. Diamond turned metal mirrors can have damage thresholds ~1 - 3 GW/cm^2, but this may represent the upper limit because damage to metal mirrors appears to be caused by absorption.

The principal cause of damage to transparent media and optical coatings is the presence of included defects. Several types of evidence for this, such as irregular damage morphology, site to site and sample to sample damage threshold variations and a dependence of damage threshold on the area (volume) irradiated can be cited. As a result of certain experiments where care was taken to try to avoid any defects, it was concluded that the intrinsic damage mechanism was electron avalanche breakdown. While there is general agreement that the ultimate intrinsic damage mechanism is avalanche breakdown, recent results suggest that defects may still be responsible even in experiments where the irradiated volume is so carefully selected.

In this paper experimental data for 10.6 μm and 3.8 μm pulsed laser damage thresholds to a variety of infrared optics will be reviewed and the mechanisms responsible will be discussed.

IRREVERSIBLE LASER DAMAGE IN IR DETECTOR MATERIALS

F. Bartoli, L. Esterowitz, M. Kruer and R. Allen
Naval Research Laboratory
Washington, D.C. 20375

Irreversible laser damage in infrared (IR) detector materials is reviewed and new results are presented. Infrared detector materials are quite susceptible to thermal damage due to intense laser radiation, since their absorption coefficients are usually large, i.e. between 10^3 and 10^5 cm^{-1}. Typical absorption mechanisms for these materials include band-to-band absorption for photodiodes and intrinsic photoconductors, and lattice absorption for uncoated pyroelectric detectors. At sufficiently high optical flux levels, free carrier absorption can also be substantial. A theoretical analysis of laser damage in these materials must treat not only the relevant absorption processes but also the time-dependent heat conduction occurring for a specific sample geometry.

Four thermal models for laser-damage employing closed-form solutions to the heat diffusion equation are reviewed. These models treat a uniformly irradiated semi-infinite solid, a semi-infinite solid irradiated by a Gaussian beam of arbitrary diameter, and two composite layered constructions irradiated uniformly. These models are successful in calculating damage thresholds for certain detector configurations and irradiation conditions. However none of these models can treat both radial heat conduction and the effects of the composite layered construction of the detector. These models also assume that the material properties are independent of temperature and optical flux.

A generalized two-dimensional numerical model based on a finite element technique is presented which treats both radial heat conduction and the layered detector construction. This model takes into account all relevant details of detector geometry and thermal configuration, as well as time-dependent irradiant conditions and changes in material properties with temperature and optical flux. This model has been found to successfully describe laser-damage for cases where the closed-form solutions do not apply.

Our recent experimental results on HgCdTe photodiodes, which illustrate the need for the numerical thermal model, are shown in Fig. 1 together with experimentally determined damage thresholds for HgCdTe material. As shown in the figure, significant differences in measured thresholds were obtained between uniformly irradiated samples and those irradiated by

a small Gaussian beam. Models based on closed-form solutions were not able to account for these differences since they do not treat both radial heat conduction and the composite layered construction of the detector. The two dimensional numerical model was employed and found to agree well with the experimental data.

Laser-damage thresholds have been determined experimentally for a wide variety of IR detector materials, chosen for detector operation in the 1-3 μm, 3-5 μm and 8-14 μm spectral regions. As an example, threshold values of laser energy density E_0 are plotted in Fig. 2 as a function of irradiation time for several 8-14 μm detector materials. The magnitude of the damage thresholds and relative vulnerability of the different detector materials are analyzed. The overall susceptibility of the various generic classes of detector materials are summarized and explained in terms of the relevant physical processes and thermal configurations.

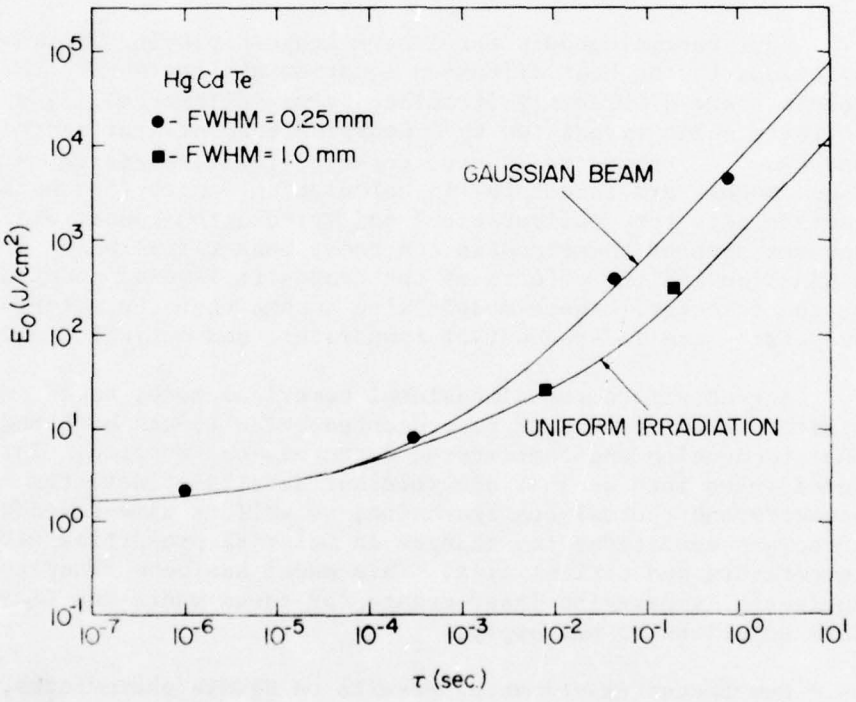

Fig. 1. Calculated energy density damage thresholds as a function of irradiation time for HgCdTe photodiodes. Experimental data on HgCdTe material are shown for two different irradiation conditions (circles-Gaussian beam, squares-approximately uniform irradiation).

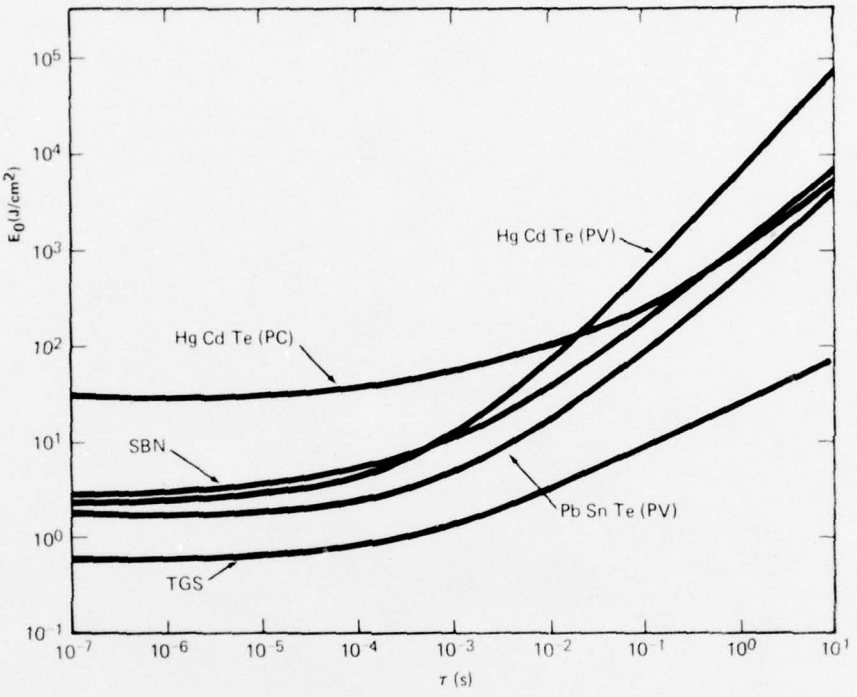

Fig. 2. Values of Eo as a function of irradiation time for several 8-14 μm detector materials. These theoretical curves have been validated experimentally.

(Invited Paper)

INFRARED STUDY OF ANOMALOUS EXCITATIONS IN GLASSES

A. J. Sievers

Laboratory of Atomic and Solid State Physics
and
The Materials Science Center
Cornell University
Ithaca, New York 14853

An intriguing feature of amorphous dielectrics is the presence of low frequency anharmonic modes, these are qualified as "anomalous" since they contribute to large deviations from the expected crystalline behavior. The first clear evidence that these anomalous modes represented a general phenomenon in glassy materials was obtained from the low temperature specific heat and thermal conductivity measurements of Zeller and Pohl[1]. For a variety of glassy materials they found a linear temperature dependence of the specific heat and a thermal conductivity whose temperature dependence and magnitude were the same for all glasses. Extensive measurements of the specific heat[2] of a large number of glasses have confirmed the presence of anomalous excitations in the energy range below a few cm^{-1}. Additional evidence for such low frequency excitations comes from ultrasonic attenuation experiments[3]. Finally the observation of boundary scattering in small glass fibers has shown that Debye-like phonons carry the heat (as in a crystalline solid) and that the excess excitations observed in specific heat measurements do not themselves carry heat through the crystal[4]. To account for these special modes a localized tunneling model[5,6] has been proposed in which atoms, ions or groups of particles quantum mechanically tunnel between two or more equivalent sites. The linear dependence of the specific heat has been obtained from this model by including a statistical distribution of barrier heights and asymmetries for the local potential. One straightforward prediction which this model makes is that the

temperature dependence of the far infrared absorption coefficient should be determined by the occupation numbers of a small number of energy levels associated with the tunneling manifold. For example a distribution of infrared-active two-level systems will produce an infrared absorption which decreases with increasing temperature in a well-defined way. In this talk, we shall discuss a variety of measurements of the temperature-dependent absorption coefficient of amorphous dielectrics in the far infrared. In one restricted temperature and frequency regime a decrease in absorption coefficient with increasing temperature is observed as expected while in another temperature and frequency range the absorption coefficient increases with increasing temperature[7]. A complete mapping of the absorption coefficient versus frequency and temperature for a number of glasses demonstrates that both ground state and excited state transitions are observed in the far infrared. In addition the results are consistent with the presence of widely spaced manifolds of energy levels. All of these results can be explained with an asymmetric tunneling potential model. At frequencies above 10 cm^{-1} a modest temperature dependence indicates that resonant mode transitions are being measured. Apparently the spatial inhomogeneities in glass provide a natural habitat not only for Debye-like phonons but also for localized modes, resonant modes and tunneling states - excitations which in the past were associated exclusively with slightly perturbed single crystals[8].

* Work supported in part by Energy Research and Development Administration, Grant No. E(11-1)3151.

1. R.C. Zeller and R.O. Pohl, Phys. Rev. B4, 2029 (1971)
2. R.B. Stephens, Phys. Rev. B8, 2896 (1973).
3. W. Arnold, S. Hunklinger, S. Stein and K. Dransfeld, J. Non. Cryst. Solids 14, 192 (1974).

4. R.O. Pohl, W.F. Love and R.B. Stephens, in Amorphous and Liquid Semiconductors, J. Stuke and W. Brenig, eds. (Taylor and Francis, 1974), pg. 1121.

5. P.W. Anderson, B.I. Halperin and C.M. Varma, Phil. Mag. 25, 1 (1972).

6. W.A. Phillips, J. Low Temp. Phys. 7, 351 (1972).

7. K.K. Mon, Y.J. Chabal and A.J. Sievers, Phys. Rev. Letters 35, 1352 (1975).

8. A.S. Barker, Jr. and A.J. Sievers, Rev. Mod. Phys. 47 Suppl. 2 (1975).

MULTIPHONON ABSORPTION IN MIXED As_2S_3- GeS_2 GLASSES

D.S. Ma, P.S. Danielson, C.T. Moynihan and P.B. Macedo
Vitreous State Laboratory
Catholic University of America
Washington, DC 20064

Glasses in the mixed chalcogenide system $As2S3$-$GeS2$ are presumed to possess a network structure consisting of pyramidal $AsS3$ and tetrahedral GeS_4 cooordination centers bridged by sulfur atoms. According to the Molecular Model of Lucovsky and coworkers the AsS_3 and GeS_4 coordination centers are coupled vibrationally only very loosely, so that the IR and Raman spectra in the fundamental region should consist to a first approximation of bands due to "molecular" AsS_3 and GeS_4 groups. In the multiphonon region the IR spectra are similarly expected to consist of overtones and combinations of the highest frequency fundamentals of the AsS_3 groups and of the GeS_4 groups. Due to the loose coupling of the neighboring AsS_3 and GeS groups,however no multiphonon combination bands containing contributions from both AsS_3 and GeS_4 groups are expected. If these hypotheses are correct, then the absorption coefficient at a given frequency in the multiphonon region of a mixed As_2S_3-GeS_2 glass should be given by the sum of the absorption coefficients of the end member glasses weighted by their respective volume fractions:

$$\alpha = f_1\alpha_1 + f_2\alpha_2 \qquad (1)$$

where α is absorption coefficient, f is volume fraction, and subscripts 1 and 2 refer respectively to the pure As_2S_3 and GeS_2 glasses.

A series of mixed As_2S_3- GeS_2 glasses have been synthesized and their IR spectra measured in the region where absorption is due to two and three phonon multiphonon processes (500-1250 cm^{-1}, 8-20 μm). Good agreement is observed between the experimental absorption coefficients and those calculated from the end member spectra via Eq. (1). These results thus support the Molecular Model of Lucovsky and coworkers as a first approximation account of multiphonon processes in network glasses containing more than one type of coordination center.

AN ASSESSMENT OF Ge-As-Se 8-12 μm INFRARED OPTICAL GLASSES FOR APPLICATIONS IN THERMAL IMAGING SYSTEMS

A N Pitt, J A Savage and P J Webber

Royal Signals and Radar Establishment
Malvern, England

SUMMARY

There is much interest in infrared (IR) scanning systems and pyroelectric vidicons for thermal imaging at wavelengths within the range 8 to 12 μm. Lens materials of excellent optical quality are required to obtain the optimum performance from such systems. Generally a single germanium lens is used, but if the highest resolution is required then the small degree of chromatic aberration in germanium must be corrected by means of an additional component which could be made from a chalcogenide glass possessing a refractive index of about 2.5 and an appropriate value of reciprocal dispersive power within the range 100 to 200. The reciprocal dispersive power between 8 and 12 μm, V_{8-12}, may be defined as $\frac{n_{10}-1}{n_8-n_{12}}$, where n is the refractive index. Other requirements are, that the uniformity of refractive index be maintained within $\pm$ 0.00005 in an optical blank, that the glass transition temperature be in excess of 150°C, that the glass should be thermally stable when made in batch sizes of 5 Kg, that the mechanical strength and surface hardness should be as high as possible, and that the thermal expansion should be as low as possible.

In 1964[1] the glass forming region for 20 gm melts in the Ge-As-Se system was reported together with information showing that the oxide impurity absorption in these glasses could be greatly reduced and hence that these glasses were in principle suitable for 8-12 μm applications. Since that time work has been done to establish the physical properties of selenide glasses[2,3] and this has enabled industrially makeable glasses to be idenified.

This paper will demonstrate the influence of oxide impurity on the IR transmission of the three glasses, Ge20 Se80, As40 Se60, and Ge30 As15 Se55 from the Ge-As-Se system. Graphs of IR transmission will be presented and quantitative plots of oxygen concentration against IR oxide absorption coefficient will be shown. A brief account will be given of the preparative techniques which enable glass to be made with oxide contents of the order of 1 ppm wt as measured by a gamma photon activation technique. Measured data will be presented on glass transition temperature, thermal expansion coefficient and refractive index. The range of V_{8-12} from 110 to 159 for the glasses in this system will be discussed in relation to the basic physical properties of these materials and it will be shown that useful glass compositions for bulk synthesis are available in the system.

1 J A Savage and S Nielsen, Phys Chem Glasses 5 (3) 1964, 82.

2 C Jones and H Hafner, Texas Instruments research on infrared optical materials Report No AFAL-TR-68-348, 1969.

3 P J Webber and J A Savage, J Non Crypt. Solids 20 (1976) 271.

NOTES

Temperature Derivative of the Refractive Index of Diamond,
John Fontanella and Richard Johnson, Physics Department, U. S. Naval Academy, Annapolis, MD 21402 and Carl Andeen, Physics Department, Case Western Reserve University, Cleveland, OH 44106

The dielectric constant for diamond is measured at audio frequencies over the temperature range 5.5 - 400 K. The temperature derivative of the refractive index is calculated from the data and compared with the predictions of recent theories.

ANALYSIS OF INFRARED REFLECTIVITY IN THE PRESENCE OF ASYMMETRICAL PHONON LINE

F. Gervais and J.L. Servoin

Centre de Recherches sur la Physique des Hautes Températures
C.N.R.S., 45045 Orléans, France

Lithium niobate and lithium tantalate are ferroelectric crystals which undergo a ferroelectric → paraelectric phase transition at high temperature, 1480 K and 891 K respectively. Their technical importance is well known. The present paper reports several methods of analysis of infrared reflectivity spectra applied to these important materials taken as an example, in the situations where either the spectra are incomplete, that is the present case, and consequently a Kramers-Kronig analysis appears unsuitable, or when a KK analysis would be of doubtful validity due to experimentaluncertainties in certain spectral ranges where reflectivity data play a dominant role in the calculation of the phase. In addition, casting aside the lattice dynamics of the so-called soft mode which is extensively studied, we will consider the behavior of all TO and LO A_1-type modes in both compounds and consequently the dielectric function and optical constants that they yield, in the vicinity of the phase transition. Recent results in quartz indeed[1] have focused attention on the possible "critical" behavior of any vibrational mode in the vicinity of phase transitions.

The temperature dependence of the infrared reflectivity is presented from room temperature up to 1175K in $LiNbO_3$ and up to 1280 K in $LiTaO_3$ for the extraordinary ray. Room temperature data had been fitted with the classical dispersion theory (3 parameters per polar mode : oscillator strength, TO frequency and TO damping) by Barker et al.[2] We were unable to fit the spectra obtained at higher temperature with this model. We have tried the factorized form of the dielectric function

$$\varepsilon = \varepsilon_\infty \prod_j \frac{\Omega_{jLO}^2 - \omega^2 + i\gamma_{jLO}\omega}{\Omega_{jTO}^2 - \omega^2 + i\gamma_{jTO}\omega} \qquad (1)$$

which contains a fourth parameter per polar mode, viz. the damping γ_{jLO} of the longitudinal mode and may yield better fit in the case of wide reflectivity bands as shown previously,[3] but we did not succeeded for most of the spectra. This is due to an asymmetry of both TO near 600 cm^{-1} and LO near 400 cm^{-1} lines. Mode-mode coupling or a frequency-dependent damping function may cause asymmetrical line shapes whereas the model eq. (1) involves constant dampings and thus is not appropriate.

The two-mode coupling model proposed by Barker and Hopfield[4] has been considered. The factorized form (1) of the dielectric function can be easily modified to account for such a coupling. Non-diagonal terms of the form $k_{12}^2 + i\gamma_{12}\omega$ in the 2x2 coupling matrix should be merely inserted into the product of resonance terms. Two TO coupled modes plus a set of uncoupled modes can then be described by

$$\varepsilon = \varepsilon_\infty \frac{\prod_j (\Omega_{jLO}^2 - \omega^2 + i\gamma_{jLO}\omega)}{\{(\Omega_{1TO}^2 - \omega^2 + i\gamma_{1TO}\omega)(\Omega_{2TO}^2 - \omega^2 + i\gamma_{2TO}\omega) - (k_{12}^2 + i\gamma_{12}\omega)\}\prod_{j>2}(\Omega_{jTO}^2 - \omega^2 + i\gamma_{jTO}\omega)} \qquad (2)$$

On the other hand, since the damping function mirrors the two-phonon density of states, when there exists an intense peak at the frequency $\omega_{2ph} \simeq \omega_2 \pm \omega_1$, an oversimplification of the lowest-order self-energy function[5] leads to

$$\Delta\omega(\omega) + i\gamma(\omega)/2 = \Delta\omega_0 + i\gamma_0/2 + g^2/(\omega - \omega_{2ph} - i\Gamma) \qquad (3)$$

Figure 1 shows the best fits to the $LiNbO_3$ data at 1175 K with the aid of the dielectric function models eqs. (1), (2) and model 3 which is eq. (1) with the inclusion of eq. (3) for the 572 cm^{-1} TO mode only. The fit appears excellent with the last model. The temperature dependence of

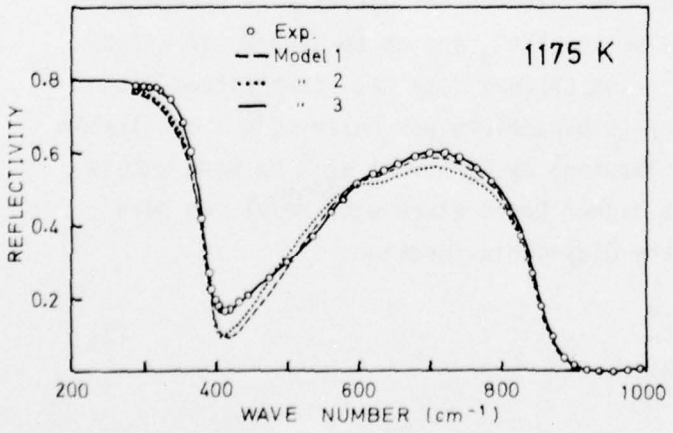

Figure 1

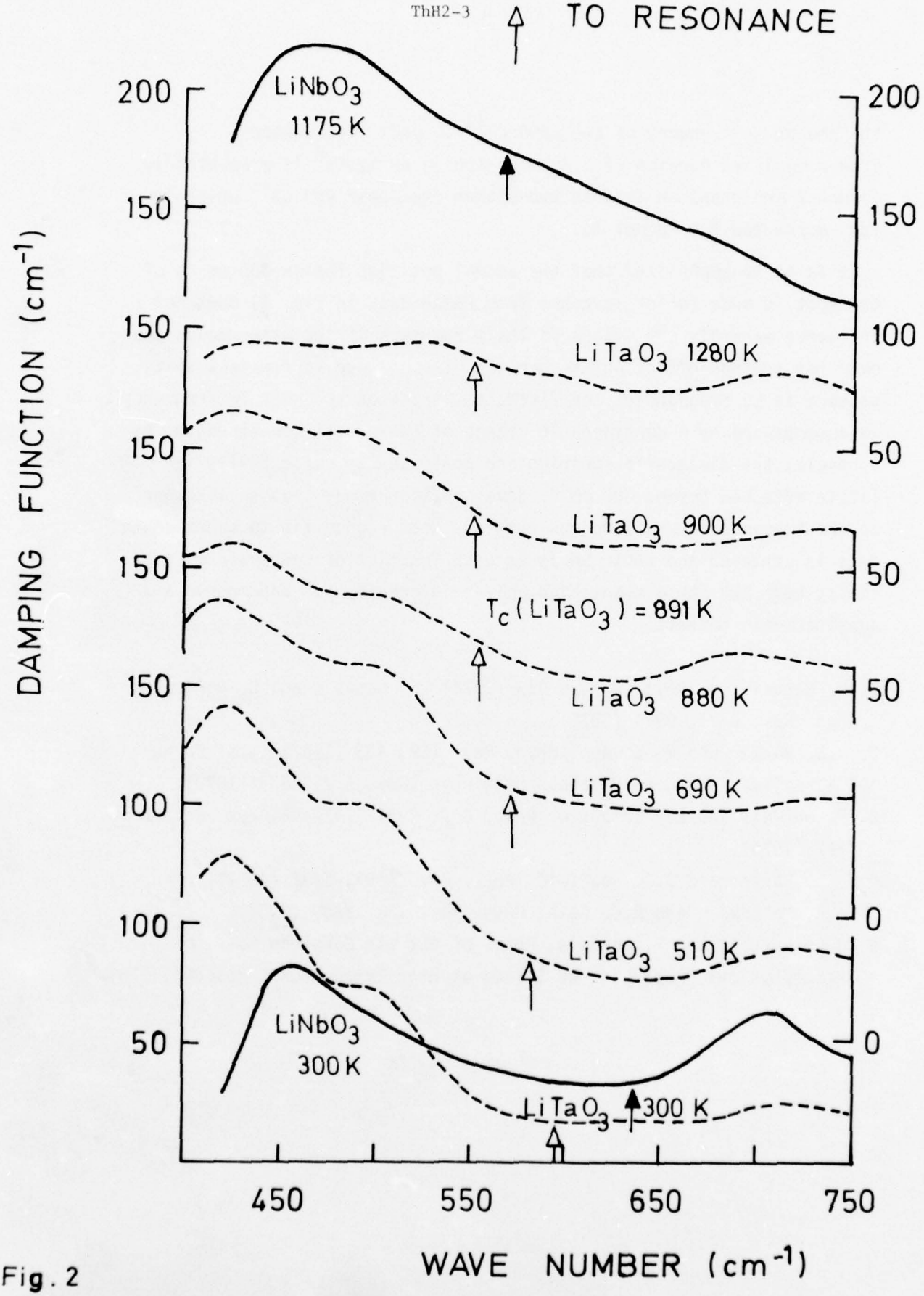
TO RESONANCE
LiNbO3 1175 K
LiTaO3 1280 K
LiTaO3 900 K
Tc (LiTaO3) = 891 K
LiTaO3 880 K
LiTaO3 690 K
LiTaO3 510 K
LiNbO3 300 K
LiTaO3 300 K
DAMPING FUNCTION (cm-1)
WAVE NUMBER (cm-1)
200
150
100
50
0
450
550
650
750

Fig. 2

the phonon self-energy of the $\sim$600 cm^{-1} TO mode calculated from a modified version of a Kramers-Kronig analysis[6] is presented in figure 2 and shows an intense two-phonon peak near 450 cm^{-1} which is thus accounted for (model 3).

It is to be emphasized that the actual position (below 300 cm^{-1}) of the soft TO mode (which is taken from Raman data in fig. 1) does not influence markedly the values of the parameters of the other modes and even has a minor effect on its own γ_{TO}. This is due to the fact that, as soon as LO frequencies are fixed, the shift of the soft TO frequency is accompanied by a considerable change of the oscillator strength. As a result, the dielectric function and consequently reflectivity is little affected beyond 300 cm^{-1}. Some confidence may thus be attached to the frequencies and dampings obtained when a good fit to experimental data is achieved and their analysis as a function of temperature, especially near the phase transition, gives information on anharmonic and quasiharmonic effects.

1. F. Gervais, J. Phys. C 7, L 415 (1974). F. Gervais and B. Piriou, Phys. Rev. B 11, 3944 (1975).
2. A.S. Barker and R. Loudon, Phys. Rev. 158, 433 (1967). A.S. Barker, A.A. Ballman and J.A. Ditzenberger, Phys. Rev. B 2, 4233 (1970).
3. F. Gervais and B. Piriou, J. Phys. C 7, 2374 (1974) - Phys. Rev. B 10, 1642 (1974).
4. A.S. Barker and J.J. Hopfield, Phys. Rev. 135A, 1732 (1964).
5. A.A. Maradudin and A.E. Fein, Phys. Rev. 128, 2589 (1962).
6. J.L. Servoin and F. Gervais, Proc. of the 5th European Conf. on Thermophysical Properties of Solids at High Temperature, Moscow (1976).

FIR EMISSION FROM n-TYPE $Hg_{.8}Cd_{.2}Te$ IN ELECTRIC FIELDS

G. Nimtz and E. Tyssen
II. Physikalisches Institut der Universität zu Köln
Zülpicher Strasse 77, D-5000 Köln / Germany

We report about a strong FIR emission which was observed when electric fields are applied to n-type $Hg_{1-x}Cd_xTe$. The composition ratio was $x = 0.2$. (The sample data are at 77 K : $n = 1.... 10 \cdot 10^{14}$ electrons/cm^3 and $\mu = 300\,000$ cm^2/Vs). The radiation occurs in electric fields of the order of 1 V/cm and was observed in pulsed as in d.c. fields. The intensity of the emission varies linearly with electric fields up to a field strength at which a sample heating takes place. For a sample surface of 1 cm^2 a total intensity up to 10^{-7} W has been measured. The spectral analysis carried out by a Fourier spectrometer revealed the emission of a line at 120 cm^{-1} and a band above 150 cm^{-1}. Typical results are shown in Fig. 1. It was found that the radiation does not depend on magnetic fields at least in fields up to 5 T. As seen from Fig.1 the application of a magnetic field does not shift the frequencies of the radiation. The emission was observed in the temperature range between 4.2K and 300 K.

At present this FIR radiation emission is not fully understood. However, there were observed main properties i) an independence of the radiation of the magnetic field. This reveals that con - duction band states are not involved in the emission process. Since the effective carrier mass in the conduction band is very small a magnetically induced shift of the emission lines of some meV would be expected if conduction band states are involved in the transitions. ii) the emission line is observed at the very frequency of the HgTe-type reststrahl. It was experimen - tally proved that the emission is not generated in potential barriers in zones of contacts. Also various methods of preparation of the sample surface have been applied as different

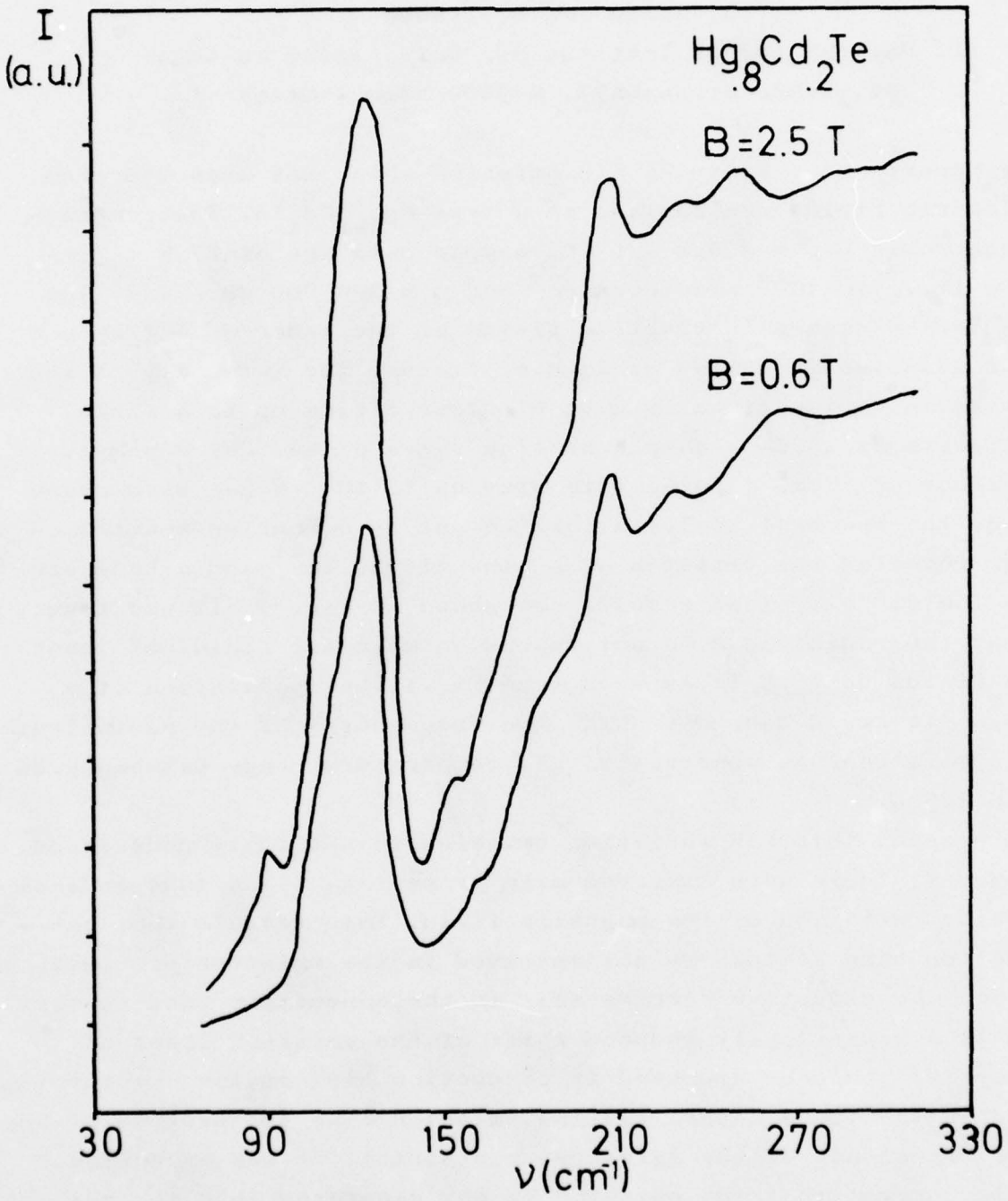
I
(a.u.)
$Hg_{.8}Cd_{.2}Te$
B=2.5 T
B=0.6 T
30
90
150
210
270
330
ν(cm⁻¹)

chemical etchings and mechanical polishing. However, the emission was not significantly influenced by these different procedures of sample preparation. Tentatively we assume the FIR emission to be due to acceptor states. There was reported in some investigations e.g.[1] about the evidence of acceptor states corresponding to Hg - vacancies in the mixed crystal system. At present it is assumed that in pure crystals acceptor and donor states caused by lattice defects particularly vacancies are determing the extrinsic carrier densities. And it is well known that the number of these defects limits the high performance of IR detectors. At the moment we assume that the emission corresponds to such a lattice defect having energy levels 3.7 meV and 18.6 meV above the valence band.

1) R. Dornhaus and G. Nimtz, Springer Tracts In Modern Physics, Vol. 78 (1976)

Fig. 1 : FIR emission spectrum from n-type $Hg_{.8}Cd_{.2}Te$ at two magnetic fields. (T = 4.2 K, E = 4 V/cm)

INFRARED PROPERTIES OF STOICHIOMETRIC AND NON-STOICHIOMETRIC RUTILE TiO_2

F. Gervais and J.F. Baumard

Centre de Recherches sur la Physique des Hautes Températures
C.N.R.S., 45045 Orléans, France.

Rutile TiO_2, which is not ferroelectric, exhibits however high values for the static dielectric constant ε_0. It has large refractive indices and the present study reports an appreciable increase of the dielectric constant ε_∞ "seen" by the infrared region, in non-stoichiometric samples. ε_∞ indeed increases from 6 for the ordinary ray of TiO_2 up to 8.3 in $TiO_{1.96}$, for example.

While stoichiometric rutile has insulating properties at room temperature, the absorption coefficient in the transparent regime between 1500 and 3000 cm^{-1} is found to increase with temperature above 1200 K much more rapidly than one would expect from the laws for multiphonon absorption, as widely discussed in recent years, when compared to corundum[1] for example. Rutile indeed becomes a semiconductor compound at high temperature or even at room temperature when the sample is partially reduced, owing to loss of oxygen, and absorption by charge carriers may play a dominant part.

The present paper reports the infrared reflectivity (270 - 3000 cm^{-1}) of TiO_{2-x} samples with x varying from 0.001 to 0.1. The temperature dependence of infrared reflection spectra of stoichiometric rutile with emphasis on "ferroelectric" properties has been studied recently.[2] In TiO_{2-x}, the frequency of the plasmon which is found increases up to 530 cm^{-1}. Due to the overdamped character of the plasmon excitation, the dampings of the LO phonon-plasmon coupled modes are much higher than those of corresponding TO phonon modes so that the classical theory of dispersion (which implies essentially equal damping for TO and corresponding LO modes, as

discussed previously) with an additional Drude term fails and does not allows one to fit the reflection spectra.

A dielectric function model expressed in the form

$$\varepsilon = \varepsilon_\infty \{ \prod_{j,ph} \frac{\Omega_{jLO}^2 - \omega^2 + i\gamma_{jLO}\omega}{\Omega_{jTO}^2 - \omega^2 + i\gamma_{jTO}\omega} - \frac{\Omega_p^2 + i(\gamma_p - \gamma_0)\omega}{\omega(\omega - i\gamma_0)} \} \qquad (1)$$

is proposed and found to fit the data satisfactorily. In the present model, the Ω_{jTO}'s are the transverse phonon frequencies, the Ω_{jLO}'s the frequencies of the uncoupled LO phonons, Ω_p the plasmon frequency, γ_p its damping and γ_0 the damping at the zero "transverse frequency". Longitudinal coupled modes are the zeroes of equation (1), and their frequency and life time can be obtained from the function $\omega\mathrm{Im}(1/\varepsilon)$ which is known when a good fit to the data is achieved. LO phonon-plasmon coupled mode parameters could be obtained independently by fit with the now almost usual factorized form of the dielectric function.[2] But it is more advantageous to analyse decoupled excitations in the subsequent step of the study.

On assuming that the oscillator strengths $\Delta\varepsilon$ of the polar modes in TiO_2 are unaffected by small departure from stoichiometry, the frequencies of the uncoupled LO phonons may be evaluated on the basis of the new value of ε_∞. An increase of ε_∞ shifts LO phonon modes towards low frequency according to

$$\Omega_{LO}^2 = \Omega_{TO}^2(1 + \Delta\varepsilon/\varepsilon_\infty)$$

for a single reflection band. The coupling with the plasmon mode increases the frequency. The balance between both effects provides a coupled mode frequency which is not very different from that of the LO frequency in stoichiometric TiO_2.

On heating (at ~400 K only to avoid reoxidation), the plasmon frequency increases by 100 cm^{-1}. Phonon dampings are only little affected. Their increase due to filling of phonon levels according to laws determined in the stoichiometric compound,[2] possibly counterbalances a decrease due to a partial structural arrangement as a consequence of annealing. The disorder indeed introduced in the reduced then quenched samples, changes the phonon dampings in a quantity which increases monotonically with x and reaches 10 to 50 cm^{-1}, while TO phonon frequencies remain

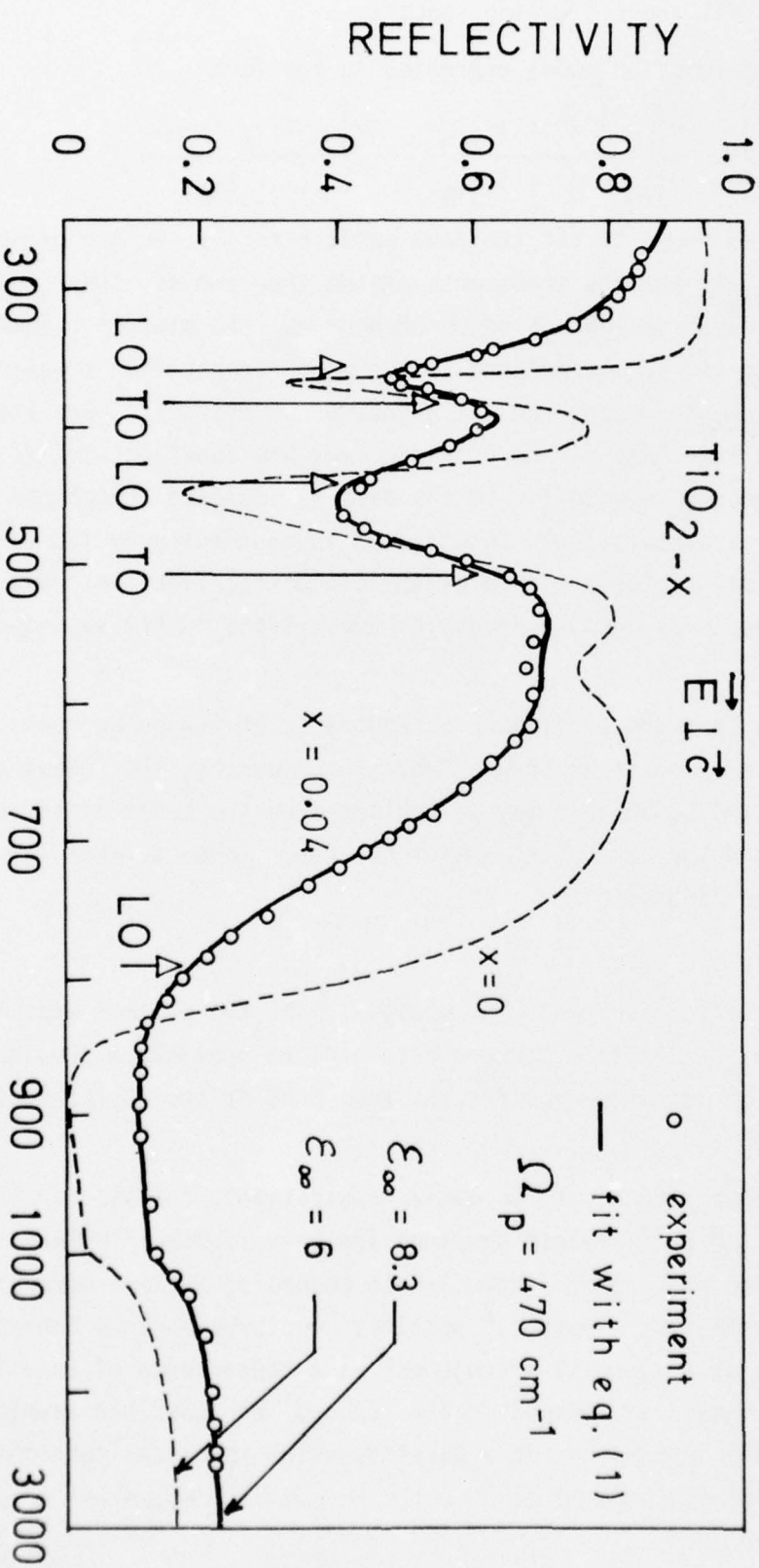
REFLECTIVITY
1.0
0.8
0.6
0.4
0.2
0
300
500
700
900
1000
3000
FREQUENCY (cm⁻¹)
TiO2-x
E ⊥ c
o experiment
— fit with eq. (1)
Ωp = 470 cm⁻¹
ε∞ = 8.3
ε∞ = 6
x = 0.04
x=0
LO TO LO TO
LO

practically unchanged in TiO_{2-x}.

1. F. Gervais, D. Billard and B. Piriou, Rev. Hautes Tempér. Réfract. 12, 58 (1975). D. Billard, F. Gervais and B. Piriou, Phys. status solidi (b) 75, 117 (1976).

2. F. Gervais and B. Piriou, Phys. Rev. B 10, 1642 (1974).

MAGNETOREFLECTION STUDIES OF $Hg_{1-x}Cd_xTe$ ALLOYS

M. H. Weiler, R. L. Aggarwal, and B. Lax

Francis Bitter National Magnet Laboratory*
and Physics Department
Massachusetts Institute of Technology
Cambridge, Massachusetts 02139

ABSTRACT

Infrared magnetoreflection measurements have been made on $Hg_{1-x}Cd_xTe$ single crystal samples for alloy compositions in the range $0.18 \leq x \leq 0.30$, and at both liquid helium and liquid nitrogen temperatures. A number of samples were oriented with reflecting faces perpendicular to (100) or (111) crystal axes. Peaks of $\Delta R/R$ from approximately 0.5% to more than 20% have been observed using circularly polarized radiation from 19 to 2.5 μm, in applied magnetic fields up to 15 T.

The observed magnetoreflection peaks have been identified as transitions between the Landau levels of the valence and conduction bands. The peak positions have been compared to theoretical calculations using the quasi-Ge model which treats exactly the interactions among the conduction, valence and split-off bands. A least-squares fit has been made to each set of data, to yield the $Hg_{1-x}Cd_xTe$ band parameters as a function of temperature, alloy composition, and crystal orientation with respect to the applied magnetic field.

*Supported by the National Science Foundation

NOTES

A HIGH ENERGY $LiNbO_3$ TUNABLE SOURCE

R.L. Byer & R.L. Herbst
Applied Physics Department
Stanford University

and

H. Ito
Tohoku University
Sendai, Japan

I. INTRODUCTION

We describe progress on a new broadly tunable narrowband $LiNbO_3$ parametric oscillator system called a "parametric tuner" that is based on a previously published optical scheme,[1] but offers a significant improvement in tuning characteristics. The narrowband, high energy parametric oscillator system is now recognized as a useful tool for applications in laser chemistry, nonlinear spectroscopy and remote monitoring.

II. Nd:YAG SOURCE

The operation of a parametric oscillator requires a diffraction limited pump laser source. We have previously used a TEM_{oo} mode laser/amplifier system which provided 370 mJ of output energy at up to 10 pps. To more efficiently utilize the Nd:YAG rods we have investigated a Nd:YAG unstable resonator oscillator.[2] Our presented design uses a 6.3 mm diameter oscillator rod followed by a 9 mm amplifier rod and generates 780 mJ in a 10 nsec Q-switched pulse at 10 pps. The unstable resonator Nd:YAG oscillator provides over 150 mJ output which is substantially diffraction limited and has been doubled, tripled and quadrupled in KD^*P and ADP to generate 30 mJ, 12 mJ and 10 mJ of .5320, .3547 and .2660 μm output. More importantly, the $LiNbO_3$ parametric oscillator operates with an improved threshold and conversion efficiency with the unstable resonator pump.

III. $LiNbO_3$ PARAMETRIC TUNER

The $LiNbO_3$ parametric oscillator operates over the 1.4 - 4 μm tuning range shown in Fig. 1 as a singly resonant oscillator (SRO) with the 1.4 - 2.1 μm signal wave resonated within a 13 cm long optical cavity formed by a grating and 50% reflecting output coupler. The grating provides linewidth control to less than 2 cm^{-1} even to degeneracy. In addition the grating provides an absolute frequency reference to within ±1 cm^{-1} over the tuning range of the oscillator.

The parametric tuner is controlled by an interactive software program using a PDP11E10 minicomputer acting through a CAMAC controller. The software allows the initial wavelength, scanning rate and scan range to be set and also allows for pressure and etalon control. Figure 2 illustrates a coherent anti-Stokes Raman spectra of H_2 taken with the $LiNbO_3$ tuner by mixing the tunable output between 1.912 and 1.8939 μm to generate the red anti-Stokes output. The spectra clearly shows the 0.25 cm^{-1} grating steps over the 50 cm^{-1} tuning range. This spectra was taken single ended and serves to illustrate the stability of the source.

Comparison of the $Q_o(1)$ peak frequency relative to 1.064 μm showed that the grating was calibrated to within ±1 cm^{-1}. Furthermore, rescanned spectra showed that the grating resettability was ±.25 cm^{-1} or one motor step. The conversion efficiency in this CAR spectra was high enough to warrant four sheets of computer paper prior to the photo-multiplier to prevent saturation.

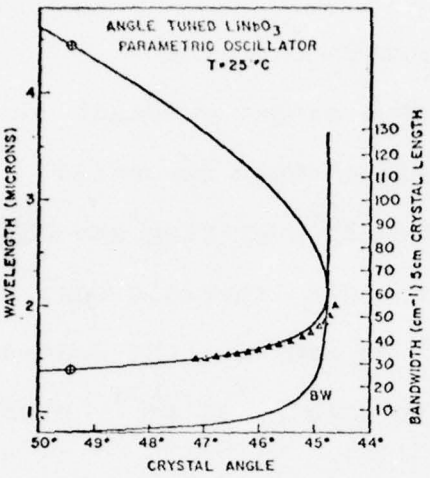

FIG. 1--Tuning range and gain bandwidth for the angle tuned 1.06 μm pumped $LiNbO_3$ parametric oscillator tuner.

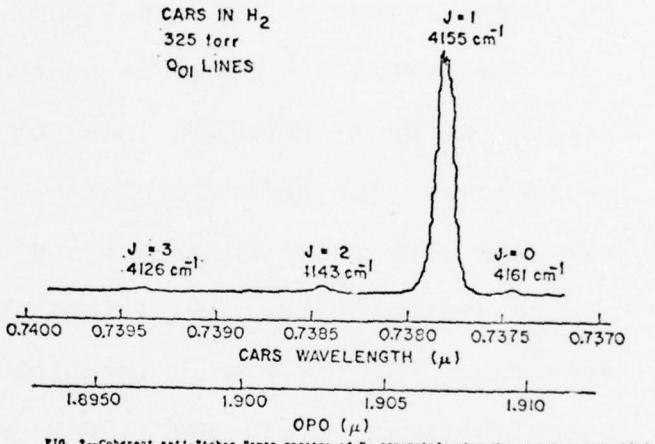

FIG. 2--Coherent anti-Stokes Raman spectra of H_2 generated using the computer controlled $LiNbO_3$ source.

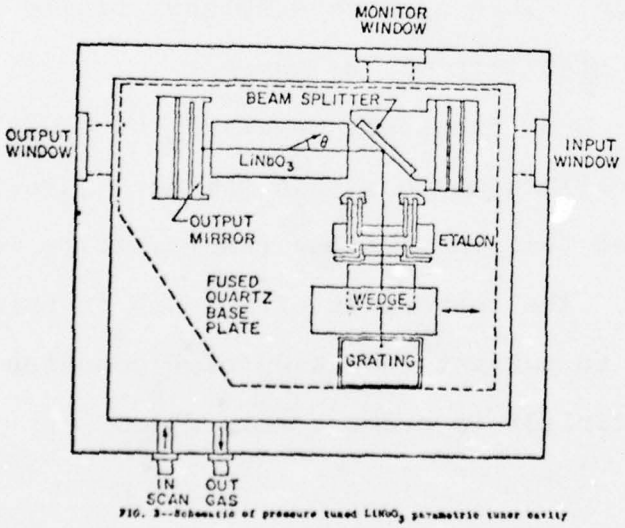

FIG. 3--Schematic of pressure tuned $LiNbO_3$ parametric tuner cavity

To further improve the linewidth and frequency control of the $LINbO_3$ tuner we have developed a compact, pressure tuned, fused silica stabilized optical cavity. The schematic of the cavity is shown in Fig. 3. The cavity uses a grating and air spaced tilted etalon for linewidth narrowing. As the pressure scans both elements tune synchronously at a rate of approximately 1 cm^{-1} per atm of argon. The cavity mode frequency, however, does not scan in synchronism with the etalon and grating due to the presence of the $LiNbO_3$ crystal within the cavity. Therefore, we invented a Brewster angle fused silica wedge, scanned by a stepper motor, to compensate for the cavity tuning rate and to allow single axial mode tuning over the few wavenumber range.

The present $LiNbO_3$ parametric tuner provides a unique near infrared tunable source. Frequency extension into the far infrared is possible by mixing and into the visible by harmonic generation. Improvements in the parametric tuner linewidth and frequency control can be extended to a much wider spectral range providing the possibility of a very widely tuned coherent source.

REFERENCES

1. R.L. Byer, R.L. Herbst and R.N. Fleming, "A Broadly Tunable IR Source", published in Laser Spectroscopy, ed. by S. Haroche, J.C. Pebay-Peyroula, T.W. Hansch and S.E. Harris, Springer-Verlag, Berlin. p.207-225, (1975).
2. R.L. Byer, "Parametric Oscillators", presented at the Tunable Laser Spectroscopy Conference, Loen, Norway, June 1976, (to be published).

PHONON INDUCED TRANSPARENCY OF TELLURIUM NEAR 11 /um WAVELENGTH

K.-H. Müller and G. Nimtz
II. Physikalisches Institut der Universität zu Köln
Zülpicher Strasse 77, D-5000 Köln / Germany

Tellurium shows a strong absorption line at wavelengths near 11 /um for radiation polarized parallel to the c-axis. The absorption coefficient of this line is proportional to the number of holes, therefore the line is called p-band. Tellurium is a strongly piezoelectrical material, thus by acousto-electric amplification phonon domains of extremely high acoustic flux density can be generated. The domains which can be excited by voltage pulses of approximately 1 /usec length travel with the velocity of sound through the sample. The electrical field strength necessary for the amplification is of the order of 100 V/cm. The spectral dependence of the absorption coefficient of the p-band as changed by the phonon flux is shown in Fig. 1. The spectroscopy was carried out with the different emission lines of a tunable CO_2 laser system. The results show that in the presence of an acoustoelectric domain the absorption decreases strongly and even shows a minimum at the wavelength where the absorption maximum is observed without acoustic flux. As seen from Fig. 1 the absorption maximum of the unperturbed absorption line is shifted to larger wavelengths with increasing temperature and obviously the phonon induced minimum is shifted, too. This phonon induced transparency will be explained by the following model. The absorption band corresponds to transitions between two valence bands separated by about 110 meV, thus the absorption being proportional to the number of holes in the first valence band. It is assumed that this number of holes in the first valence band is markedly reduced by a carrier heating in the high density flux of the domains. The carrier occupation of the second band, however, is increased by the carrier heating yielding a stimulated emission at any further carrier redistribution. The estimated carrier temperature in the acousto-electric domain is about 400°K which is in agreement with the theoretical model of Bugaev et al.[1]. Thus the observed phonon induced transparency is assumed to be a hot carrier effect in the field of the high density flux. The effect is ob-

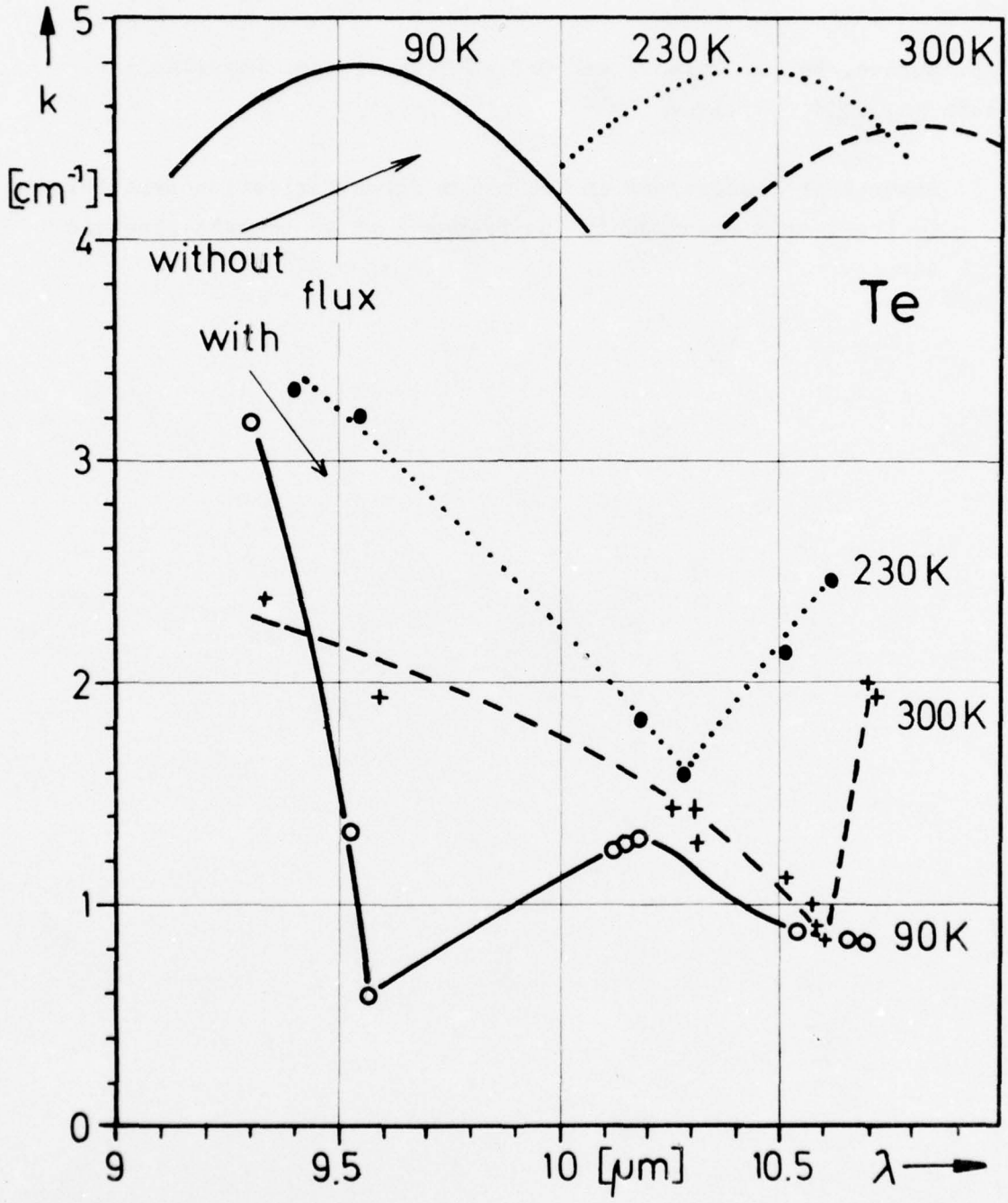
k
[cm⁻¹]
5
4
3
2
1
0
90 K
230 K
300 K
without flux
with
Te
230 K
300 K
90 K
9
9.5
10 [μm]
10.5
λ

served with radiation near 11 /um independent of the intensity of the laser radiation. The switching time of this effect is of the order of 1 /usec.

1) A.S. Bugaev, Yu. v. Gulaev, and G.N. Shkerdin, Sov. Phys.-Solid State 12, 2133 (1971)

Fig. 1: Absorpiton coefficient in Tellurium for polarization parallel to the c-axis measured in the presence of an acousto-electric domain.

EFFICIENT NEAR INFRARED STIMULATED RAMAN SCATTERING IN GLASS FIBER WAVEGUIDES

by

Chinlon Lin, R. H. Stolen, L. G. Cohen,
G. W. Tasker* and W. G. French*
Bell Telephone Laboratories
Holmdel and Murray Hill*, New Jersey

SUMMARY

We report observation of efficient high order stimulated Raman scattering in the near infrared in small core glass fiber waveguides. Many nonlinear optical processes have been observed in fiber waveguides in the visible region with low powers. High conversion efficiency is possible because high intensity, confined optical interactions can be maintained over long lengths of fiber waveguides. Particularly interesting is the near infrared region where intensive research, stimulated by optical communication applications, has produced highly transparent glass fiber waveguides. These low loss glass fiber waveguides are attractive media for Raman lasers and amplifiers in the near infrared. In our present experiments with low loss single mode and low mode silica fibers we have observed efficient high order stimulated Raman scattering. Using a 1.06 μ pulsed Nd:YAG laser as the source and with a pump power of 250 W in a 175 m silica fiber of 6 μ core diameter, we obtained four orders of Stokes at 1.11 μ, 1.17 μ, 1.22 μ, and 1.28 μ respectively. We also observed three orders of Stokes generated with similar

pump powers in a 4 m, 3 μ core diameter pure germania fiber. Germania has a Raman cross-section an order of magnitude larger than that of pure silica, but the usable length is limited by the large loss of the present fiber. In another experiment with a pure silica core fiber pumped by a near infrared dye laser ($\lambda \sim 0.78$ μ) of large spectral width (~ 100Å) a near infrared broadband continuum spanning more than 1000Å in the .8 - .9 μ region was observed. In both the discrete pump (Nd:YAG laser) and the broadband pump (dye laser) experiments the time characteristics of various wavelength components showed clearly the processes of efficient sequential Stokes generation. Typically the pump and the lower order Stokes are two-peak pulses with completely or partially depleted center regions while higher order stimulated Stokes pulses appear as narrower single pulses. The overall duration of the broadband near infrared continuum is ∿10 ns, slightly less than that of the dye laser pump. This continuum should be useful for nanosecond excited state spectroscopy. The discrete, multi-wavelength emissions (1.06 μ - 1.28 μ), are in a region of particular interest for fiber waveguide studies because this is the region of lowest loss and minimum material dispersion. Recently glass fiber waveguides with loss < 1 dB/km between 0.95 μ - 1.37 μ and < 20 dB/km between 0.5 - 1.9 μ are reported.[1] Such glass fibers offer the possibility of efficient Raman lasers and amplifiers for the 1-2 μ region.

REFERENCE

1. M. Horiguchi and H. Osanai, Electron. Lett. 12, 310 (1976).

INFRARED GENERATION BY NONLINEAR 4-PHOTON MIXING IN GERMANIUM*

N. Lee, R. L. Aggarwal†, and B. Lax†

Francis Bitter National Magnet Laboratory‡
Massachusetts Institute of Technology
Cambridge, Massachusetts 02139

ABSTRACT

We are developing a high power step-tunable radiation source in the 8 to 13 μm region by 4-photon mixing of two or three CO_2 laser beams in germanium. Germanium is chosen because of its relatively large third-order nonlinear susceptibility,[1-4] availability of high-purity single crystals in large sizes[5] and high transparency in the above spectral region.[6] The efficiency of output is strongly dependent on the high order multiphonon losses in the crystal.

We have achieved,[7] for the first time, phase-matched 4-photon mixing in germanium using the noncollinear mixing geometry. With 3 MW/cm^2 peak input intensity from each of two CO_2 TEA lasers operating at ω_1 = 1045.02 cm^{-1} (P22) and ω_2 = 945.98 cm^{-1} (P18), 1 mJ of energy per pulse was obtained at 8.7 μm ($\omega_3 = 2\omega_1 - \omega_2$) using an 8.3 cm long crystal of germanium. Assuming that the output energy is contained in a 100 nsec (FWHM) pulse, the corresponding peak power generated at 8.7 μm was 10 kW, which was in reasonable agreement with our theoretical calculation of 22 kW.

*Supported in part by Massachusetts Institute of Technology Funds and in part by the Advanced Research Projects Agency through the Office of Naval Research
†Also Department of Physics, Massachusetts Institute of Technology
‡Supported by the National Science Foundation

Since the damage threshold of germanium is approximately 100 MW/cm^2, one can conservatively increase the input intensity to 10 MW/cm^2 for each of the two input beams. Using beams of 1 cm^2 in cross section and 10 MW/cm^2 in input intensity and a 20 cm long AR coated germanium crystal, the projected output energy at 8.7 μm is well over 100 mJ per pulse, or the projected output power is above MW level. It is quite obvious that the output power can be further linearly scaled up with input beams of the same intensity but larger cross section.

Similar 4-photon mixing experiments were also attempted for the generation of radiation at $\omega_3 = 2\omega_2 - \omega_1$ in the 12 μm region. However, there is a large discrepancy between observed and calculated values taking into account absorption losses as obtained in the literature. We are currently looking into this discrepancy.

We have demonstrated the tunability of the FIR radiation[8] by difference-frequency mixing of two CO_2 lasers in GaAs with frequency spacing as small as 0.01 cm^{-1} when both the CO_2 lasers are simultaneously step tuned by a line at a time. Similar tunability can be obtained with our 4-photon mixing in germanium by choosing different lines for the two input CO_2 lasers. Orders of magnitude more combinations of frequencies can be obtained by using three different CO_2 lasers. Thus, this 4-photon mixing may prove to be a very versatile and practical technique for the generation of step-tunable coherent radiation in the 8 to 13 μm region because of its room temperature operation, scalability to larger crystal and higher power densities and high power handling capability due to relatively low losses.

REFERENCES

1. C.K.N. Patel, R.E. Slusher, and P.A. Fleury, Phys. Rev. Letters 17, 1011 (1966).
2. J.J. Wynne and G.D. Boyd, Appl. Phys. Letters 12, 191 (1968).
3. S.S. Jha and N. Bloembergen, IEEE J. Quant. Electronics QE-4, 670 (1968).
4. J.J. Wynne, Phys. Rev. 178, 1295 (1969).
5. R.N. Hall, in Proceedings of the Twelfth International Conference on the Physics of Semiconductors, Stuttgart, 1974 (B.G. Teubner, Stuttgart, 1974), p. 363.
6. E.D. Capron and O.L. Brill, Appl. Optics 12, 569 (1973).
7. N. Lee, R.L. Aggarwal, and B. Lax (submitted to Appl. Phys. Letters).
8. B. Lax, R.L. Aggarwal, and G. Favrot, Appl. Phys. Letters 23, 679 (1973).

NOTES

NOTES

Second and Fourth Order Nonlinear Processes in Chalcopyrites, H. Kildall, G. W. Iseler, N. Manyuk, and J. C. Mikkelsen, Lincoln Laboratory, M. I. T., Lexington, MA 02137

The I-III-VI_2 and II-IV-V_2 chalcopyrites have received considerable attention because of their semiconducting and nonlinear optical properties. The compounds of most interest for nonlinear applications in the infrared are $AgGaS_2$, $AgGaSe_2$, $CdGeAs_2$, and $ZnGeP_2$, which are transparent and phasematchable over part or all of the 1 to 18μm region. Some of the optical properties of these four compounds are listed in Table 1. For comparison purposes Table I also lists these properties for Te, GaSe, and Ag_3AsS_3.

Use of the chalcopyrites has been quite limited because it is difficult to grow crack-free single crystals of sufficient size and optical quality, and crystals of these materials are not commercially available. Recently, however, improved techniques for the growth of $AgGaS_2$ crystals have been described in the literature. In this paper we report progress made in our laboratory on the growth and applications of $AgGaSe_2$ and $CdGeAs_2$.

The linear thermal expansion of the chalcopyrites is highly anisotropic. Therefore polycrystalline boules, and even single crystals that are not properly oriented, have a strong tendency to crack during cooling from the growth temperature. By using a seeded vertical Bridgman technique we have succeeded in obtaining crack-free single crystals of $AgGaSe_2$ up to 50 cm^3 in volume. Crystals grown from nominally stoichiometric melts exhibit marked optical attenuation in the 0.7 to 10μm range due to scattering by second-phase precipitates that form during furnace cooling to room temperature. Most of these precipitates can be eliminated by annealing samples in evacuated, sealed ampoules for a few hours at temperatures above 600^{o}C, then quenching in air. By using this technique we have reduced the scattering at 5μm sufficiently to obtain an increase of 30 percent in power conversion efficiency for frequency doubling CO_2 laser radiation in an 8 x 8 x 2 mm^3 crystal. However, quenching cannot be used for large $AgGaSe_2$ crystals, which crack when

FB1-2

PROPERTIES OF INFRARED NONLINEAR MATERIALS

Material	Index of refraction n	Nonlinear coefficient $d \times 10^{22}$ (As/V^2)	Nonlinear figure of merit d^2/n^3 (relative units)	Laser-induced surface damage threshold at 10μm (J/cm^2)	Transmission range (μm)
Te	4.9	57	405	--	4 - 25
$CdGeAs_2$	3.6	26	215	5 - 6	2.5 - 17.5
$ZnGeP_2$	3.1	6.6	22	--	0.7 - 12
GaSe	2.6	5.0	21	--	0.65 - 18
$AgGaSe_2$	2.6	2.9	7	1.5 - 3	0.7 - 19
$AgGaS_2$	2.4	1.1	1.2	3 - 3.5	0.5 - 12.5
Ag_3AsS_3 (+)	2.6	1.1	1	1.9	0.64 - 13

they are cooled too rapidly. As an alternative, we have obtained as-grown crystals with reduced scattering by growth from Se-rich $AgGaSe_{2+\delta}$ melts; the best optical quality has been achieved for initial values of δ between 0.02 and 0.04.

Most of our nonlinear experiments have been performed with $CdGeAs_2$, which has a figure of merit about 30 times that of $AgGaSe_2$. The crystals were grown by the unseeded vertical Bridgman technique, since our attempts at seeded growth of $CdGeAs_2$ have been unsuccessful. The largest crack-free crystals obtained so far have volumes of a few cubic centimeters. Most of them are p-type, with hole concentrations that range from 1.5×10^{15} to 2×10^{16} cm^{-3} at room temperature and decrease by 2 to 5 orders of magnitude on cooling to 77 K. Because of this carrier freeze-out, cooling to 77 K significantly reduces the optical absorption. (Scattering is not important for $CdGeAs_2$.) The absorption observed at 77 K, which is not decreased by cooling to still lower temperatures, may be due to transitions from the valence band to acceptor levels located about 0.3 eV above the valence band.

To take advantage of the decrease in absorption on cooling, all our nonlinear optical experiments with $CdGeAs_2$ are performed at 77 K. Cooling also increases the thermal conductivity. As a consequence of the two effects the cw damage threshold for our best crystals is increased from about 1 W at room temperature to over 20 W at 77 K for irradiation with a CO_2 laser beam focused to a 100 μm spot size. Cooling has little effect on phasematching angles, since the reduction it causes in birefringence is compensated by a decrease in dispersion. Thus the phasematching angle for second harmonic generation (SHG) with 10 μm radiation changes by less than 1 deg between room temperature and 77 K.

For SHG with pulsed CO_2 laser radiation, the highest external energy conversion efficiency that we have achieved is 24 percent, which was obtained with an AR-coated $CdGeAs_2$ crystal 12 mm long. The highest external conversion efficiency we have obtained

with $AgGaSe_2$ is 7 percent (corresponding to an internal efficiency of 14 percent), which was measured using an uncoated crystal 16 mm long. The SHG conversion efficiency in $AgGaSe_2$ increases linearly with input intensity up to the damage threshold, while for $CdGeAs_2$ the efficiency saturates below the damage threshold.

The highest outputs for SHG with CO_2 laser radiation have been achieved by using $CdGeAs_2$. Pumping with a TEA laser has given a maximum output energy of 200 mJ per pulse, while Q-switched and chopped cw lasers have given maximum values of 1.1 W and 75 mW, respectively, for the average output power.

We have observed SHG with CO_2 laser radiation in mixed crystals of several compositions in the $CdGe(As_{1-x}P_x)_2$ and $AgGa(Se_{1-x}S_x)_2$ systems. In these materials the birefringence and therefore the phasematching angle are functions of alloy composition. In the case of $CdGe(As_{1-x}P_x)_2$ we have found that the type II phasematching angle increases from 49 to 67 deg as x is changed from 0 to 0.2. From this result we estimate that 90-deg phasematching would be obtained for $x \sim 0.3$.

In addition to SHG, we have also obtained phasematched fourth harmonic generation in $CdGeAs_2$ pumped with CO_2 laser radiation. Observation of this process has enabled us to make the first measurement of the fourth order susceptibility tensor for $CdGeAs_2$.

Both $CdGeAs_2$ and $AgGaSe_2$ can be used to generate coherent radiation by sum and difference frequency mixing, as well as by SHG. By mixing CO and CO_2 laser radiation it should be possible to obtain output wavelengths over most of the region from 2.5 to 18 μm. In experiments with cw lasers we have determined the phasematching curves for difference-frequency generation between 12 and 17 μm. Over this range the type I phasematching angle for $CdGeAs_2$ changes by only 5 deg. For $AgGaSe_2$ the angle changes by about 30 deg, so that two crystals would be necessary to cover the whole 12-17 μm range.

STUDY OF THIN FILMS USING LEAKY SURFACE EM (SEM) AND INTERFERENCE EM (IEM) WAVES IN THE INFRARED*

W. P. Chen, A. Hjortsberg and E. Burstein
Department of Physics and the Laboratory for Research on the Structure of Matter, University of Pennsylvania, Philadelphia, Pa. 19174

We have carried out theoretical and experimental studies of thin films on metal surfaces, using excitation and reradiation of leaky SEM waves and interference EM waves.

The configuration used is an Otto prism-air-metal structure, in which the investigated thin film is deposited on the metal surface. Volume infrared radiation of finite beam width incident from the prism side is used to excite leaky SEM waves and interference EM waves. The beam width is chosen to be of the same order of magnitude as the propagation length of the leaky modes (mm). Excitation occurs when the wavevector parallel to the interface and the frequency of the incident beam match those of the leaky mode. Resonant excitation can be obtained either by scanning the incident angle at a fixed frequency, or by scanning the frequency at a fixed angle.

The excited leaky waves are found to build up along an "excitation region" and to propagate as damped free-running waves beyond it. At resonance, the spatial dependence of the "reflected" intensity along the interface exhibits a double peak structure at the leading edge of the "excitation

---

*Research supported by the U.S. Office of Naval Research and the National Science Foundation.

region." This is caused by destructive interference between the "mirror reflection" from the prism-air interface and the reradiation from the leaky wave generated. The radiation from the "free-running region" shows an exponential decay, and is emitted at an angle defined by the dispersion relation of the leaky mode.

Experimentally, the excitation is observed by monitoring the "reflected" intensity either from the "excitation region" or from the "free-running region." When the incident angle or the frequency is scanned through resonance, the reflection from the "excitation region" shows a dip, and the radiation from the "free-running region" exhibits a peak. The intensities from these two regions give complementary information about the excitation, and both can be used as experimental EM probes. For studies of mode characteristics and surface properties, it may, however, be advantageous to use the radiation from the free-running waves, since this directly reflects the properties of the leaky mode.

SiO films of various thickness deposited on the metal (Ag)-air interface have been investigated in the infrared using both methods. A 100 Å thick SiO film is found to modify the reradiated intensity strongly in the infrared, and to completely quench it in the 10 μ absorption band of SiO. The experimental results have been used to make a comparison of the finite beam and the plane wave excitation of leaky waves. Advantages and limitations of these techniques will be discussed and compared to the conventional external reflection case. A straightforward theoretical extension to the Kretschmann prism-metal-air configuration will be presented.

OPTICAL CONSTANTS OF THE ACCUMULATION LAYER IN SILICON MOS STRUCTURES

H. C. Chien and G. Sadasiv
Department of Electrical Engineering
University of Rhode Island
Kingston, Rhode Island 02881

INTRODUCTION

Modulation in the optical spectral region achieved with laser beams guided along thin films or epitaxial structures has led to the rapid development of integrated optics. It is interesting to consider the possibility of achieving such effects in the infrared. Though there are more experimental problems in the ir one advantage is that silicon can be used as the optical material. At 10.6 μ, for example, pure silicon is transparent and the optical constants can be modulated by changing the free carrier concentration.

In this paper we consider the modulation of the optical constants by an applied voltage in the simple silicon planar MOS structure shown in Fig. 1. By applying an appropriate voltage to the gate an accumulation layer is formed in the silicon at the Si-SiO_2 interface. We have calculated the optical constants as a function of depth x in the silicon. The calculations were made for n- and p-type silicon, with different substrate doping levels N_I, and for various values of the field E_S at the silicon surface.

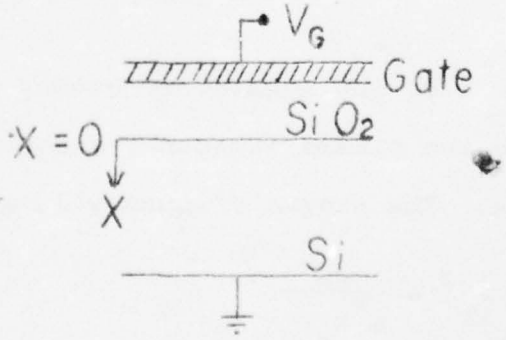

Fig. 1 Planar MOS structure.

CALCULATIONS

We assume non-degenerate statistics and neglect the minority carriers in the silicon. The potential distribution $V(x)$ in the silicon is then obtained by solving simultaneously Poisson's equation and Boltzmann's equation:

$$\pm \frac{d^2V}{dx^2} = \frac{N_I e}{\varepsilon_s \varepsilon_o} \left[\exp \left\{ \pm \frac{eV}{k_B T} \right\} - 1 \right] \qquad (1)$$

where ε_s is the relative permittivity of silicon, N_I is the impurity concentration in the substrate, the $\pm$ signs refer to n- and p-Si respectively, and the physical symbols have their usual meaning. This is solved numerically with the boundary conditions $\left.\frac{dV}{dx}\right|_{x=o} = -E_S$, and $V(\alpha) = 0$. We thus obtain N, the hole or electron concentration in the silicon, for any specified value E_S of the electric field at the silicon surface.

The optical constants n and k are then calculated from the expressions

$$2nk = \varepsilon_s \left[\frac{\omega_p^2 \tau}{\omega(1+\omega^2\tau^2)} \right] \qquad (2)$$

$$n^2-k^2 = \varepsilon_s \left[1 - \frac{\omega_p^2 \tau^2}{1+\omega^2\tau^2} \right] \qquad (3)$$

where ω is the angular frequency of the ir radiation, and ω_p and τ are the plasma frequency and relaxation time for the free carriers. The plasma frequency is given by

$$\omega_p^2 = \frac{Ne^2}{m^* \varepsilon_s \varepsilon_o} \qquad (4)$$

In the calculations the values of the optical effective mass m^* was taken to be 0.26 m_o for electrons, and 0.377 m_o for holes. τ was calculated from the experimental values of the DC conductivity σ of silicon, from the expression $\sigma = (Ne^2\tau/m^*)$.

RESULTS

The values of n and k as functions of x were calculated for values of N_I ranging from 10^{14} cm^{-3} to 10^{19} cm^{-3}, and for values of the electric field at the silicon surface of up to 10^7 V/cm. Typical results are shown in Figures 2 and 3. The depth from the surface is plotted in units of the modified Debye length L_D in the figures.

A detailed analysis of all the results will be presented, and the degree of modulation of ir radiation which can be achieved by applied voltages will be discussed.

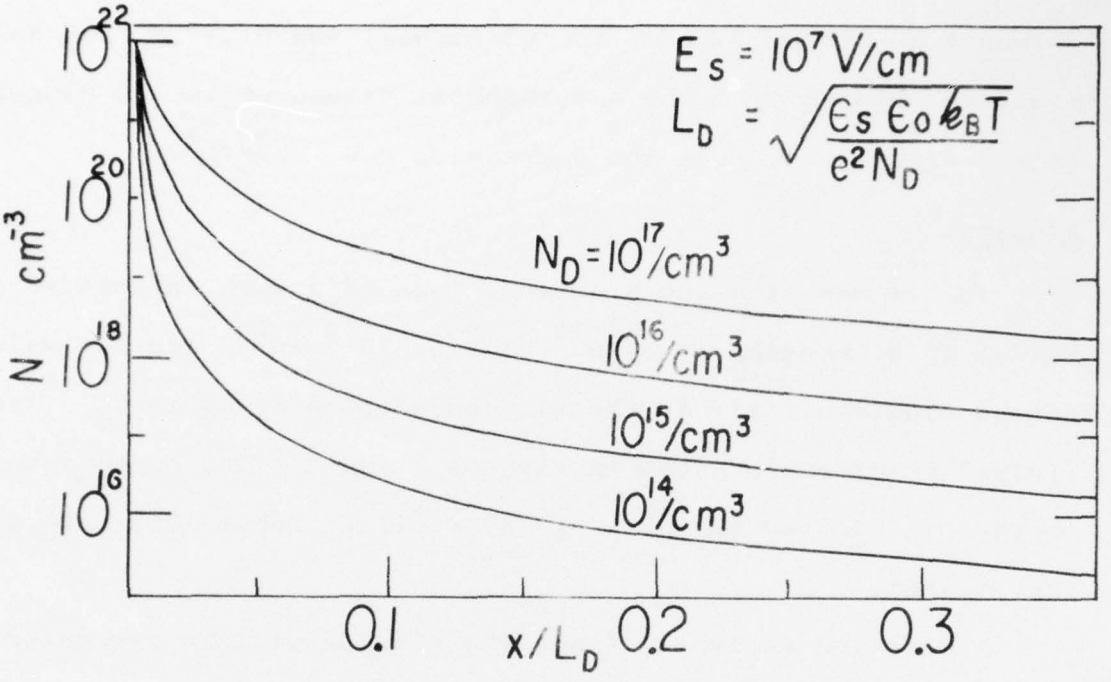

Fig. 2 Free carrier concentration in silicon.

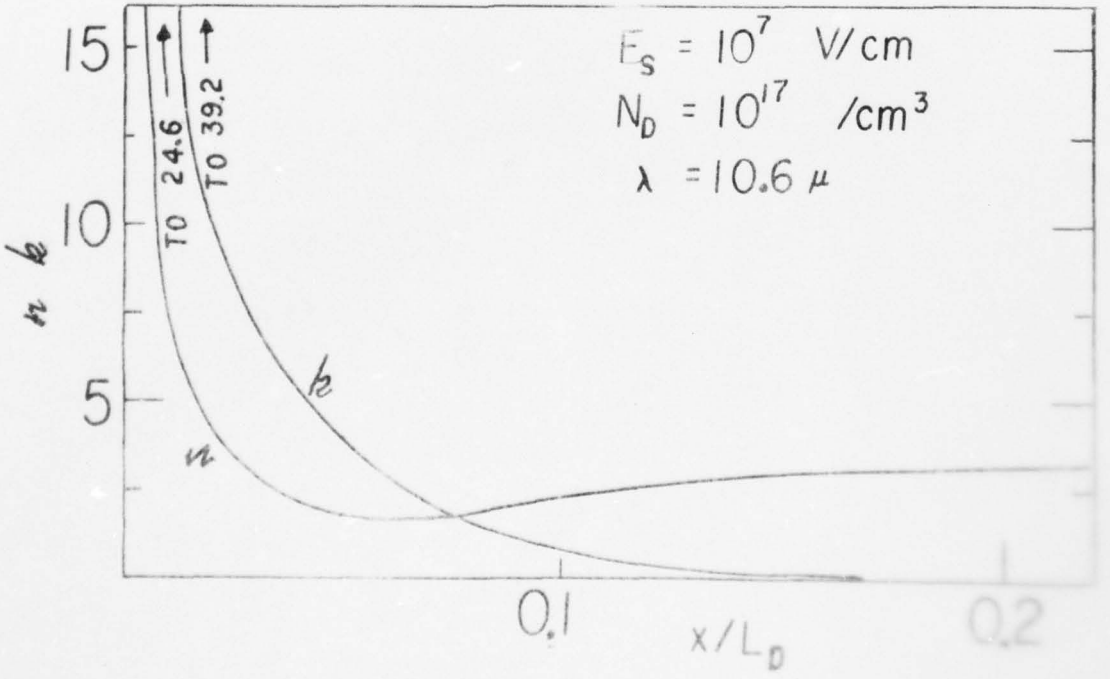

Fig. 3 Optical constants in silicon with $N_D = 10^{17}/cm^3$

AD-A037 737 OPTICAL SOCIETY OF AMERICA WASHINGTON D C F/G 20/6
OPTICAL PHENOMENA IN INFRARED MATERIALS.(U)
1976 AF-AFOSR-3061-76
UNCLASSIFIED AFOSR-TR-77-0163 NL

3 OF 3
AD A037737

END
DATE FILMED
4-77

SEMICONDUCTOR-BASED INFRARED INTEGRATED OPTICS*

I. Melngailis

Lincoln Laboratory, Massachusetts Institute of Technology
Lexington, Massachusetts 02173

SUMMARY

Integrated optical circuits (IOCs) will provide a major new capability in certain future technology areas. Together with optical fibers IOCs at infrared wavelengths in the 0.85 - 1.3 μm range will find applications in high speed communications and data transfer. Special waveguide devices and IOCs will enhance the capabilities of laser radar and atmospheric laser communications at various wavelengths from 0.85 to 12 μm. Devices primarily at the shorter infrared wavelengths will also offer new possibilities in both digital and analog data processing.

For fiber optics communications a simple integrated receiver-transmitter terminal including a waveguide detector, a directional coupler switch, and a laser-modulator combination could be a useful standard circuit. For laser radar an integrated heterodyne receiver containing a wavelength-tunable diode-laser local oscillator would be of interest. For signal processing, acoustooptic Fourier transform devices and high speed analog-to-digital converters could provide very significant extensions to present capabilities.

Semiconductor compounds have unique advantages for implementing various IOC schemes in the form of compact monolithic structures. The basic properties of these compounds in some cases permit the construction of all of the components required (waveguides, sources, detectors, modulators and directional couplers) and the techniques for selective epitaxial growth of monolithic structures are either well developed or could be developed with additional effort.

Table I summarizes the properties of four semiconductor systems that are of particular interest for different infrared wavelength ranges. The GaAs-AlGaAs system is the most

* This work was sponsored by the Department of the Air Force

developed and most used for waveguide devices at short wavelengths. (It should be pointed out that this materials system is useful for waveguide devices at longer wavelengths as well, provided there is no need for a monolithically integrated diode laser source.) A good lattice match of AlGaAs to GaAs permits the growth of epitaxial layers with low dislocation densities that are necessary for long-lifetime diode lasers and for microplasma-free avalanche diodes. A direct energy gap permits highly efficient radiative carrier recombination in light emitting diodes and diode lasers. The electrooptic effect can be used effectively in modulators and directional-coupler waveguide switches.

While the 0.85 - 0.95 wavelength range is satisfactory for many fiber-optics systems the optical wavelength for both minimum attenuation and minimum dispersion in silica fibers is near 1.3 μm. Thus for long distance (> 10 km) communications at wide bandwidths (> 100 MHz) the InP-GaInAsP system is of major importance. The use of the quaternary alloy GaInAsP makes it possible to achieve a nearly perfect lattice match to InP. The optical and electrical properties of this system are similar to those of the GaAs-AlGaAs system since both belong to the class of III-V compounds.

For longer wavelengths, which are of particular interest for systems based on high-power gas lasers, such as HF (2.7 μm) DF (3.8 μm) and CO_2 (10.6 μm) the II-VI compounds CdTe-HgCdTe and the IV-VI PbTeSe-PbSnTe are possible candidates. In the CdTe-HgCdTe system narrow-gap HgCdTe photodiode detectors for any desired wavelength in the 0.85 - 12 μm range could be incorporated into waveguide structures by selective epitaxial growth. A good lattice match enables the growth of high-quality layers by VPE. In addition, the CdTe-HgCdTe system has the advantage of a large electrooptic coefficient that is useful for phase shifters and modulators. The drawback of this system is the lack of sources, since attempts to realize diode lasers and efficient LED's in this material have so far been unsuccessful.

The PbTeSe-PbSnTe system has the advantage that efficient tunable diode lasers have been developed over a broad wavelength range and could be used, for example, in integrated heterodyne receivers. With the two ternary alloys a nearly perfect lattice match can be

achieved. (Other lead salt alloys could cover short wavelengths, e.g., PbS-PbSSe could cover the range from 3.8 to 8.5 μm.) The disadvantage of the lead-salt systems is that they are not electrooptic.

Table II is a summary of the waveguide devices that have been developed in the four alloy systems. For GaAs-AlGaAs all of the components that would be needed in a fiber communications terminal and in a number of other applications have been developed and could be incorporated into IOCs with additional effort.

TABLE I

SEMICONDUCTOR MATERIALS FOR OPTICAL WAVEGUIDE DEVICES

	GaAs-AlGaAs	InP-GaInAsP	CdTe-HgCdTe	PbTeSe-PbSnTe
Wavelength range of interest (μm)	0.85 - 0.95	0.9 - 1.7	0.85 - 12	6.5 - 12
Type of energy gap	direct	direct	direct	direct
Electrooptic coefficient (max) (m/V)	1.2×10^{-12} (GaAs)	unknown	5.3×10^{-10} (CdTe)	not electro-optic
Elastooptic coefficient	0.07 - 0.2 (GaAs)	unknown	.057 - .15 (CdTe)	unknown
Lattice mismatch (%)	≤ 0.35	--	≤ 0.8	--
Epitaxial growth techniques developed	LPE, VPE MBE	LPE	VPE	LPE, VPE MBE

TABLE II

WAVEGUIDE DEVICES DEVELOPED

	GaAs-AlGaAs	InP-GaInAsP	CdTe-HgCdTe	PbTeSe-PbSnTe
Double heterostructure diode lasers	X	X	--	X
Distributed feedback diode lasers	X	--	--	X
Distributed Bragg diode lasers	X	--	--	--
Optical amplifiers	X	--	--	--
Photodiode detectors	X	--	--	--
Optical waveguides	X	--	X	X
Directional-coupler switches	X	--	--	--
Electroabsorption modulators	X	--	--	--
Electrooptic modulators	X	--	X	--
Acoustooptic modulators	X	--	X	--

NOTES

KEY TO AUTHORS AND PAPERS

TECHNICAL PROGRAM COMMITTEE